ANTAL KERPELY DOCTORAL SCHOOL OF MATERIALS SCIENCE & TECHNOLOGY

Phenomena upon Brazing of Steels by Copper

A PhD dissertation submitted to Antal Kerpely Doctoral School for the degree of Doctor of Philosophy in the subject of Material Science and Technology

By

Dheeraj Varanasi

Supervisors

Dr. Peter Baumli, Associate Professor

Prof. George Kaptay, Professor

Head of the Doctoral School

Prof. Gacsi Zoltan

Institute of Metallurgy, Metal Forming and Nanotechnology

Faculty of Material Science and Engineering

University of Miskolc, Hungary

November 2020

List of Symbols

The symbols are listed according to order of appearance in the text.

Symbol	Description	Units
σ	Interfacial energy	J/m^2
ΔG_{disp}	Displacement free energy	J/m^2
θ	Contact angle	Degrees (°)
σ_{sv}	Solid-vapor interface energy	J/m^2
σ_{lv}	Surface tension	J/m^2
σ_{sl}	Solid-liquid interface energy	J/m^2
W_a	Work of adhesion	J/m^2
ΔG_D	Driving force	J/m^2
ϕ	Dihedral angle	Degrees (°)
L	Penetration depth	m
R	Universal gas constant	8.3145 J/molK
P_0	Atmospheric pressure	1 bar
$\Delta_m H_s$	Melting enthalpy of solid	J/mol
$T_{m,s}$	Melting point	K
$C_{P,s}$	Heat capacity of solid	J/K
$C_{P,l}$	Heat capacity of liquid	J/K
$V_{m,s}$	Molar volume of solid	m^3/mol
N_{Av}	Avogadro number	$6.0223 \cdot 10^{23}/mol$
q	Correlation parameter	25.4
Ω_{sl}	Interaction parameter of solid-liquid	J/mol
$G^0_{M,s}$	Standard Gibbs energy of solid	J/mol
$G^0_{M,l}$	Standard Gibbs energy of liquid	J/mol
T_{eu}	Eutectic temperature	K
R_a	Arithmetic average of roughness profile	m
d_j	Joint thickness	m
t_L	Liquid time	s
t_h	Holding time	s
z	Semi-empirical coefficient	1/s
α_V	Volume expansion coefficient	K^{-1}
$t_{L,cr}$	Critical liquid time	s
$C_{Mn(steel)}$	concentration of manganese in steel	wt%
$C_{S(steel)}$	concentration of sulphur in steel	wt%

Table of Contents

1. Introduction

Metallic structures today play an important role in everyday life of human beings. From housing to office spaces, house-hold equipment to heavy industrial equipment world today is filled with more and more intricate structures with complex designs. Steels are the most commonly used structural materials owing to their superior properties like strength, ductility, rigidity etc. The complex structures used in industries are achieved by material joining methods. They can be of both temporary and permanent nature. Temporary joints involve bringing two materials together and joining them temporarily to perform the intended function. Temporary joints are achieved by means of mechanical fastening by using rivets, bolts and nuts, watchers etc. On the other hand, materials can also be joined permanently. They normally include various thermo-mechanical joining methods like welding, soldering and brazing. Welding includes melting of one or both the materials to be joined is carried out in presence of flux to form a permanent joint. In soldering and brazing an external material called as solder (for soldering) or braze filler (for brazing) is melted in between the two substrates so as to achieve the joint. The main difference between soldering and brazing then is in the temperature at which the respective fillers melt. Usually, soldering is a process that is carried out at temperatures below 723 K while brazing is a process that is carried out at temperatures above 723 K. Thus, generally the border between the two processes is identified as 723 K.

Brazing as a joining technique is known to man from primitive times where, noble materials like gold (Au), silver (Ag), copper (Cu) and copper alloys of brass (Cu-Zn) and bronze (Cu-Sn) were used for joining by early man. In a thermo-mechanical process like brazing, melting point of the metals to be joined and the braze play a crucial role. This is because the mechanical properties of the metals are directly proportional to their cohesive energies which increase monotonously with melting point [1-2]. The importance has to be on selection of appropriate braze filler with melting points closer to the melting point of the metals to be joined. The essence being higher the difference in melting points, weaker is the joint obtained. Thus, brazing of structural materials like steels (melting point of pure Fe is 1809 K) is not carried out by tin-based solders (melting point around 505 K). For heavy industrial applications, brazing is the most commonly employed material joining technique and is usually carried out by Cu-based or Ni-based alloys as braze fillers. However, Ni is a toxic metal and is more expensive compared to copper. More often than not, Cu is the widely

used braze metal as it is cheaper and cost-effective and is still the common practice in the industry. Hence, in depth understanding of the various phenomena occurring during brazing of two most important materials is quite necessary. The questions still persist in relation to interaction between the molten braze and steels and subsequent formation of various precipitates in the joint.

Brazing of steels include various phenomena like oxide removal from the surface, wetting and grain boundary penetration by the molten braze, dissolution and diffusion of alloying elements from bulk of steel to the joint etc. This thesis is a genuine effort in investigating the behavior of copper as a braze in joining the steels of varying compositions and understanding the different phenomena involved in the process. A comprehensive literature review was presented with identification of knowledge gap. Goals were formulated, experiments were planned, executed and analysed scientifically and were presented for reproducibility.

2. Literature review

Metallurgical bonding as a field can be said to have evolved hand in hand with early metallurgy itself dating back to the primitive times (as early as 4400 BC). All over the world, three basic elements known to mankind are gold, silver and copper. Objects of various shapes were produced by brazing technology were discovered in archaeological excavations from times as early as 2500 BC. Gold buttons and sequins brazed with Cu-Ag alloy were unearthed in Egypt [3]. Alloys of gold-copper, silver-copper, copper-zinc and copper-tin were all used as braze materials since the time of antiquity. Various objects made of brass and bronze brazes were discovered all over the ancient world from the times of bronze age [4-5]. In fact, the term brazing is a tribute to the over use of brass as braze fillers throughout the course of history [6-8]. These instances throughout history shows us that joining processes were always at the heart of human civilization and evolution right from the moment humans learned to develop articles and tools for either decoration purposes or for warfare.

Bronze and brass as filler metals once again came to forefront during the renaissance and imperialistic era, mainly in manufacturing of firearms and machetes. In fact, in the industrialized world, first known application of brazing is in fabrication of "Sheffield plate" [9]. Sheffield plate as its namesake comes from Sheffield, England. It was invented by Thomas Boulsover in 18^{th} century as a cheap alternative to then standardized silver cutlery. The process involved sandwiching copper between two silver plates and heating the sandwich system to about 1073 K in air. Thus, formed sandwich of Ag/Cu/Ag is used in domestic cutlery [10].

Joining in simple terms is bringing together parts of similar or dissimilar materials so that the resulting joint could satisfy an intended function [4-5, 11] Various metal-joining techniques currently in use are classified based on various schemes. One way of classification is based on type of conditions imposed at the time of joining operation (pressure, temperature etc). The other type depends on the metals being joined (homogenous, heterogenous, autogenous). The classification can also be made on basis of physical state of material at the interface to be joined (solid state, liquid state etc). All the above-mentioned schemes are based on Bauer [11] and summarised in Fig.2-1.

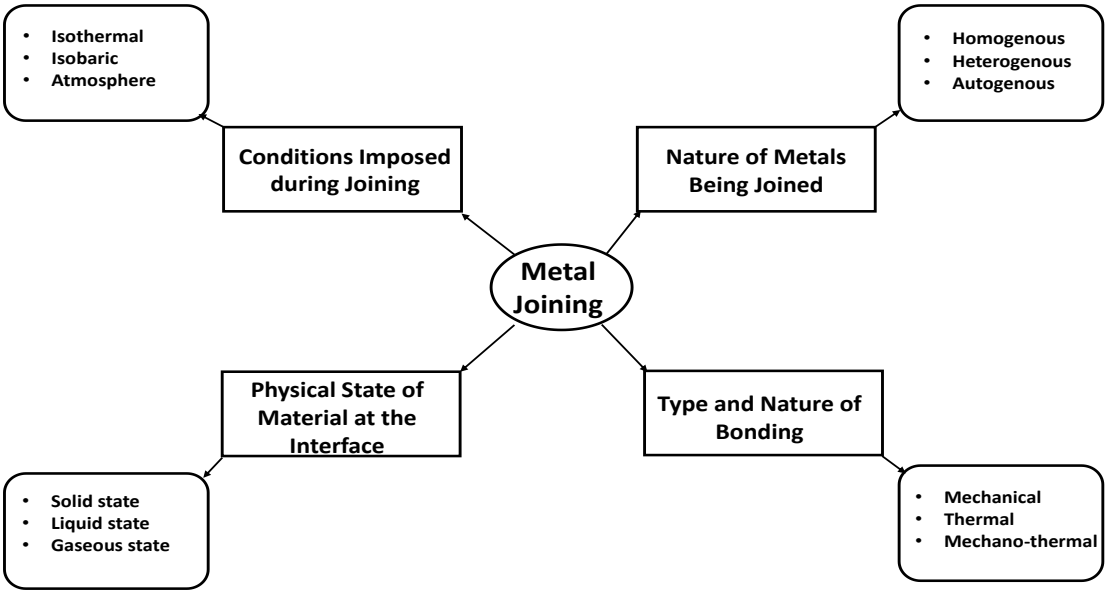

Fig.2-1. Sketch of classification of metal joining methods, based on [11]

Welding, soldering and brazing fall under both thermomechanical and liquid state joining methods. I chose to provide the classification in my thesis according to type and nature of bonding. Schematic shown in Fig.2-2.

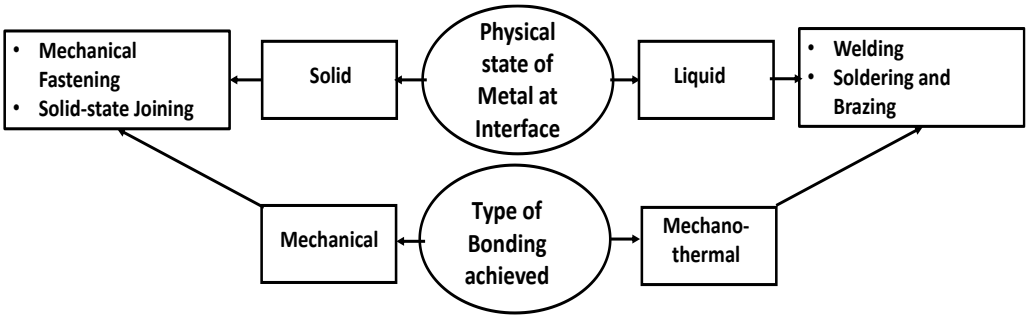

Fig.2-2. Sketch of sub classification of metal joining, based on [4, 11]

Mechanical fastening involves no real fusion between the substrates but instead a temporary joint is achieved by means of clamping, riveting, bolting etc [4, 11]. Joints are achieved on a temporary basis as no real fusion takes place at the joint. They are easy to disassemble, repair and maintain. These types of joining methods can be planned for accommodating expansion mismatches and stress tolerances. However, local stresses effect the joint quality and life in the long run and hence there is a severe restriction about the geometry of the substrates and the joint formed between the two. It also includes a weight limitation which certainly hinders its range of application.

Adhesive bonding involves use of some polymer-resin material with various additives used to achieve a sticky texture. This adhesive resin is then used to stick the two materials together

by means of a chemical reaction between the adhesive and the two materials to be joined. Main characteristic of adhesive bonding is it is very cheap and has low strength. Prime everyday life example of adhesive bonding is the application of commercial M-seal on the leaky water pipes. The adhesive is applied around the leaky joint of a water pipe and is left in air to dry. However, joints are susceptible to external loads and high temperatures.

The second class in joining techniques is when thermal energy is provided to fuse/melt the substrate or the filler to achieve a mechanical joint and hence the name thermo-mechanical joining [4, 12]. Brazing, soldering and welding fall into this category. Joint in welding is achieved by melting of surfaces of both the substrates in presence of flux. Welding is usually performed at extremely high temperatures using high energy sources. Welded joints are affected by direction of heating and heat rate. The properties of the joint to a major part depend on heat affected zone (HAZ) around the joint area. Welding processes are classified according to the types of the heat source used like the plasma welding, electron-beam welding, submerged-arc welding, arc welding etc [4].

On the other hand, soldering and brazing processes are also thermo-mechanical joining methods performed at lower temperatures (than welding). The working principle is similar where a filler material is melted at a lower temperature (than in welding) and was drawn into the small gaps between the parts to be joined by interfacial forces [1, 13]. Soldering and brazing are differentiated at the temperature of application of joint formation. Soldering is carried out at temperature below 723 K while brazing is carried out at temperatures > 723 K [4-5]. Wetting of the surfaces of metal is primal to both soldering and brazing processes and hence presence of oxide layer on surface of parts like steels hinders the wetting process by the solder/braze and results in a bad joint. Since soldering is done at a lower temperature, a flux is used in tandem with solder so as to prevent the oxidation of the metal surface and to keep the surfaces clean from contamination. Soldering is highly advantageous to industrial applications like electronic packaging of integrated circuits and microchips [5].

Brazing today is used in almost all heavy industrial applications for the fabrication of sturdy equipment, in automotive part manufacturing, heat exchangers for refrigeration and air-conditioning and space electronic packaging. It offers a flexibility of “suit to requirement” technology for a wide range of materials (metals/ceramics/glasses/polymers) [14]. In brazing, the materials to be joined are brought in close contact with each other and the filler is placed between the surfaces in a system resembling the sandwich and heat is applied.

Under the applied heat, the braze filler melts and flows in between the surfaces to be joined. The flow is governed by gravity and interfacial forces and the metallurgical bond established at the intersection. Brazing offers high strength joints with minimal distortions (unlike welding) and can be used on wide range of materials and temperatures (unlike soldering) [11]. Brazing also has few disadvantages. It is not a suitable joining technique for brazing extremely large assemblies. Since the physical and chemical properties of joint can be heterogenous and maybe a cause for concern [14]. Good brazed joints depend on the surface quality of the substrates. Hence, the key to a good brazed joint starts from sample preparation and pre-treatment. Braze filler should be placed in between or adjacent to the sample piece requiring brazing and heating is provided to the assembly. Care is to be taken while fixturing the components in place as any mismatch would lead to a poor wetting and a poor joint. Under the heat, the braze melts and wets the surfaces to be joined forming a metallurgical bond with or without intermetallic compounds/layers [14]. After a sufficient time, termed as "*holding time*" pre-determined by the user, the assembly is allowed to cool down.

The innovations in brazing in the last century are detailed here. Effective brazing with minimum filler wastage was discussed by [15] for cast iron-Cu brazed joints. Brazing of thin brass sections for refrigeration applications was patented [16]. The onus of the study was on providing cheaper brazing alternatives for brazing of thin sections of heat exchangers. A braze filler with a zinc non-fluxing paste is placed in between the joints helping in reducing the melting temperature and providing perfect rounded joints. Brazing of stainless steels to aluminum and aluminum alloys by treating them in a zinc bath to ensure a continuous flux on the surface of steels was invented by Chartet [17-18].

The quality and reliability of brazed joints are affected by various parameters [4, 12, 14, 19]. They are wetting and substrate interaction, filler metal and filler flow, joint clearance and atmosphere during brazing. These factors would be discussed in detail in the following subchapters linking them with the observations made during the experiments. All the experiments in the current study were conducted with an identical filler (pure Cu), at same pressure and temperature (~10^{-8} bar, 1373 K), with more or less similar joint clearance. The substrates used are various alloyed steels and therefore majority of substrate interactions with liquid Cu/liquid Sn are similar but not identical. As stated above, main focus is on the various phenomena I observed during the process of brazing. They are listed below:

1) Dissociation of oxide layer
2) Wetting of steels by liquid metal
3) Grain boundary wetting and penetration
4) Thinning of the braze joint
5) Cracking of the braze joint upon cooling

Hence, the subchapters in literature review from here on would be in the order stated above. Knowledge gap pertaining to each topic is listed at the end of each subchapter for reader's convenience.

2.1 The role of the oxide layer in brazing

The presence of oxide layer hinders the ability of filler to flow on the surface [3, 20]. The poor wetting between oxides and metals is well known in the literature [21]. Hence, removal of oxide layer is important for establishing good wetting between the braze filler and substrate surface.

Before speaking of dissociation of oxide layer, let us in brief look at the various atmospheres under which brazing is carried. Since brazing is a high temperature process and normally done without a flux, the chances of metal/filler being oxidized are higher. Hence usually it is carried out in an inert gas environment like Ar, N_2 or under vacuum in a furnace. Inert gases ensure no external surface modification reactions take place during the process, keeping the sample pure. Brazing environment more often than not dictates the type of reactions occurring at the interface and hence more care around the world is being put on controlling the braze parameters, brazing environment being one of them [4]. Usually, brazing environments are classified depending on the atmosphere-constituents reactivity into three types. They are – a) oxidizing (in air), b) reducing – hydrogen/carbon monoxide or
c) controlled/inert – nitrogen/vacuum.

a) **<u>Oxidizing environment:</u>** The most fundamental atmosphere available for brazing is air. The major advantage with air brazing is that no specialized handling equipment is needed and ease of access to the substrate-filler system during the entirety of the brazing process. However, the major problem associated with atmospheric brazing

is in maintenance of the purity of the surfaces of either the filler or the substrate as they are prone to oxidation specially at elevated experimental temperatures. To counter balance the oxidation, usually a flux is used at the molten filler/substrate interface. Fluxes are known to remove the oxide layers physically/chemically.

b) **Reducing environment:** Reducing environment is the one where the surface contaminants can be removed chemically. Gases like hydrogen (H_2) or carbon monoxide (CO) are the principally used gases for creating reducing environments during brazing.

c) **Inert environment:** Inert environment is termed inert because it is neither oxidizing nor reducing. From practical standpoint, it is not possible completely to exclude the oxygen interaction with the substrate during experimentation. The technical definition of inert atmosphere is an environment where presence of residual oxygen does not adversely affect the bonding. Inert gases like argon (Ar) or nitrogen (N_2) are typically used for inert environments and are characterized in terms of residual partial pressure of oxygen (P_{O2}). Besides inert gases, vacuum is typically used for metal-joining processes [22]. In fact, vacuum environment is mostly used for brazing in industry. The major advantage of vacuum system over inert gas system is the ability to control the partial pressure of oxygen inside the furnace. For a furnace brazing application under vacuum, normal oxygen partial pressure is about one-fifth of vacuum pressure. Besides, vacuum is also very useful in controlling the most common surface contaminants on steels – oxide layers.

We have established the need for better environment-controlled furnaces and why we need them. The next phase of this subchapter deals with literature on the oxidation of steels and the removal of the oxide layers during heating. Steels are inherently covered by a metallic oxide layer under normal atmospheric pressure and temperatures. To know the oxides forming on steels, it is vital to know the high temperature oxidation behavior of iron and carbon steels. The most common oxides found on steels are Fe_2O_3 or Cr_2O_3, depending on the composition of the respective steel.

Study on oxide film formation on Cr and Cr-Ni steels was taken up as early as 1957 by Yearian [23]. They observed the growth of oxide films on these respective stainless steels by heating them in air up to 973 K and then subjecting the samples to electron diffraction techniques under both reflective (EDR) and transmission (EDT) modes. Study on the high temperature oxidation of Cr-Mn steels in air with temperatures between 1073 K to 1273 K

was discussed by Gesmundo et al. [24]. They found a continuous chromium oxide layer forming on the steel at temperatures above 673 K. They also observed that activity of Mn breaks chromium oxide layer forming manganese oxide intermittently. They reported a complex oxide of $MnCr_2O_4$ a hybrid complex between both manganese and chromium oxides. Similar study with similar results was reported by Song et al. [25]. High temperature oxidation of low alloyed steels (total alloying elements < 3wt%) was taken up by Chang & Wei [26], while the same for iron was provided by Chen & Yuen [27] in the temperature range of 973 K to 1523 K. In both latter studies, they observed the oxidation of iron follows a parabolic trend as function of time and all three oxides of iron form on the surface. Outermost layer is comprised of Fe_2O_3 and is extremely thin. The intermediate layer is made of Fe_3O_4 and the innermost layer adjacent to the surface of steel is FeO, also supported by Young [28]. Furthermore, Chang provided the ratio of thickness of all three layers as being time independent as 100:10:1 for FeO : Fe_3O_4 : Fe_2O_3. They even opined that presence of carbon in the steel would react with the iron oxide to evolve carbon monoxide gas.

Oxidation behavior of the stainless steels at temperatures between 1073 and 1273 K was taken up by two different researchers [29-30]. Huntz et al. [29] in particular studied the oxidation behavior of the surface of steel at various partial pressures of oxygen. In both the studies, with increasing concentration of Cr and increasing temperature, chromium oxide layer was observed on the surface. At high temperatures they also reported presence of Mn at the oxide layer which supports already described study by Song et al. [25]. The evolution of raw steel surface under continuous heating was given by Doyle et al. [31]. The experiments were conducted on three different steels (one mild steel and two high Cr steels) of varying alloy compositions at temperatures between 373 to 873 K under air and vacuum. The samples under vacuum showed different behavior with rise in temperature. On mild steel, they observed decreasing concentration of surface oxygen on steels with a continual increase in temperature. This coincided with an increase in the surface concentrations of metallic Fe particularly above 723 K. In other two steels which have high concentrations of Cr, there is no trace of metallic Cr on the surface which is still present in oxide state even at 873 K. Their experiment is proof enough for the above statement that different steels will form different oxides at their surfaces. As per the samples heated in air, no real change in states of either of the oxides was reported. More recent studies were taken up on the oxidation behavior of the high Cr steels and chromium oxide formation was reported on the

surface of steel with increasing temperature [32-33]. The studies presented here are summarized in Table 2.1-1.

We have seen the studies conducted on the oxidation behavior of various steels. This next phase deals with the removal of oxide layer from the surface of steels. Removal of oxide layer from steels was further studied in 1980's [34-35]. Ishigami et al. [34] studied the vacuum heating of stainless steels between temperatures of 1173 K to 1373 K. They observed the growth of oxide layer on steels between temperatures of 473 K to 973 K, which later disappeared with increased temperature to around 1173 K. They analysed the results thermodynamically and concluded the removal of oxide layer is by the reactivity with the solute carbon in the steel. The study by Ishigami et al. was followed by Arata et al. [35] around the same time in 1983. The focus was on the dissociation of oxide film from surface of stainless steels and the spreading of molten braze under vacuum. The growth of oxide layer on steel surfaces observed and confirmed by the both studies between the 823 K to 1023 K range. The main conclusion from their study is the confirmation of the dissociation by carbon activity in the steel. They have observed a marked increase in the CO gas in the furnace around the dissociation temperatures. Similar observations and opinions were shared by Kozlova et al. [36-37]. They observed a wetting transition of Cu-Ag eutectic braze filler on the surface of austenitic steels at temperatures above 1123 K. The experiment was conducted on SS304steel under vacuum levels identical to the vacuum levels used in my experiments (~ 10^{-8} bar). They observed the transition of the melt from non-wetting to wetting sessile drop. They opined that the observed transition is due to the dissociation of oxide layer present on the surface of steel at higher temperatures. They further theorized the observed dissociation is due to the activity of carbon in the steel which reacts with the oxide, i.e. leads to the dissociation of metallic oxide into pure metal and CO evolution. This was further supported by the observed increase in CO gas concentration within their furnace at temperatures above 1123 K. The opinion of activity of carbon being responsible for the removal of oxide layer at high temperatures was also given by Doyle et al. [31]. More recent studies in the field were given by Rosseau et al. [38]. They reported on the vacuum heat treatment of high-speed steels. They observed oxide layer removal around 1073 K coinciding with an increase in CO evolution and a reduction in carbon content in the steel. This was also confirmed by the scanning electron microscopy (SEM) on the samples before and after the experiment. Additionally, Rockwell hardness response was measured before

and after the experiment and considerable change in the hardness values were reported. The summary of the literature on oxide removal is provided in Table 2.1-2.

Table 2.1-1. Summary of the literature on growth of oxide layer on surface of steels

Reference	Experimental Method	Observation	Experimental Environment
[24]	XRD	Oxidation of Cr-Mn austenitic steel in air	1073-1273 K, air
[25]	SEM, XPS & XRD	Oxide film formation on surface of Austenitic SS304 steel	300-1073 K, air
[26]	Fe-O phase diagram	Oxide film formation and on surface of carbon steels (< 3 wt% of alloying elements)	473-973 K, air
[27]	Review paper	Oxide film formation and on surface of pure iron	973-1523 K, air
[29]	XRD, XPS	Oxidation of AISI 304 and AISI 439 steels	1123-1223 K, different $p(O_2)$
[30]	XPS & AES	Oxide film formation on the surface of stainless steels, SS316L	300-1253 K, air
[31]	XPS during the experimentation	Iron oxide layer evolution on stainless steels (SS304, SS316) as function increasing temperature	300-873 K, vacuum at 10^{-9} bar
[32]	XRD, FE-SEM & TEM	High temperature behavior of SS321	1073 K, Ar + 20% O_2
[33]	TEM & XRD	Oxidation behavior of Fe-Mn-Si-Cr-Ni stainless steel	1073 K, in air

Table 2.1-2. Summary of the literature on removal of oxide layer from the surfaces of steels during heating under vacuum

Reference	Experimental Method	Observation	Experimental Environment
[26]	Theoretical paper on the basis of Fe-O phase diagram	Dissociation of oxide layer (Fe_2O_3) from the surface of steel	1653 K, air
[34]	Measuring the brightness of surfaces using optical microscope during the experiment	Oxide layer removal from the surface of stainless steels (~ 18 wt% Cr- 10 wt% Ni steels) by carbon reduction	1173-1423 K, vacuum at 10^{-5} bar
[35]	Observing the changes to the Surface of the steels during vacuum heating by using optical microscope	Removal of oxide layer on surface of SS304 and SS321 steels (Cr-Ni steels) by carbon reduction	1133 K, vacuum at 10^{-8} bar
[36]	By observing the wetting transition temperature of liquid Cu-Ag alloy on the surface of steels	Removal of oxide layer from the surface of SS304, SS316 (Cr-Ni steels) by carbon reduction	1123 K, vacuum at 10^{-8} bar
[38]	Nano scanning electron microscopy and hardness testing on samples before and after the experiment	Oxide layer removal from the surface of M35 High speed steel (Cr-V-Mo-W-Co) by carbon reduction	1123 K, N_2

From above summary tables, one can notice that oxide layer formation and oxide layer removal studies were conducted before but the steel types were mostly limited. While the studies confirm the oxide layer removal under reduced environments [35-38], there is need for further experiments. How does the dissociation temperature on the same steels change according to changing pressure? The studies by Ishigami et al. and Arata et al. both observe and relate the oxide film removal to the increased brightness of the surface of steels. Can we describe the oxide layer removal precisely by using the pictures taken from optical microscope? There is a clear need for further confirmation of these observations by accurately used scientific methods. The reviews mentioned [26-27] discuss the oxide layer formation using theoretical means of Fe-O phase diagram and previous literature under similar parameters of temperature and pressure. However, Chang et al. further described the oxide layer dissociation with further increase of temperature, while Chen et al. does not discuss on this. Furthermore, there is no information on the oxide layer dissociation on various other steel types such as mild carbon steels, low alloyed steels. The composition of steel and pressure dependency needs to be examined clearly. The brazing industry needs to know a method of calculation that for a given steel composition at which temperature / gas

pressure / gas composition the surface of the steel will be covered by an oxide (meaning brazing is impossible) and under which temperature / gas pressure / gas composition the surface of the steel will be free of oxide (meaning brazing is possible). According to the state of the art of the literature today this general knowledge / method is missing. So, further experiments and modelling is needed to get closer to this final goal.

Knowledge gap: Although there are many papers in the literature that studied the conditions of the removal of the oxide layer from the surface of steels, these studies are focused only on limited range of steels (stainless steels or high-speed steels). A systematic study is missing on the other steels such as carbon steels or low-alloy steels. The effect of engineering parameters of pressure and composition of steels on the dissociation temperature of oxide needs to be investigated.

Following the dissociation of the oxide the next immediate observation is the spontaneous wetting of the steels by molten braze.

2.2 Wetting of steels by liquid metals

Wetting has become an important sub-field of chemistry and material science since the 19th century. Wetting is an important parameter for brazing. It can be understood that for a good joint formation in a mechano-thermal process like brazing, wetting plays an important under-role. The spread of liquid on top of solid surface continues until the surface energies are balanced according to Eq. (1) [39-40] represented in Fig.2.2-1.

$$cos\theta = \frac{\sigma_{sv}-\sigma_{sl}}{\sigma_{lv}} \quad (1)$$

where σ_{sv} (J/m^2) is the solid-vapor interface energy, σ_{sl} (J/m^2) is the solid-liquid interface energy and σ_{lv} (J/m^2) is the surface tension of the liquid (liquid-vapor), θ (degrees) is the contact angle between the droplet edge and solid surface at the triple point.

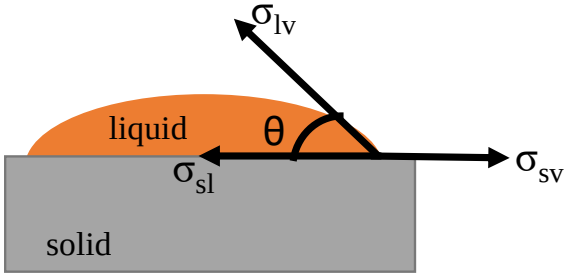

Fig.2.2-1. Illustration of sessile drop wetting technique, most commonly used method for determining the wettability of solid-liquid systems.

Following Eq. (1), it can be understood the behavior of liquid droplet on solid surface is expressed by θ, where good wetting implies an angle between 0-90° and poor wetting implies angles > 90°. Wetting is usually enhanced by adhesion between the solid-liquid pair. As follows from Young's equation, work of adhesion defined by Dupree as the work required to be done in order to separate the solid-liquid interface by introducing a third vapor/gas interface.

$$W_a \equiv \sigma_{sv} + \sigma_{lv} - \sigma_{sl} \quad (2)$$

Substituting Eq. (2) into Eq. (1) we arrive at Eq. (3) which is the Young-Dupré equation:

$$W_a = \sigma_{lv} \cdot (1 + cos\theta) \quad (3)$$

In addition to interfacial energies, wetting is also decided by other experimental factors like surface roughness, temperature and pressure [19]. These were further discussed [41-42]. In paradigm of brazing the braze filler is the liquid metal which wets the surface of solids. Before we delve into the braze fillers, first let us see the literature on wetting of steels by the liquid metals bein used in my study – Sn and Cu.

Wetting of metallic liquids like Cu, Ag, Au on their own solid surface, the contact angle θ was found to be in the range of 0-10°, which shows excellent wetting of metal/metal systems [21, 43-44]. For semiconductor metals like Si and Ge, the contact angle is a bit higher around 10-30° [45-46]. But overall, good wetting exists between metal-metal systems. For the molten liquids involved in the study such as Sn and Cu, the contact angles on the surface of Fe are found in literature for Sn/Fe at 1023 K as around 40° albeit under H_2 gas environment [46]. For liquid Cu/steel the contact angle at 1373 K was found to be ~5° under flux environment [47]. The contact angle of 40° was reportedly achieved by liquid Cu-Ag eutectic on the surface of stainless steels [36]. More recently, the limiting contact angle of ~50° by liquid copper on the surface of SS304 steel was reported in [48]. However, the experimental environment was not provided by them. Complete wetting of pure liquid copper on Fe and stainless steels was reported by Bernardo et al. [49] under inert N_2-H_2 environment at 1bar. However, copper could not wet Fe substrate under Ar-atmosphere at same 1bar pressure [49].

Tin is mainly used for soldering applications as it has considerably lower melting point compared to copper. The contact values attained by liquid tin on the surface of iron under inert gas environment were already discussed in [46]. However, Fe and Sn form intermetallic

compounds at the interface. The effect of formation of intermetallic compounds on the corresponding contact angles of liquid tin on iron surface were discussed by Protsenko et al. [50]. They reported the intermetallic compounds in the case of Fe/Sn pair encourages the wetting and reported final contact angles of around 30° by liquid tin on the surface of iron. Wetting behavior of liquid tin on gold [51] and bismuth [52] substrates under gas flux environment was reported in the temperature range of 523 K to 703 K and contact angles of around 20° (Au-Sn) and 90° (Bi-Sn) were reported. Wetting behavior of Sn-based alloys like Sn-In, Sn-Au and Sn-Cu were measured on Cu and Ni substrates [53]. The contact angles below 40° were observed for all the Sn-based alloys in the study on both Cu and Ni substrates. Especially the spreading of Sn-Cu alloy on Cu substrate yielded contact angles of < 5° which is partly explained by the dissolution of Cu in Sn [53]. Wetting of Cu and Al by Sn-Zn alloy was carried out by Pstrus et al. [54]. The experiments were carried out at ambient pressure under N_2 protective environment between the temperatures of 523 K to 773 K. The spreading of Sn-Zn alloy on the surface of copper does not depend on the temperature at least up to 673 K was reported by them. They also opined that Sn-Zn alloy does not wet the copper surfaces if a protective environment was not provided.

For brazing which is a joining technology carried out at temperatures higher than the ones used in soldering, selection of an appropriate high temperature braze filler is of utmost importance. In the introduction, the author pointed that pure copper is the braze filler used in the study owing to its higher melting point (1358 K).

Considerable research was done in using copper-based alloy as braze filler over the years. Various Cu-based fillers with varying additions of Ni and P were patented by Risannen [55] for ball bearing part manufacturing. The effect of carbon content in steel having an effect on the wetting of Cu/steel pairs was discussed by Rassoul [56]. The wetting between stainless steels and copper fillers during brazing was reported in [57-58]. Among other studies with pure copper as braze filler, [59-60] investigated the reactivity with copper as braze filler with advanced high strength steels. Wetting and brazing of various Cu-alloyed fillers with stainless and other metals was discussed in other studies [61-68]. Good wetting was reported between the liquid Cu-solid substrate pairs in these studies.

Knowledge gap: Wetting of metal surfaces particularly iron/steels by liquid metals such as Sn and Cu was studied in literature. However, these studies are associated with various experimental parameters such as temperature, environment (vacuum, inert or ambient),

interaction between the solid-liquid pair (reactive, nonreactive) etc. However, knowledge about the effect of steel composition on the wetting behavior of these liquid metals is mostly missing. Most studies with Sn were associated on Cu or Ni substrates while their interaction with steels under various experimental environments was missing. As per steel-Cu interactions, the information is missing for the various steels available such as medium carbon steels, low alloyed steels, tool steels etc. The investigations in this regard would help the industry and scientific community in creating a comprehensive databank for steel/molten Sn and steel/molten Cu interactions.

2.3 Grain boundary wetting and penetration

Grain boundary (GB) wetting is the wetting of GB of a solid substrate by a molten liquid. To understand this phenomenon, we need to first define and understand what are grain boundaries and what role they play in metals.

Grain boundary is defined as the separation between two adjacent grains in a metal differing in orientation, composition or dimension of crystal lattice [69]. The grain boundaries were also defined as the boundaries separating two adjacent crystal grains within a phase, under classification of "*homophase boundary*" [70-73].

The concept of grain boundaries originated in the early years of 20^{th} century and were thought to be amorphous layer [74]. However, it was later noticed that the grain boundaries were crystalline [75]. In fact, all polycrystalline materials have grain boundary regions inherent to them [70, 76-77]. For a long time, the properties of grain boundaries were thought to be similar to the properties of bulk crystal in a metal which is untrue [78-79]. Grain boundaries essentially have conjugate crystal orientation which make their properties and energy states different from the bulk crystal of same material [72-73]. Thus, from the perspective of metals which are crystalline, grain boundaries also form an important field of study. Grain boundaries today are described by their degrees of freedom (six for the interface and three for the orientation) [78]. Under the paradigm of joining processes like brazing, the need for grain boundary accountability and design of joints going forward was provided in [73,76]. GB come to the fore at the braze/substrate interfaces and hence they significantly affect the joint properties.

Though the phenomena of GB wetting and GB penetration are unavoidable mostly, they are also not desirable specially when the aim is to join the materials. Grain boundary penetration is the phenomenon which occurs when the liquid metal infiltrates the grain boundaries of solid. It originates from supply of liquid from an external reservoir penetrating the solid grain boundaries continuing onto the bulk of solid [80]. It is an extremely fast process proceeding at rates up to 100µm/s [80-81].

The inherent condition for penetration of a solid GB by a molten metal is given in Eq-s. (4-5) [82-85].

$$\sigma_{GB} \geq 2\sigma_{sl} \tag{4}$$

$$cos\left(\frac{\varphi}{2}\right) = \frac{\sigma_{GB}}{2\sigma_{sl}} \tag{5}$$

Where, σ_{GB} (J/m^2) and σ_{sl} (J/m^2) are the grain boundary energy and solid/liquid interface energy respectively, φ is the dihedral angle and is defined as angle between the liquid layer and the intersecting solid GB, see Fig.2.3-1.

It should be known that grain boundary penetration is only possible when the above condition is satisfied and GB penetration occurs only when dihedral angle φ is 0°. For wetting but non-penetrating systems, the dihedral angle represents the measure of penetrability [83].

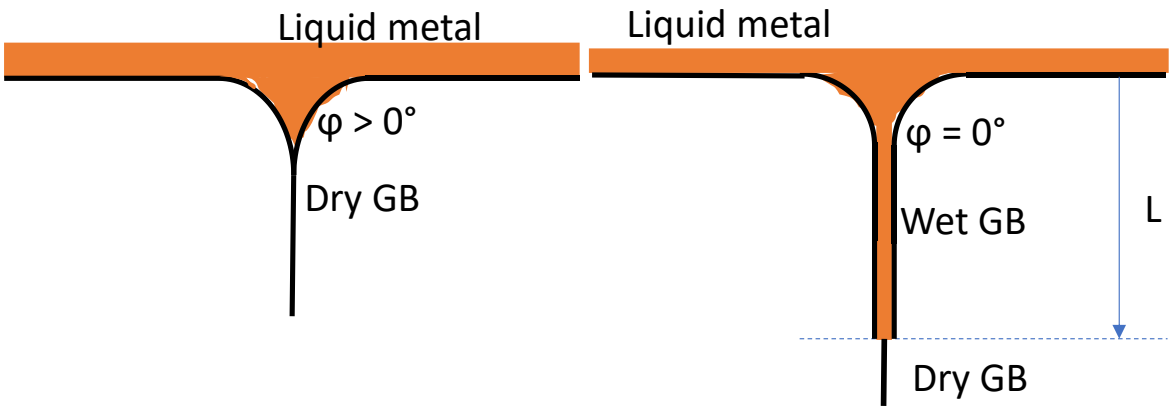

Fig.2.3-1. Schematic of grain boundary penetration by liquid metal showing both dry and wet GB, corresponding dihedral angles and GB penetration depth

Thus, grain boundary penetration can be understood as a complex process following grain boundary wetting.

GB wetting of Fe/steels by tin was studied with particular focus on intergranular cracking observed in steel grain boundaries. Intergranular fracture of steel grain boundaries due to the presence of "trap elements" at the grain boundaries was discussed by Briant and Banerji [86]. The common list of elements leading to such embrittlement was also provided further which includes tin, phosphorus, sulfur, silicon, antimony among others. Grain boundary strength of a Ni-Cr steel was investigated in [87] under the effect of Sn, P and Sb. They opined that the presence of impurity element at the grain boundary of high Cr-Ni steels would lead to embrittlement of the grain boundaries. This is in agreement with previous findings by Briant and Banerji [86]. Complete GB wetting of Zn by liquid Sn was studied as function of Sn concentration and temperature was reported by Evans et al. [88]. Similar observations pertaining to complete GB wetting and penetration of liquid Sn along the grain boundaries of Al was reported by Dolgopolov et al. [89]. They observed an increase in penetration depth achieved by liquid tin in Al GB as it approached triple GB junction. They also inferred formation of Sn-Al intermetallics along the triple junctions in the GB of Al. GB cracking in steels due to the embrittlement induced by the interaction between liquid tin was investigated [90]. They concluded the presence of tin on the surface and its corresponding interaction with the steel GB leads to GB cracking and penetration by liquid tin.

The focus on interactions between molten copper/steel or molten/iron systems increased since late 1950's [91-93]. Fisher observed the diffusion and penetration of a molten liquid occurs rapidly along a GB interface compared to interior of crystals. Mullins described in particular, the mechanism of grain boundary groove formation in a polycrystalline material when subjected to heating. He established that the process of grooving in a heated polycrystal follows a time dependent profile proportional to $t^{0.5}$ correlating his work to that of Fisher. A study on combining the two theories of Fisher and Whipple was attempted by Young et al. [94]. They confirmed the square root of time dependence of penetration depth.

The interactions between molten copper/steels was soon taken up by various researchers [82,95-96]. Savage et al. described mechanism in which braze joints of steels/Cu/steel systems fail due to the penetration of steel grain boundaries by liquid copper. The so called "*intergranular cracking*" occurs when liquid copper wets the grain boundaries of stainless steels. The adhesive energy between steel GB and liquid copper is greater than the cohesive energy within the liquid and hence, this becomes the driving force for the penetration. Once,

the liquid metal penetrates the GB, intergranular stresses [97-98] are caused leading to intergranular cracking and failure of the joint at the steel/braze interface.

Fe dissolution from the bulk steel into molten copper was found in both the studies. Additionally, penetration of molten copper into the iron and steel GB was reported by Ishida after experimentation at temperature ranges between 1373-1673 K. This work provided the first account of liquid metal incipient into solid GB. His studies provided initial mechanism of liquid metal penetration into solid grain boundary. He also explained a three-step mechanism where liquid metal diffuses and penetrates the GB region of solid at the solid/liquid interface region. Second step, is complete GB penetration by the liquid metal and finally the grains of iron dissolving in liquid copper. He also provided the comparative study of penetration by liquid Cu and Cu-Ag eutectic on steels and observed the reduced penetration in case of Cu-Ag melt which he attributed to the silver addition in Cu. Investigations of high alloyed structural steels penetration by copper were further carried out [56, 99-100]. Rassoul et al. [56] discussed the effect of carbon content on diffusion and penetration of copper in steels and established an inverse relation between the two. Steward et al. [99] experimented with the grain boundary penetration system in SS304 stainless steel/Cu systems. They found Cu penetration into the GB and brittle interlayers at the interface between the steel and Cu. The work of Fredriksson et al. [100] in 2001 is perhaps the most closely related work to my present thesis and provides a comprehensive outlook on behavior of molten Cu on iron and steels. They studied the process of liquid copper penetration into iron grain boundaries. They established that during melting of copper and its interaction with iron GB, iron grains would be separated and dissolved in liquid copper. This would lead to a subsequent channel formation which is immediately filled by the liquid copper causing LME (liquid metal embrittlement) in the GB of iron. This LME effect leads to further cracking and penetration of the molten metal into the substrate. The process is driven by the energy difference as shown in Eq. (5). The simultaneous diffusion and dissolution of Fe will also lead to groove formation at the interface as previously theorized by Mullins. They also provided a comprehensive mathematical expression for the observed penetration as function of Gibbs free energy, Eq. (6). He gave mathematical proof of the same as following:

$$\Delta G^{tot} = \Delta G^{\sigma} + \Delta G^{s} + \Delta G^{diff} \quad (6)$$

where, ΔG^{tot} is the total Gibbs energy change (J/mol); ΔG^{σ} is the Gibbs energy required to form new interfaces of S-L (J/mol); ΔG^{S} is the driving force required to suck in the liquid

(J/mol); ΔG^{diff} is the driving force for diffusion of copper and vacancies (J/mol). They also provided a general penetration distance relation for this case where the penetration distance varies as function of holding time with a power of ¾ as opposed to the usual power ½ as followed from Fisher and Young, Eq. (7).

$$L \propto f(t^{0.75}) \tag{7}$$

where L is the penetration distance observed (m); t is holding time (s).

Among other studies on GB wetting and GB penetration on various metallic solid/liquid pairs include [101-107]. All these studies showed good GB wetting and penetration of steel by molten liquids, both of which are undesirable. Thus, we can see that phenomena of grain boundary wetting and grain boundary penetration are inseparable and form an intricate part of brazing process. The studied literature is summarized in Table 2.3-1.

Table 2.3-1. literature available on various steels and pure Cu filler

Reference	Solid/liquid pair	GB wetting and GB penetration
[56]	Mild steels/Cu	yes
[82]	Steel/Cu	yes
[95]	Carbon steels/Cu	yes
[96]	Iron/Cu	yes
[99]	SS304/Cu	yes
[100]	Iron/Cu steel/Cu	yes
[102]	1045 low-alloyed steel	yes

Knowledge gap: Though the literature exists on steel/Sn and steel/Cu interactions with regards to grain boundary wetting and grain boundary penetration, the extent of these studies was only limited to high alloyed stainless steels. Data pertaining to the same is insufficient for other structural and carbon steels. GB wetting and penetration of steels by liquid tin was mostly discussed as a phenomenon leading to embrittlement. Further studies are required to observe if this is the case for all the steel systems or only in high alloyed steels. It is also not clear if the GB penetration is true for all steel types by liquid copper.

2.4 Thinning of the braze joint

To understand the significance of the thickness of brazed joint, we need to first discuss the significance of joint gap and control of joint gap. Joint gap comes into play because of the nature of brazing in it being a capillary joining technique. Generally, the braze fillers should

and will possess exceptional flow characteristics, specially the pure metal fillers like Cu which is used in this thesis work. At this point it is also worthy to point that under brazing, "a filler with necessary flow characteristic would flow towards the hottest part of the joint. This is true even for the cases, where the flow is against the gravity" [3]. Normally for a brazing application under air, a limit of 0.05 mm joint gap exists for production of good joints. This goes down further for brazing operations under vacuum to 0.025 mm joint gap. This establishes the narrower the gap maintained, better is the action by capillary forces to suck the molten braze and form a good joint. Besides, study by Zimprich et al. [108] among others have also shown the same is followed in soldered joints.

Besides, joint gap, thickness of braze filler also plays important role in the efficiency and reliability of the joint. The investigation of effect of joint thickness on the braze joint strength of brazed Al structures using Al-Si foil was carried out by Hashemi et al. [109]. They observed a decrease in the thickness of the joint due to the increased formation of Al-Si eutectic with an increase in holding time above 5 minutes (300 s). Porosity in the joint was found to increase at higher holding times which also contributed to the reduction in the joint strength.

Since the first half of this decade, prominence of filler thickness and their effect on joint microstructure is increasing not just in brazing but in other joining industries like welding. The properties of TiNi-steel alloys welded by Cu-fillers was investigated by Li et al. [110]. The thickness of the Cu-filler was varied while keeping other experimental parameters constant. They found a qualitative increase of the weld joint and Cu-filler thickness [110]. The Cu-content across the weld zone increased which also resulted in an increased joint strength. A significant reduction in the thickness and quantity of intermetallic compounds (IMC) was also noticed. This reduced the overall brittleness in the joint contributing to the joint strength. Continuing the trend, qualitative experiments of laser welded steel/NiTi joints using Cu-fillers of varied thickness was done by Zoeram et al. [111]. They concluded that increasing the thickness of filler promoted an increase in joint strength.

More recent trend of studies in the understanding the effect of joint thickness has turned towards brazing. Steel brazed joints with a Cu-interlayer added to the filler was studied where the thickness of the interlayer was varied and corresponding changes to the microstructure were analyzed [112]. Varying the thickness of Cu-interlayer reduced the amount of IMC's formed at the joint and increased the shear strength of the joint as reported

[112] However, effects of varying filler thickness on the quality of the joint was investigated by [113-114]. They found optimized thickness-temperature parameters for obtaining a superior joint.

The literature presented above were on the usage of fillers of varying thickness and how the thickness effects the joint microstructure or strength. However, in my studies I used braze filler of same thickness throughout my experiments. I observed a significant reduction in the thickness of the filler post brazing. To the best of my knowledge, this was neither reported nor discussed before. I present my observations regarding the thinning of the joints in the due course of the thesis.

Knowledge gap: From literature, it is discussed that for good joints thinner joint thickness is desirable. However, contradictory results were also provided in few studies. Furthermore, it is not known how the joint thickness depends on different brazing parameters, such as brazing time, temperature, steel composition, brazing atmosphere, etc.

2.5 Cracking of the braze joint upon cooling

Once, all the necessary parameters and conditions of brazing are satisfied and the materials are brazed, the focus shifts to the qualitative analysis of the joints – microstructure. Under normal circumstances, the microstructure of the joints is reliable and show good bonding. Sometimes, cracks are observed in the joints which cause hindrance to the joint life and serviceability of the brazed structures. This subchapter deals with the cracks in the brazed joints, the reasons for cracking and conditions which contribute to cracking of the brazed joints.

Crack is understood as a break in the bulk of material without complete splitting or separation of the material. Cracking of the joint is not desirable as it will lead to eventual split and failure of the joint and the brazed structure as a whole. Cracking effects the intended function and hence the reliability of the joint. Cracking of brazed joints have been observed and analyzed in the literature. There are two main conditions under which brazed joints crack – externally loaded and unloaded.

Cracking of the joint under external loading condition happen when the joints are subjected to mechanical tests like tensile/shear/torsion etc. The joints fail under the applied force/pressure and the magnitude at failure is given as the strength of the joint. More often

than not, liquid metal embrittlement causes the majority of failures of the braze joints under external loads [97, 115]. On the other hand, cracking of the joints under no external loading conditions is very vital to understand. This type of cracking occurs due to the inherent nature of various precipitates being formed in the joint layer during cooling down period of a brazed system. For example, when an ionic precipitate like sulfide or phosphide form in a metallic braze joint, and the system cools down from relatively high temperatures, the joint cracks due to the imparted thermal stresses at the joint/precipitate interface [115].

Considerable research was done on cracking of brazed joints under external loading conditions. Liquid metal embrittlement (LME) as the name suggests, is the phenomenon in which the metal in contact with liquid metal at higher temperatures becomes brittle and cracks when subjected to external loads. Initial studies in the field were focused on the brittle fracture of solid metal due to contact with liquid metal [98, 116]. Nicholas et al. [116] gave the pre-requisites of LME, in which they discuss the parameters like external stress, temperature and crack propagation etc.

First studies on the LME phenomenon in connection with cracking in brazed joints was discussed in [117-119]. They found cracking in the brazed joints of various steels/Cu systems where the steel was embrittled by molten copper and later was cracked under external loading. Particularly Heiple et al. focused the study on stainless steel embrittlement by molten Cu, Ag and Sn. They concluded the primary reason for cracking of the joint under strain was due to LME. LME as we can recall is connected with liquid metal penetration of grain boundaries (subchapter 2.5).

More recent studies in the field were carried out by Maciejewski et al. [120], Yue et al. [121] and Ghovanlou et al. [122]. Maciejewski et al. [120] investigated the intergranular fracture of stainless-steel pipe surfaces at the brazed joint interface. He found accumulated copper in the grains of steel which ultimately led to failure of the joint under operation. Yue et al. [121] investigated the mechanical properties of stainless steels brazed with Ag-Cu braze filler. Ductile fracture under shear was observed by them. They also established an inverse relation between shear strength and applied braze temperature.

The study carried out by Ghovanlou et al. [122] on the brazed joints between low carbon steels using pure Cu filler is of particular interest to me as it directly falls within the scope of my experimental study. Two modes of failure were established by them – rupture and dendritic failure. Their observations of rupture and dendritic failures fall under both the

categories. Rupture failure is due to dissolved Fe in the copper joint. Whereas, the dendritic failure was attributed to precipitate formation more particularly manganese sulfide (MnS) precipitates in the joint. The joints when subjected to shear lead to failure at the interface of MnS/copper.

There is a possibility of braze joints being failed without any additional mechanical loading.

The concept of intergranular cracking of steels was investigated as early as 1970s [82]. They reported the penetration of steels by liquid copper during brazing of steels. They opined that intergranular cracking of grain boundary of certain steels is due to the penetration by copper which creates intergranular stresses [115] in steel. This stress leads to failure of the joint at the grain boundary of steels.

Steels are composed of various elements like Cr, Ni, Mn, Mo etc. besides Fe and C. They also consist of non-metallic elements like Si, S, P etc. The alloying elements readily form compounds with inclusions during processing [123]

The most commonly formed non-metallic inclusions in steels are manganese sulfide (MnS). They are very common in most steels, as almost all steels contain Mn and S albeit in small amounts if not higher [124]. MnS is an ionic precipitate forming one of the largest indigenous inclusions in steel matrices. They form during the cooling down process of steel casting and form near the grain boundaries and surfaces. Modelling and characterization of various shapes and distribution of MnS in steels was also investigated and published [123, 125].

Precipitates form indefinitely in the brazed joint under cooling. Initially, the braze filler is free of any precipitates or elements but the alloying elements would accumulate in the joint due to diffusion from steel under the experimental conditions. Of these, MnS specifically is known to cause failure of alloyed steels by inducing pitting corrosion. The behavior of high alloyed steels such as SS304 and SS316L steels under humid environment and their eventual failure was exclusively discussed [126-128]. They realized MnS inclusions in steel microstructure form the source of localized stresses resulting in initiation of pitting corrosion. More recent findings of the spring steel corrosion and observed the corrosion is due to presence of manganese sulfide inclusions around the corrosion pits was presented by Shi et al. [128]. Moreover, they quantitatively analyzed the inclusion size and its dependence on the crevice formation. They also provided an upper limit of 5μm for size of the inclusions probable of initiating a crack.

In addition to pitting corrosion, MnS was also found culpable for failure of other materials elsewhere. Failure analysis of knuckle joints in an aluminum sheet straightening machine was carried out by Pantazopoulos et al. [130]. The ductility of the joint purportedly was deteriorated by the presence of heavy inclusions of MnS. These inclusions when subjected to the high torsional distortions lead to the failure of joints. The failure of carbon steels due to fatigue development around the regions of sulfide inclusion clusters was reported by Temmel et al. [124]. It is due to the fact that MnS inclusions normally are spherical shaped. But, during the processing the morphology of the inclusion changes and this leads to anisotropy in the structure. This anisotropic change is associated with reduced mechanical properties of the inclusions and lead to cracking, supported by Sojka et al. [131].

Knowledge gap: Literature regarding the cracking of brazing joints has been studied before, it focusses on cracking of the joint under external loading conditions. No real contribution was made in the study of cracking of brazed joints under no-load conditions. There is a gap in understanding if and why the joints crack under no-load conditions. The knowledge is also missing in systematic qualitative investigation of brazed joints of steel/Cu system as function of various alloying elements in the steel and their dependence on the holding time.

In addition to this, manganese sulfide precipitates were methodically shown to cause cracking of steels under various working environments and is attributed as corrosion inducer in steels. However, formation and precipitation of MnS in the brazed joints was not conclusively linked with cracking of an unloaded braze joint under cooling. There is a need to confirm if such a relationship exists between precipitation of manganese sulfide and cracking of the brazed joint. If yes, then how does the concentration of Mn, S in steel and holding time of brazing effect the final joint quality.

The engineering industry requires a database on the quality of the brazed joints as function of holding time, composition of steel and temperature. As composition of steels vary from steel to steel, there is a need to contribute to this databank for better understanding of the effect of various parameters on the quality of the brazed joints.

3. Scientific goals

After careful literature review and identification of knowledge gap, the following scientific goals have been defined:

3.1 Identify the conditions of spontaneous removal of the oxide layer from the surface of steels.

3.2 Investigate the wetting behavior of liquid copper and liquid tin on the surface of various steels.

3.3 Investigate the grain boundary penetration of steels by molten copper and molten tin.

3.4 Observe the change in the thickness of the joint as function of holding time during brazing for various steel compositions.

3.5 Braze of steels by copper and investigate the microstructure of the joint. Establish conditions of spontaneous cracking of the joint upon cooling after brazing, if any.

4. Materials and methods

The material and methods section is provided for the reproducibility by the reader. The study is focused on various phenomena taking place during brazing of steel sandwiches by using a copper foil under vacuum.

4.1 Materials

All the experiments with regards to oxide layer dissociation, wetting, GB wetting and penetration and brazing were conducted with five different steels of varying composition. The composition of these steels was tabulated below, Table 4.1-1.

Table 4.1-1. Composition of steels used in the thesis (Source: X-ray Florescence)

Steel standard		Cr wt%	Mn wt%	S wt%	C wt%	Others (Si, P, Mo etc) wt%	Fe wt%
European	AISI						
Armco	-	0.016	0.11	0.0064	0.0010	< 0.050	Rest
C45	1045	-	-	0.030	0.45-0.50	~ 0.60	Rest
S103	-	-	0.20-0.25	0.010-0.020	0.60-1.00	~ 0.70	Rest
CK60	1060	0.15-0.20	0.75-0.80	0.070-0.075	0.25-0.60	~ 0.70	Rest
EN 1.4034	420	11-12	0.90-1.0	0.035	0.15-0.20	~ 0.50	Rest

C45 steel is medium carbon steel with excellent machinability and tensile properties. It is generally used for automotive and structural parts like gears, bolts, shafts and keys.

S103 is a low chromium steel with good thermo-mechanical properties and creep resistance. It is generally used for manufacturing of gear shafts, bolts and nuts, industrial fasteners for turbines and boiler etc. The ‘S’ is a code given for structural steels for aircraft applications.

CK60 is a carbon steel used for fabrication of mechanical parts like shaft bushes, connecting rods, agriculture tools, springs and strips etc.

EN1.4034 is a high Cr-steel with excellent corrosion resistance. They are used generally for manufacturing of kitchen knives, press plates, brake discs and surgical instruments.

Besides the above-mentioned steels, two other steels were used exclusively as part of sub-experiments. Armco steel (Table 4.1-1) was used in oxide dissociation study using liquid tin Armco steel was assumed to be the closest to pure iron in the experimental investigations as the total amount of alloying elements is < 0.2 wt%.

Pure copper foil [99.99 wt%, source: XRD] was used as the braze filler for brazing experiments. The thickness of the copper was 70micrometers, measured by using micrometer.

Pure tin [99.99 wt%, source: XRD] and pure copper were used to study the oxide layer removal and wetting experiments.

Pure Sn is a common solder metal with a low melting point of around 505 K [5]. Pure Sn has a broad liquidus range [132] and hence was chosen for the oxide layer dissociation experiments.

4.2. Methods

The experiments were conducted in a resistance vacuum furnace equipped with Pt/Pt-Rh thermocouple to measure the temperature. The heating mechanism is achieved by resistance heating by varying the amperage (I).

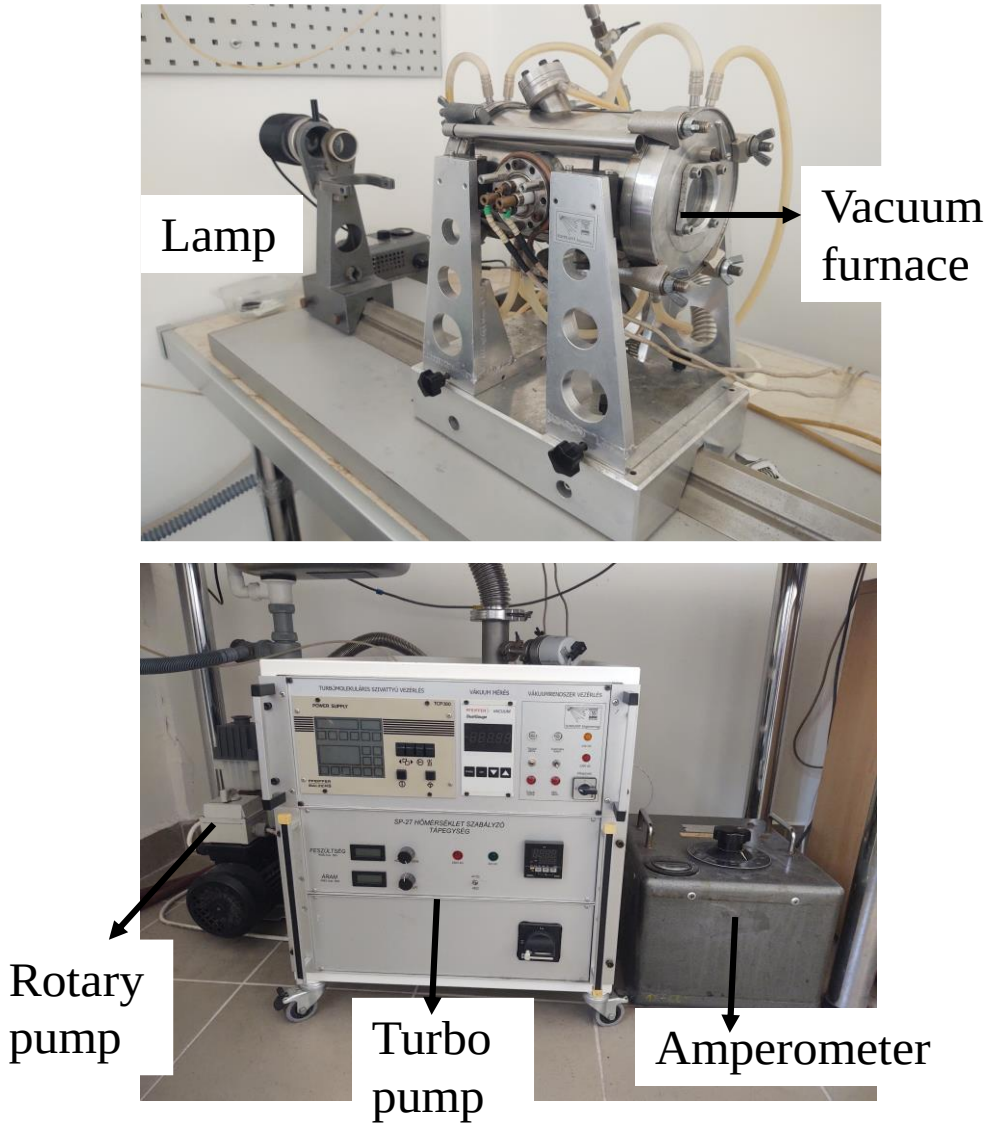

Fig.4.2-1. The experimental setup of furnace and high vacuum pump

The resistance furnace is connected to a high definition camera for recording pictures during the experimentation. The lamp shown in the Fig.4.2-1. is used to illuminate the samples inside the furnace for the camera at low temperatures. At high temperatures, usually above 873 K, the furnace begins to glow and the lamp is no longer used.

All the experiments were conducted under vacuum at pressure 10^{-8} bar. To achieve this vacuum level from atmospheric pressure, two pumps are used in two stages, a rotary pump and a turbo pump. The amperometer is used for changing the current supplied to the resistance furnace in order to change the temperature. The furnace is water cooled with water channels running around the periphery of the furnace.

All the steel samples were first cut to required dimensions of 10mm x 7mm x 4mm and ground by using sand papers of 180, 220 and 320 µm grit size. The process is carried out for duration of 180 s on each grit sized grinding paper. Water is used as cooling media during this process. The samples are then subjected to polishing on a 3 µm grit woolen cloth in a diamond media until a mirror finish is obtained. Additionally, ethylene glycol lubricating media is also used during the polishing process. Both grinding and polishing were carried out under a load of 25 N with speed of polishing disc at 300 rpm. The samples are dried immediately.

The copper and tin used in the experiments are 99.99 wt% pure materials. They are cleaned in acetone using an ultrasonic bath. This helps in removal of any external grease, dust or fats present on the foils.

To study the oxide layer dissociation/removal and corresponding wetting, a sessile drop technique is used. Sessile drop technique is the most common method employed for wetting experiments [133-134]. Sessile drop technique is the method in which a small piece of metal to be melted is placed on the surface of substrate, placed in the furnace and heated until it melts and forms a sessile drop on the surface of substrate. Hence it is called s sessile drop method.

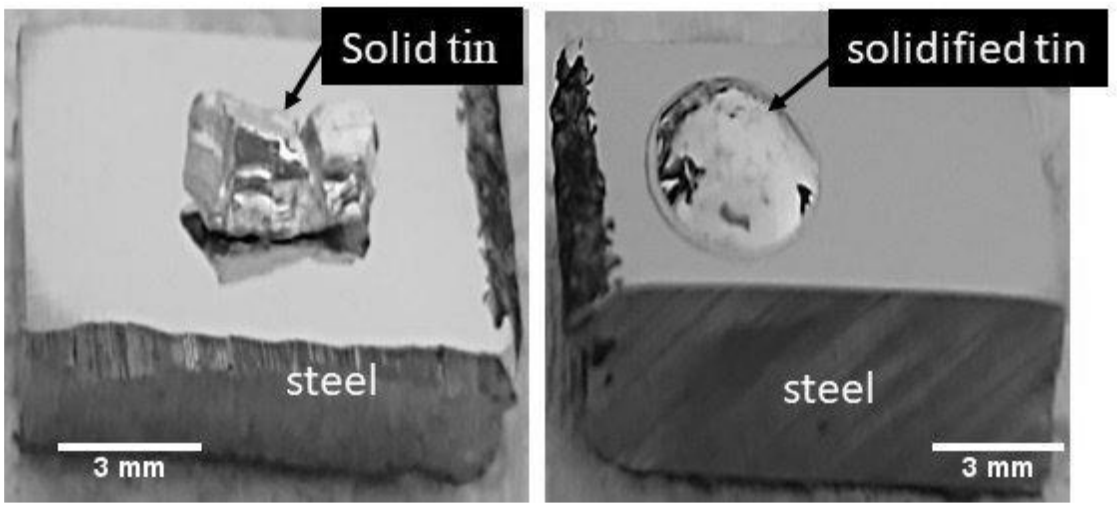

Fig.4.2-2. The tin on surface of steel, before (left) and after (right) the wetting experiments.

The change in the shape of sessile drop as well as the contact angle during the wetting and wetting transition experiments were recorded by using the high definition video camera connected to a laptop. A pre-installed contact angle measurement software (KSV surface

chemistry) was used to measure the contact angle of the sessile drop of tin and copper on the surface of steel during the experimentation.

For the purpose of brazing, the two steels and Cu foil are placed in a sandwich structure where the foil is in between the two steels, a high temperature Ni-Si wire is wound manually around the sandwich structure so as to keep them in place during the experimentation. The diameter of the wire used is ~500 µm and is used exclusively to keep the samples together during the experiment. The wire contact with samples is minimal and hence it has no effective role in the experimentation. Table 4.2-1. Shows the gravitational pressure exerted by the top steel substrate on the sandwich joint is calculated. As follows, this pressure is in the range of 267 …. 347 Pa and thus it has little effect on the joint.

For brazing, the temperature is increased from room temperature to 1373 K (experimental temperature,17 K above the melting point of Cu), where it is held for a sufficient time termed as "*holding time*".

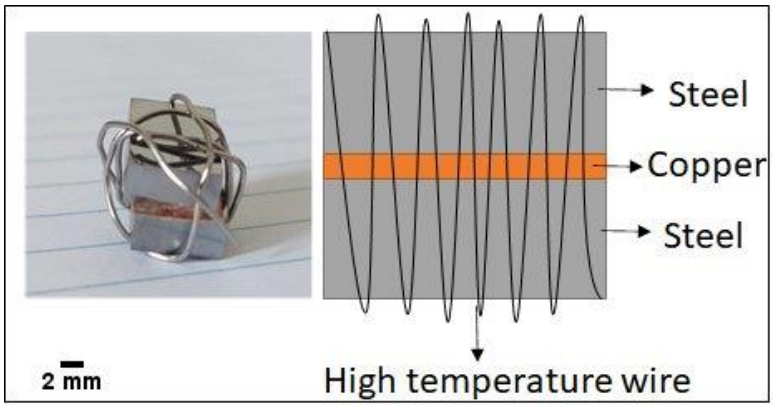

Fig.4.2-3. The sandwich structure arrangement used for brazing experiments

Table 4.2-1. The average mass of the top steel sample, surface area of copper in contact with the top steel and the pressure exerted by the steel sample on the copper sandwich

Steel	Mass of the top steel substrate (g)	Surface area of copper in contact with top steel (m^2)	Pressure applied on the joint by the top steel sample (Pa)
C45	2.20 ± 0.10	$7.00 \cdot 10^{-5}$	307 ± 15
S103	2.48 ± 0.36		347 ± 43
CK60	1.91 ± 0.24		267 ± 28
EN1.4034	2.01 ± 0.07		281 ± 1.0

4.3 Post experimental processing

Post experimentation, the samples are left in the furnace to cool down overnight. They are later removed from the furnace, weighed and mounted in bakelite resin for microstructural examination. The mounted sample is again grounded, polished and dried as explained in section 4.2 before subjecting to microstructural examination. The microstructural examination is conducted by using scanning electron microscopy – energy dispersive spectroscopy (SEM-EDS) [135-136].

Two different scanning electron microscopes were used in this study, Carl Zeiss EVO MA10 and Hitachi S-4800. EDAX Genesis APEX2 and Bruker AXS EDS were used for carrying the elemental analysis at the microstructure. An acceleration voltage of 20KV was used. All the pictures were taken under back scattered scanning electron microscopy (BSD-SEM) mode. The GB penetration of the steels by liquid Cu was observed in SEM investigation and the depth was measured using imageJ image analysis software as the vertical length of the copper channel formed in steel GB perpendicular to the steel/Cu interface.

5. Results

5.1. The role of the oxide layer in brazing and wetting of steels by liquid tin

From the literature, it was clear that the steel surfaces are covered by a native oxide layer. Presence of oxide layer creates hindrance to wetting of solids by molten metals. The experiments are focused on observing the conditions under which this native oxide layer disappears during wetting. This will lead to wetting transition of the liquid metal on the surface of steel. Wetting transition is defined as the transition of the contact angle of a liquid in contact with a solid surface from angle > 90° to an angle < 90°.

For our purposes a metal is needed that satisfies the following requirements: i) have a wide temperature range of its stability in liquid state, ii). wetting steels of unoxidized surface with contact angle below 90°, iii). wetting steels of oxidized surface with contact angle above 90°. The latter condition is satisfied for the majority of liquid metals. Our final choice is tin. It has a relatively low melting point (505 K) and it is stable as a liquid up to 1,155 K at the residual pressure of 10^{-8} bar in vacuum (see Fig.5.1-1). Moreover, it is widely used as a basic component for soldering. The calculation is done by using the data by [137] and a method described in [138]. So, all the experiments will be conducted in this work by liquid tin.

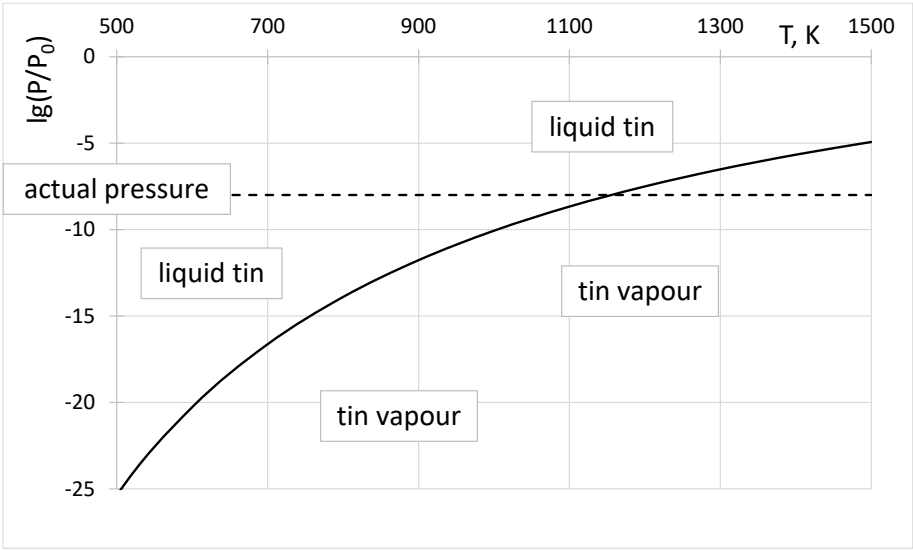

Fig.5.1-1. Equilibrium vapor pressure of tin plotted as function of temperature calculated from data by [137]. The actual residual pressure in the furnace is shown by a horizontal dotted line; under these conditions tin is a stable liquid below 1155 K.

These “wetting transition experiments”, were conducted using liquid tin as tin has a broad liquid temperature range. The experiments on wetting transition of tin were conducted with five steels (Armco, C45, CK60, S103 and EN1.4034), composition given in Table 4.1-1., at two different vacuum levels – 10^{-8} bar and 10^{-5} bar. The experiments were conducted between room temperature and temperature where wetting transition of tin was observed on respective steel surface. The range of temperature for all the steels was in between 673-1273 K.

First observation is that the liquid tin upon melting (around 505 K) formed a closely resembling spherical ball shape on the surface of steel. This phenomenon is called poor wetting and is evidently due to the presence of oxide layer. Later as the temperature is increased, the spherical ball slowly and gradually turns to spherical cap or a sessile drop shape (see Fig.4.2-2.). The temperature above which this transition occurs strictly depends on the composition of steel and native oxide on the surface of the steel. This wetting transition observation is shown in Fig.5.1-2, below.

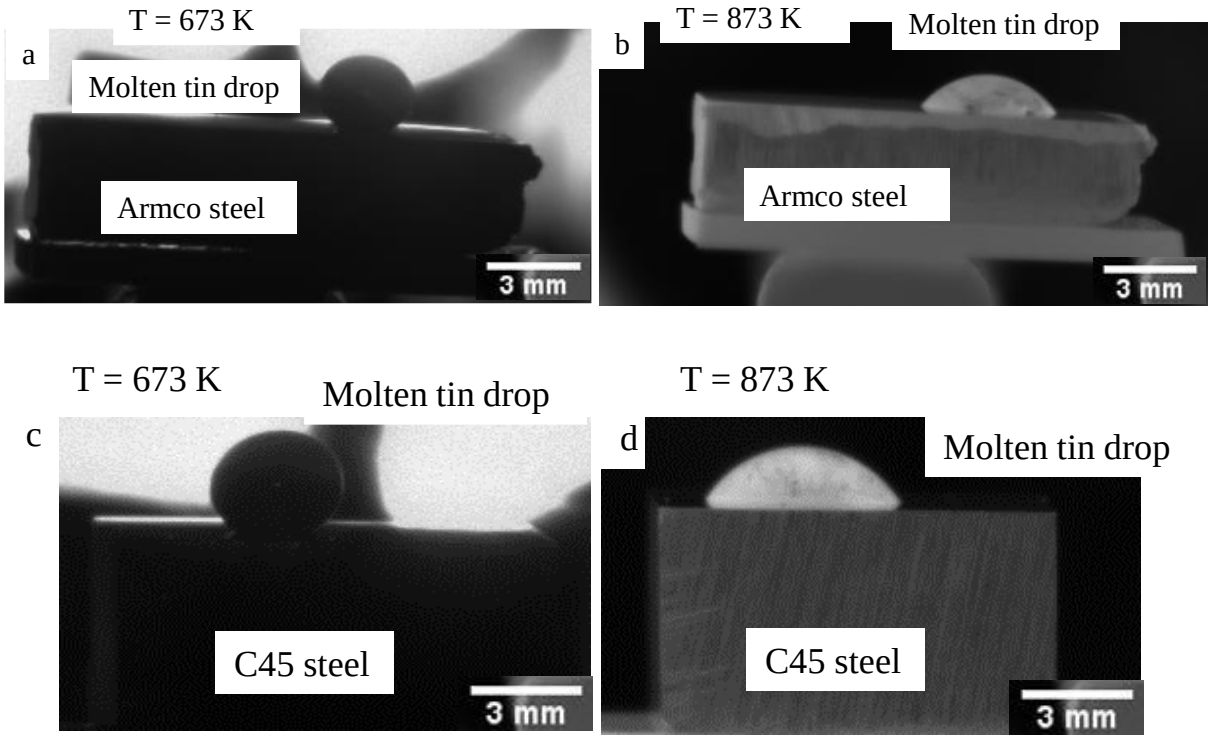

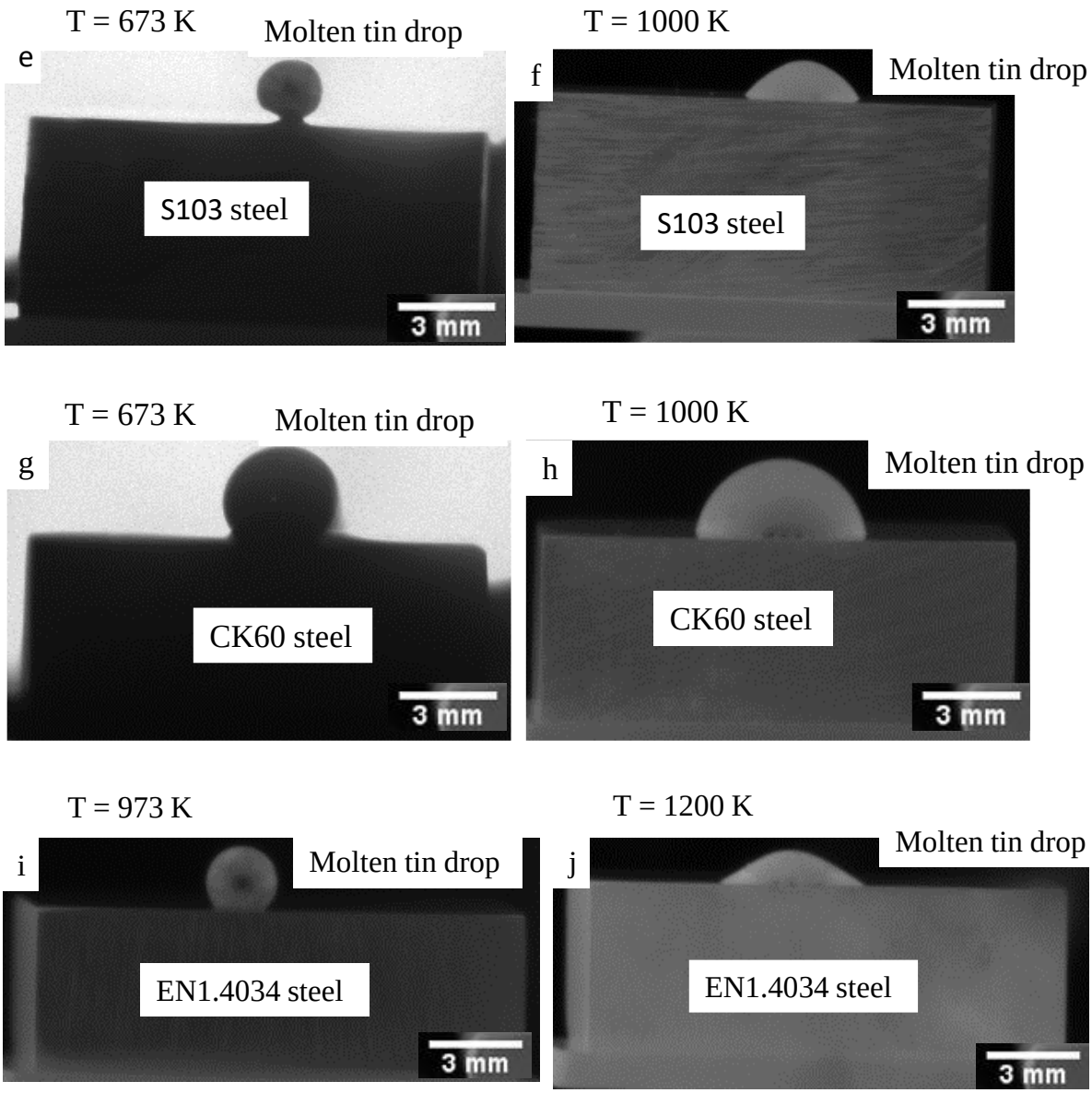

Fig.5.1-2. Non wetting and wetting shapes of Sn sessile drops. Fig-s a, c, e, g, i show the low-temperature non-wetting Sn drops on the surfaces of Armco, C45, S103, CK60 and EN1.4034 steels, respectively. Fig-s b, d, f, h, j show the high-temperature wetting Sn drops on the surfaces of same steels in the same order as described above.

The transition temperatures were noted and the frames were continuously recorded using the camera. The contact angle was calculated for all the steels using the contact angle software and is plotted as function of temperature. The experiments were repeated at two different vacuum pressures. The transition temperatures for all five steels at two vacuum pressures were noted below, Table 5.1-1. A series of experiments were conducted under the identical experimental conditions at temperatures ~20 K lower than the measured transition temperatures for the respective steels. In these experiments, no wetting transition was

observed by liquid tin on the surface of steels, confirming the reported data in Table 5.1-1. The non-wetting to wetting transition of liquid tin on the surface of steels was identified by the measured contact angles reading the intersection with 90° horizontal line as shown in Fig.5.1-3 and Fig.5.1-4.

Table 5.1-1. Non-wetting to wetting transition temperatures of various steels at two different vacuum pressures.

Steel	Transition temperature (K) at 10^{-8} bar	Transition temperature (K) at 10^{-5} bar
Armco	773-793	773-793
C45	823-843	8323-843
S103	913-933	963-983
CK60	923-943	973-993
EN1.4034	1133-1153	No transition below 1323 K

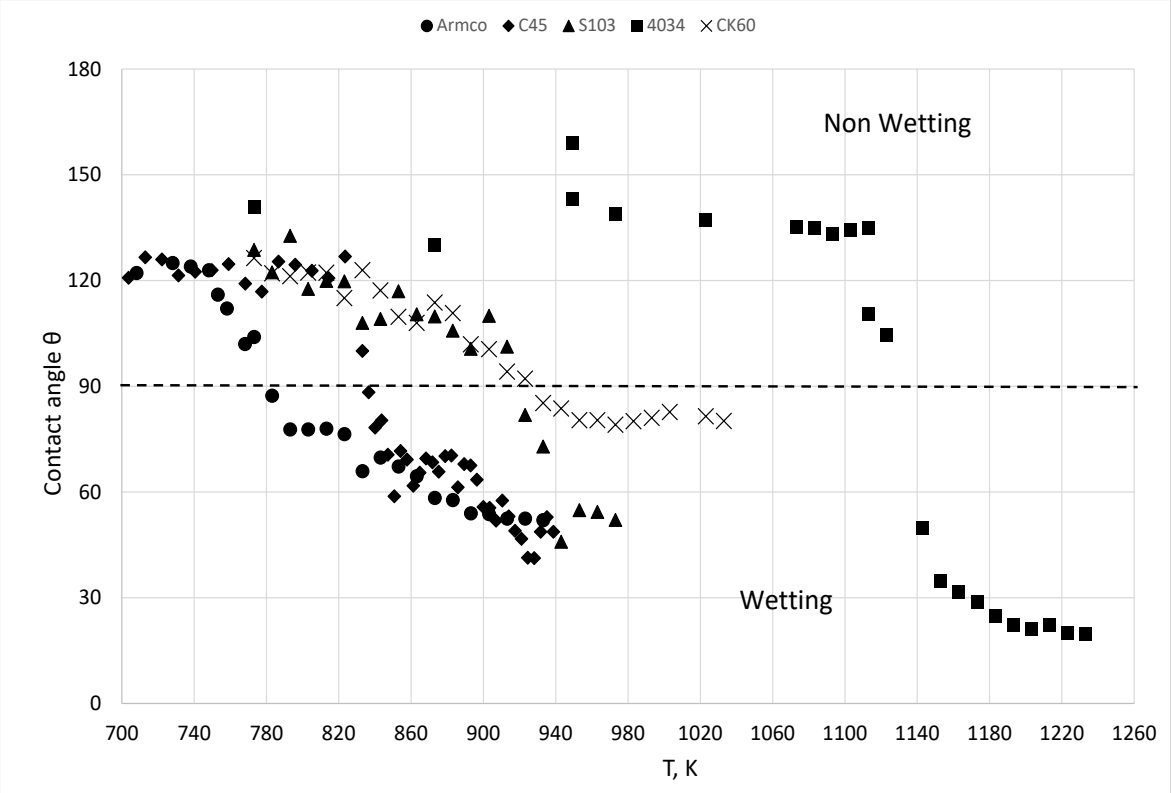

Fig.5.1-3. Contact angle of liquid tin on different steel substrates as function of temperature at vacuum pressure of 10^{-8} bar.

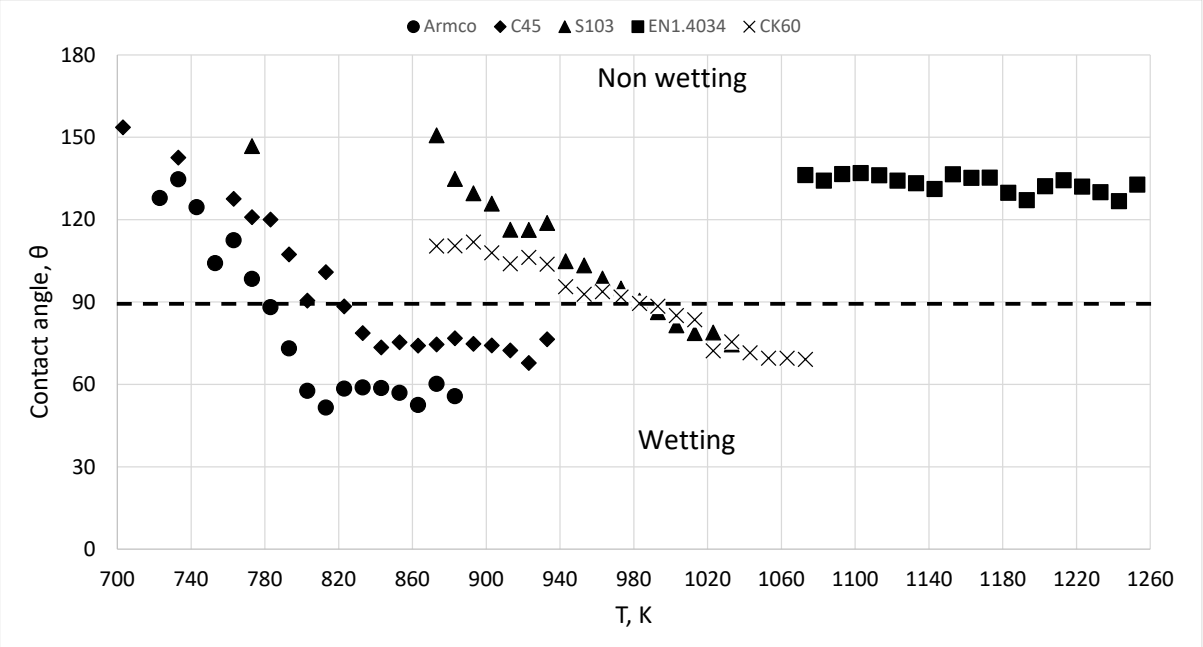

Fig.5.1-4. Contact angle of liquid tin on different steel substrates as function of temperature at vacuum pressure of 10^{-5} bar.

From Fig-s 5.1- 3-4, we can see the wetting transition temperatures of the same steels under two different vacuum pressures. There is an observed change in wetting transition temperatures of S103 and CK60 steels, which is probably due to added alloying elements and also the type of oxide layer at the surface of steel. Also, at low vacuum level, EN1.4034 steel (high Cr) has no transition observed transition temperature even after 1323 K. Due to the technical limitations of the vacuum pump, the heating was not carried above this temperature under low vacuum pressure. The observed transition is a proof of removal of oxide layer from the surface of steel. The liquid tin formed a non-wetting ball until the temperature of transition is reached beyond which the liquid metal begins to spread on the surface of steel.

During the wetting transition, the liquid metal begins to spread accompanied by a change in the dimensions of diameter and height of the droplet. This change in dimensions was calculated and plotted as function of temperature for all the experiments at two different vacuum levels as an indication of wetting transition and subsequent spreading. The diameter of the drop increases with spreading while the height of the sessile drop decreases. These parameters were calculated by image analysis from the recorded images during the experimentation and are plotted as function of temperature for all the steels, below Fig-s

(5.1-5 – 5.1-8). They are proof that the change in contact angle observed is indeed due to spreading of the droplet rather than evaporation of tin in the furnace during the experiments.

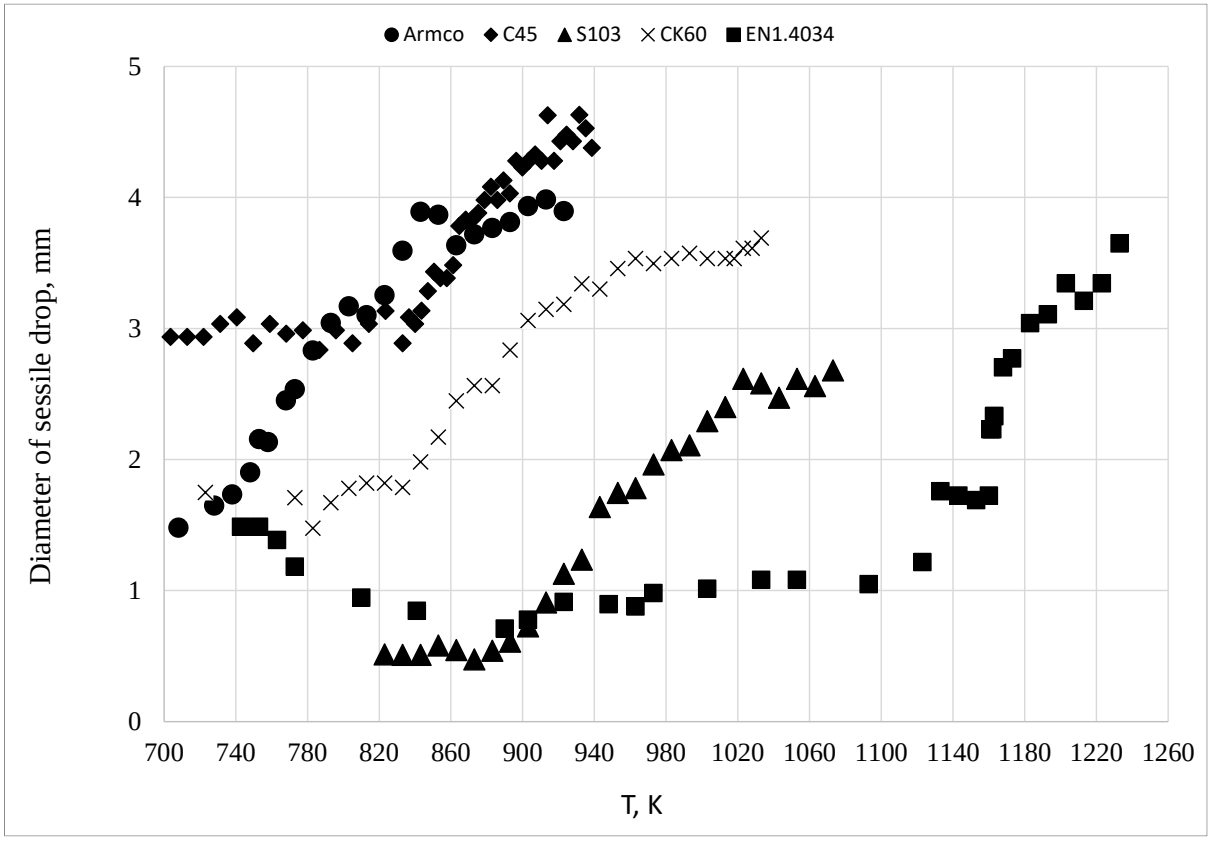

Fig.5.1-5. Contact diameter of the sessile drops plotted against temperature for all the steels at 10^{-8} bar.

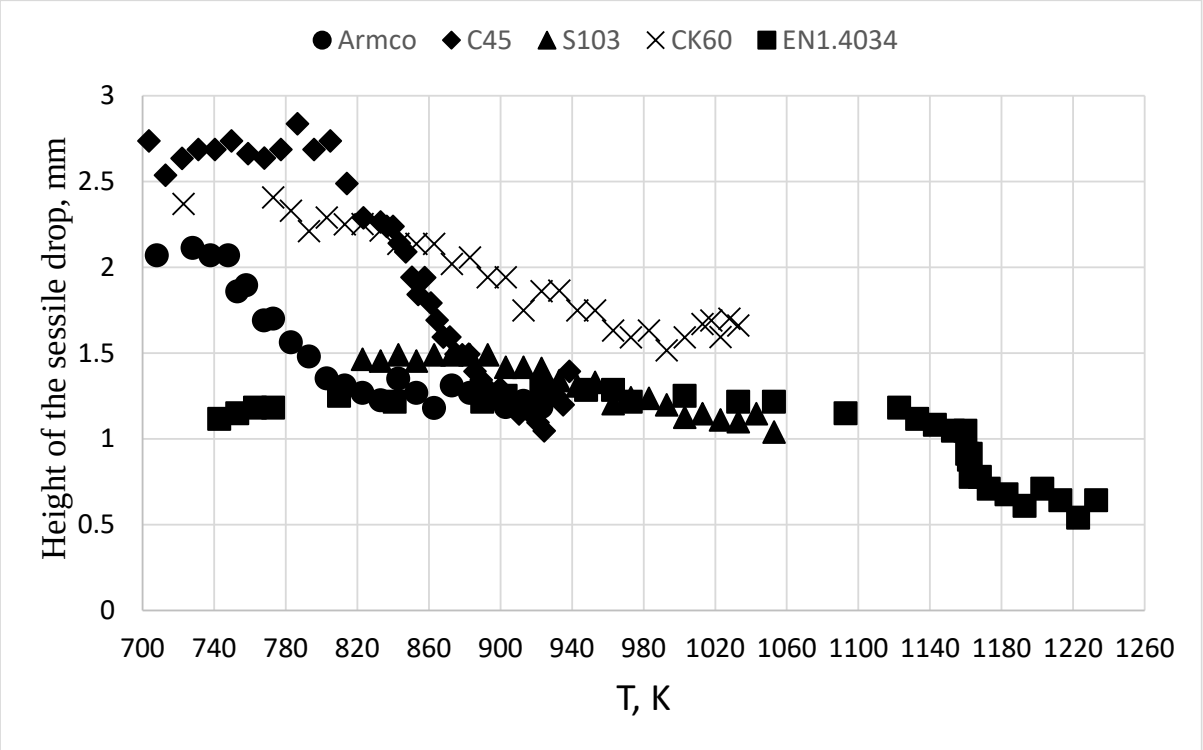

Fig.5.1-6. Height of the sessile drops plotted against temperature for all the steels at 10^{-8} bar.

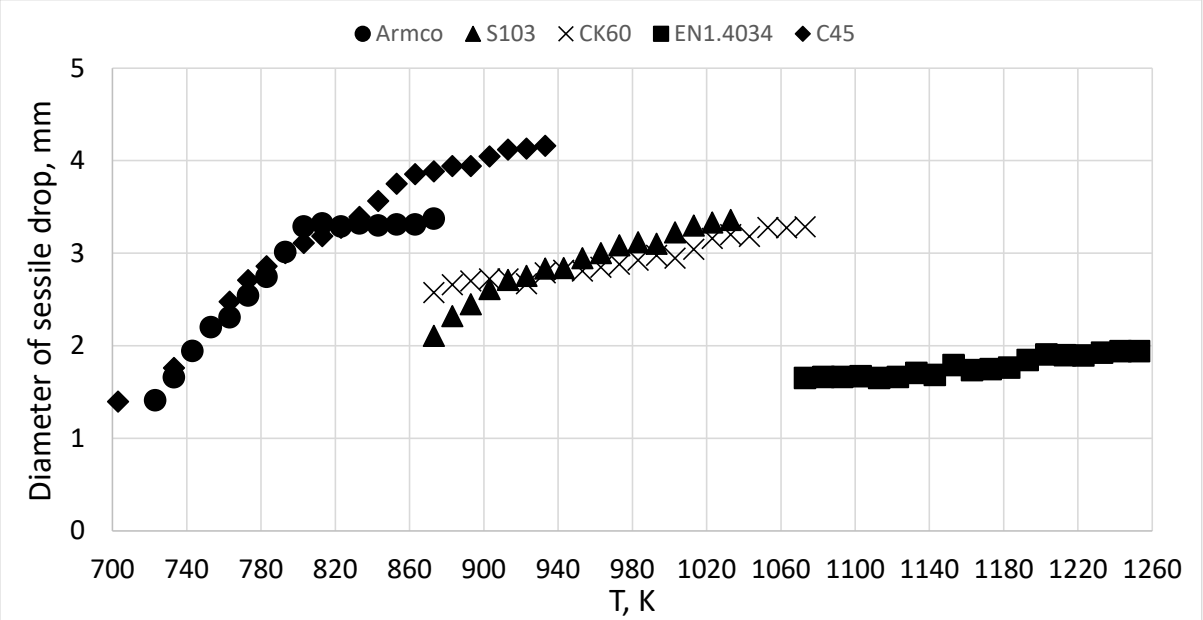

Fig.5.1-7. Contact diameter of the sessile drops plotted against temperature for all the steels at 10^{-5} bar.

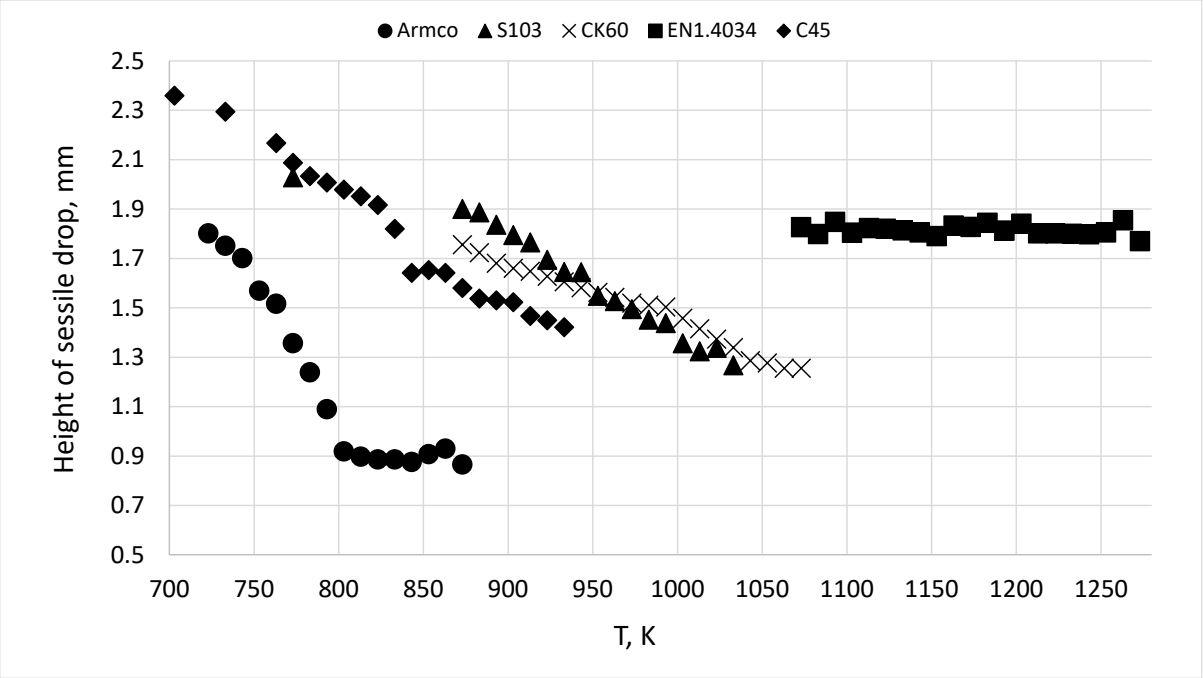

Fig.5.1-8. Height of the sessile drops plotted against temperature for all the steels at 10^{-5} bar.

After the wetting transition of liquid tin was observed on the surface of steels, wetting of the steel surfaces by molten tin follows. The final contact angles of liquid tin on the five steels were tabulated below for both vacuum pressures at respective temperatures, Table 5.1-2.

The contact angle for EN1.4034 steel at high vacuum pressure is in agreement with the reported contact angle by Kozlova et al. [36] under similar experimental conditions. Moreover, the overall contact angles of liquid tin on steels are reported between 40 – 70° [46, 48].

Table 5.1-2. Post wetting transition contact angles of liquid tin on the surface of steels

Steel	10^{-5} bar vacuum pressure		10^{-8} bar vacuum pressure	
	T, K	θ, (°)	T, K	θ, (°)
Armco steel	883	50 ± 10	923	50 ± 10
C45 steel	943	70 ± 10	933	45 ± 10
S103 steel	1033	75 ± 10	973	50 ± 10
CK60 steel	1073	70 ± 10	973	70 ± 10
EN1.4034 steel	1323	130 ± 10	1223	20 ± 10

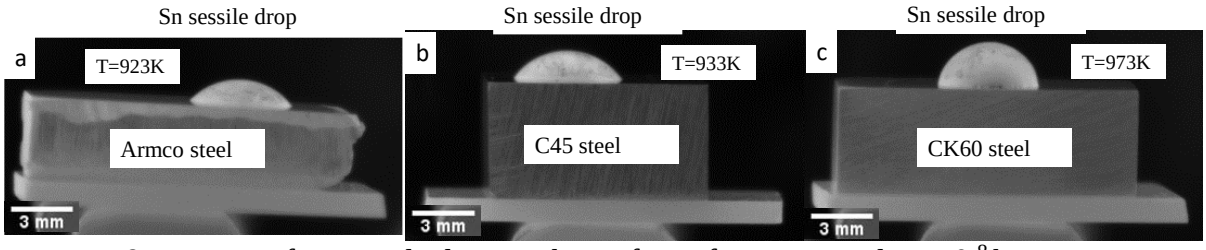

Fig.5.1-9. Wetting of tin sessile drop on the surface of various steels at 10^{-8} bar vacuum pressure and at temperature as shown in Table 5.2.1-1 for respective steels.

Wetting transition coincides with spreading as shown in Fig-s.5.1-4 – 5.1.7 coinciding with a decrease in height of the sessile drop and increase in base diameter of the drop. Spreading follows from work of adhesion and Young-Dupree equation Eq-s. (2-3). As wetting already established in the literature is attributed to imbalance of interfacial energies [39].

The contact angle of liquid tin changed from $\theta > 90°$ to $\theta < 90°$. However, this contact angle which is a measure of wetting is still comparatively higher [46]. This can be explained by the fact that intermetallic compounds and intermetallic layer of Fe/Sn was formed at the steel/tin interface in all the experiments. Dissolution of Fe from base metal in to the liquid tin and formation of intermetallic compounds of Fe-Sn were observed. From Fig.5.1-10 showing the EBSD phase identification, we observe the formed FeSn and $FeSn_2$ intermetallic compounds and layer at steel/Sn interface. The EDS spectra of the two different intermetallic compounds formed in Fig.5.1-11 is shown below, Fig.5.1-12. These intermetallic compounds once formed, are not fully metallic in nature [139]. This is further supported by the specific electric resistivity values of Fe-Sn intermetallic compounds (FeSn and $FeSn_2$) compared to specific electric resistivity values of pure Fe and Sn values in Fig.5.1-13 [140-142]. The specific electric resistivity values are one order of magnitude higher for intermetallic compounds compared to pure metals meaning they are not fully metallic. Thus, the formation of intermetallic compounds leads to decrease of adhesion energy relative to metal/metal interfaces. Hence the intermetallic compounds limit the spreading of molten tin on the surface of steels and hence higher contact angles are evidenced for molten tin-steel systems, Table 5.1-2.

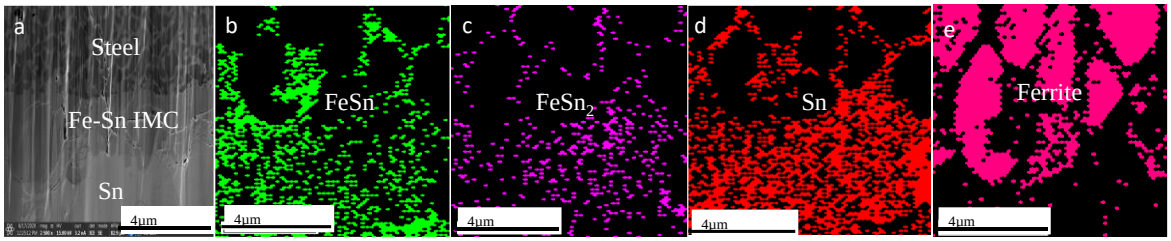

Fig.5.1-10. Identification of Fe/Sn intermetallic compounds formed at the interface between steel and liquid tin using SEM-EBSD analysis.

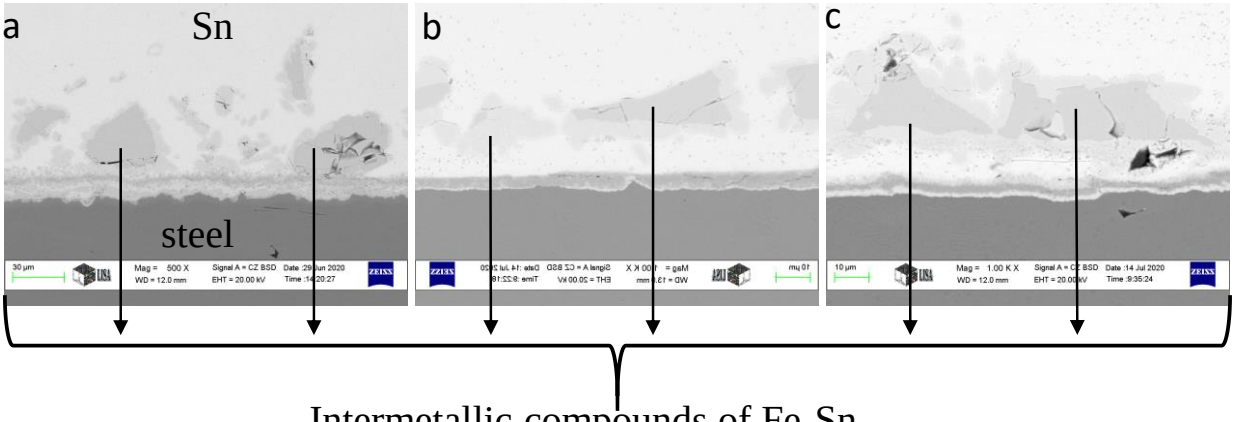

Fig.5.1-11. Microstructure of steel/Sn interface. Two different intermetallic compounds are visible at the interface, dark-gray and light-gray color. They are two different Fe/Sn IMC's. We also observe no grain boundary groove formation at the interface between steel/Sn showing no grain boundary wetting in this system. Fig a: Armco steel, Fig b: S103 steel, Fig c: CK60 steel.

Element	wt %
C K	0.7
O K	1.38
SiK	0.27
SnL	65.38
MnK	0.45
FeK	31.82
Total	100

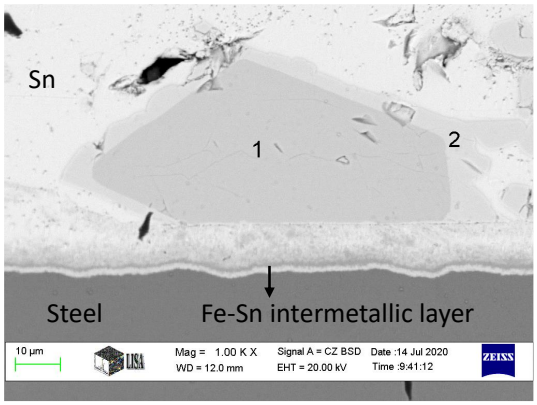

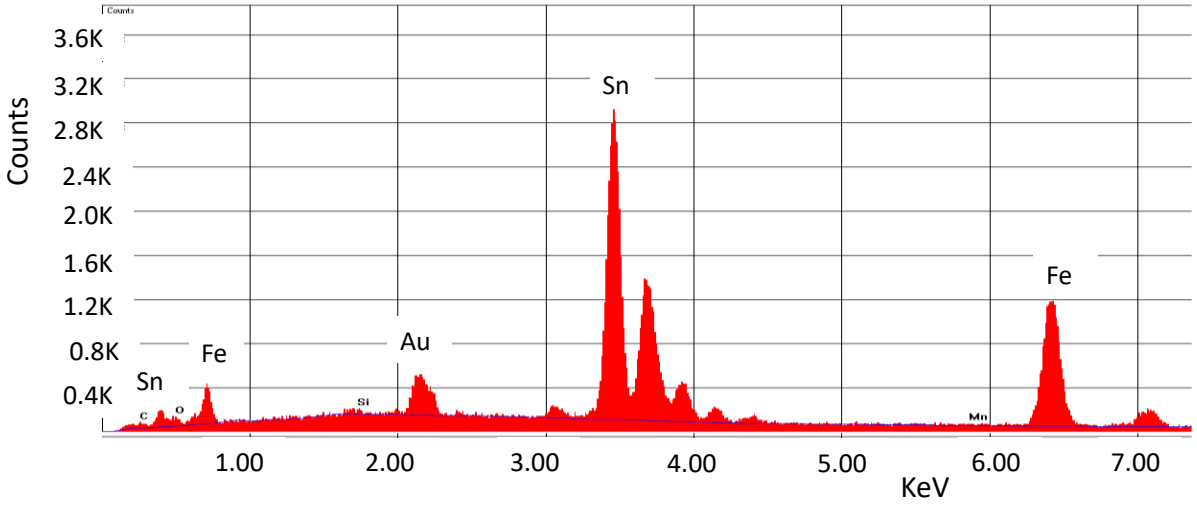

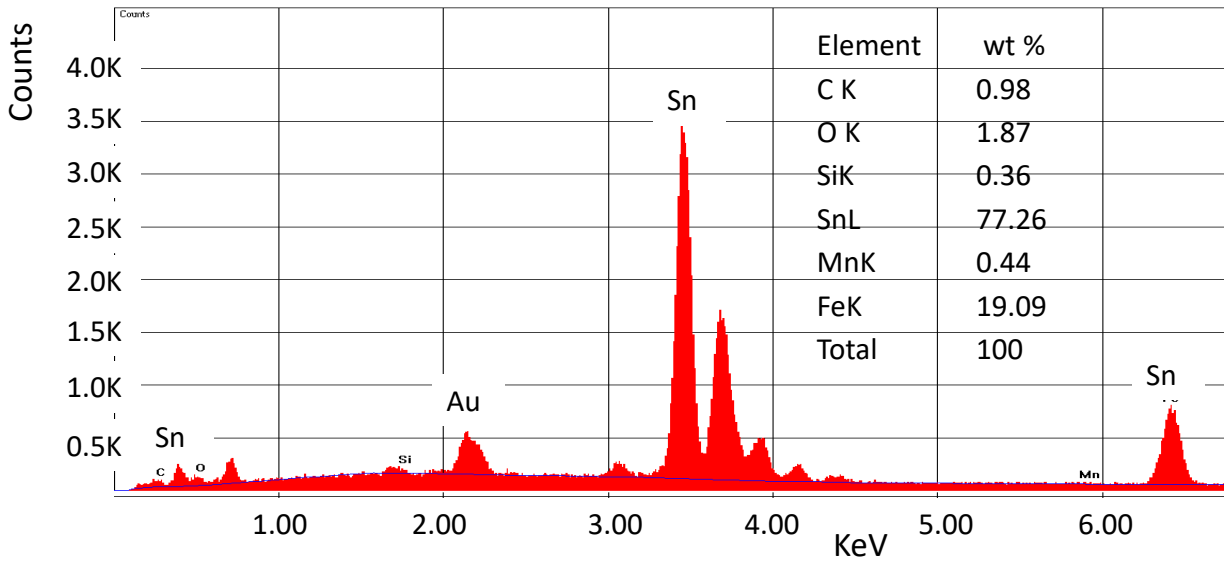

Element	wt %
C K	0.98
O K	1.87
SiK	0.36
SnL	77.26
MnK	0.44
FeK	19.09
Total	100

Fig.5.1-12. The EDS spectra of the points 1 &2 in the top picture measured using SEM. The IMC's are made of Fe/Sn as proven by the quantitative analysis shown in the adjacent tables.

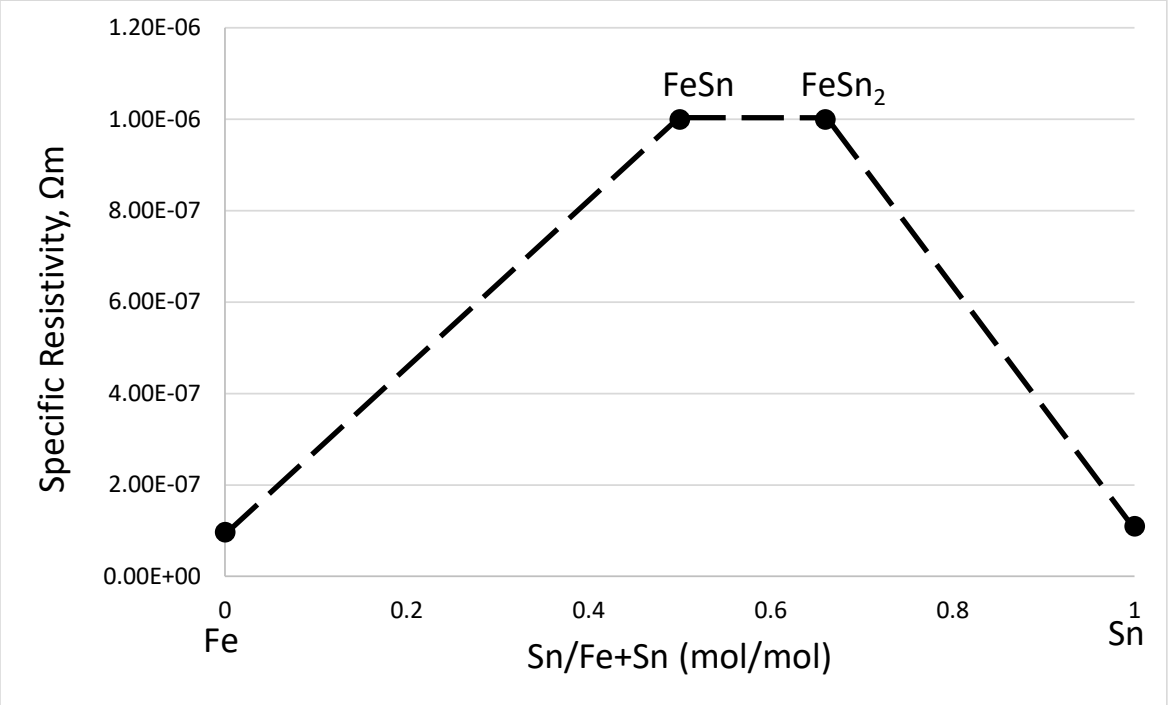

Fig.5.1-13. Specific electric resistivity values of the intermetallic compounds identified at the steel/Sn interface compared to the resistivity values of pure Fe and Sn at room temperature (T=298K).

Thus, we have seen the wetting transition temperatures of liquid tin on the surface of five steels at two different vacuum pressures. It stands to reason from the calculations made on equilibrium pressures that the steel surface is free of oxide layer after a certain temperature under the experimental vacuum pressure. The transition temperatures for five steels varying in composition at two different vacuum pressures were tabulated in Table 5.1-1. Good wetting of steels by liquid tin was observed post transition. Final contact angles of liquid tin on surfaces of all the steels was tabulated in Table 5.1-2. The spread of liquid tin on steel and higher contact angles were observed due to the formation of intermetallic compounds at the Fe/Sn interface.

5.2. Wetting of steel surfaces by liquid copper

From chapters 5.1, we see the wetting transition of molten tin on steel surfaces at temperatures much lower than the melting point of copper (1358 K) and the experimental brazing temperature (1373 K). Hence in the wetting experiments with copper, by the time copper melts, an instantaneous wetting and spreading was observed, see Fig 5.2-1. The contact angle is < 10° showing a near perfect wetting between molten copper and steels. This is observed for all the steels.

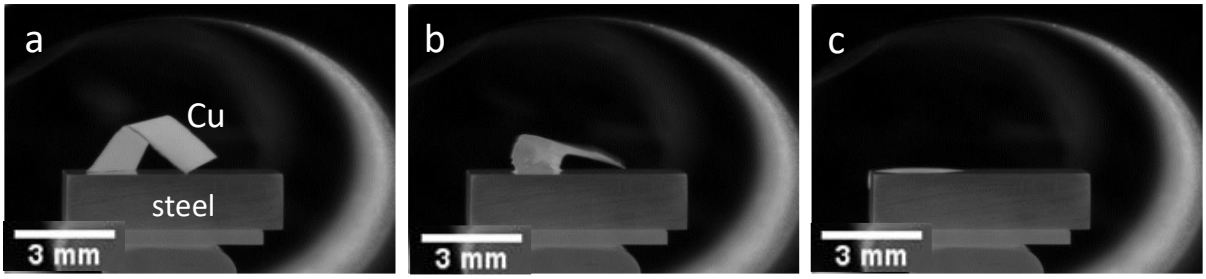

Fig.5.2-1. Instantaneous melting and excellent wetting of steel by molten Cu. This figure shows the wetting of CK60steel by liquid copper as seen through a high definition video camera.

The final contact angles of liquid Cu on the surface of steels are tabulated below. Both the angles, calculated by using the contact angle measurement software (KSV software), Table 5.2-1.

Table 5.2-1. Final contact angles of Cu on steels as measured by KSV shape analysis software

Steel	contact angle of Cu on steel (°)
C45	2.7 ± 0.2
S103	1.3 ± 0.2
CK60	2.4 ± 0.3
EN1.4034	5.0 ± 0.5

We can see from the Table 5.2-1, the contact angle measurements carried out using the software during the experiment (using the recorded pictures). Furthermore, the contact angle of C45stee/Cu was confirmed by SEM contact angle measurement, Fig.5.2-2. The measurements were in agreement with values reported in literature [36, 47-48].

Once the liquid droplet wets the surface, spreading follows. Spreading is a consequence of work of adhesion and Young-Dupree equation Eq-s. (2-3). The drive for spreading of molten copper on steels can be understood from a simple model of Fe/Cu systems. The equations are given below, Eq-s. (8-10) [2,13].

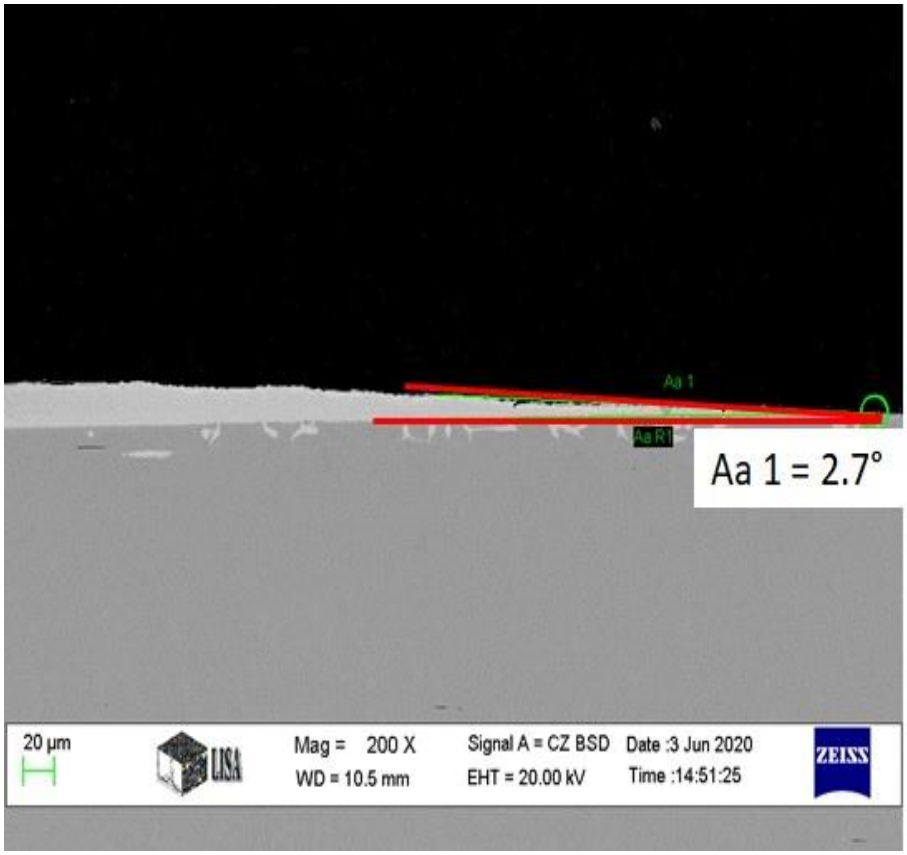

Fig.5.2-2. The contact angle of liquid Cu on C45 steel as measured using SEM

$$\sigma_{s/v} \cong \frac{\alpha_s.\left[q.R.T_{m,s} + \Delta_m H_s + \int_T^{T_{m,s}} C_{P,s} dT\right] - 2.T}{f_s.{V_{m,s}}^{2/3}.{N_{Av}}^{1/3}} \quad (8)$$

$$\sigma_{l/v} \cong \frac{0.182.\left[q.R.T_m - C_{P,l}.(T - T_m)\right] - 2.T}{1.06.{V_{m,l}}^{2/3}.{N_{Av}}^{1/3}} \quad (9)$$

$$\sigma_{s/l} \cong \frac{0.310.{f_b}^{1/3}.\Delta_m H_s + 0.343.\Omega_{s-l} + 3.3T}{{V_{m,s}}^{1/3}.{V_{m,l}}^{1/3}.{N_{Av}}^{1/3}} \quad (10)$$

where, σ_{sv}, σ_{lv}, σ_{sl} are the interfacial energies of solid-gas, liquid-gas and solid-liquid phases. α_s and f_s are the solid crystal parameters which are considered as average constants of 0.20 and 1.1 respectively. q is correlation parameter of value 25.4, R is universal gas constant, 8.3145 J/mol K, $\Delta_m H_s$ is the melting enthalpy of the solid (KJ/mol), $C_{P,s}$ and $C_{P,l}$ are the heat capacities of the solid and liquid at temperature T (J/Kmol), T is required temperature (K), $V_{m,s}$ and $V_{m,l}$ are the molar volumes (m^3/mol) of solid and liquid metals in study (Here Fe and Sn respectively), N_{Av} is Avogadro constant ($6.023 \cdot 10^{23}$ /mol), Ω_{sl} is the solid-liquid interaction energy J/mol. For metals with eutectic composition, [13] defined the interaction energy as shown in Eq. (11), below:

$$\Omega_{sl} \cong \frac{G^0{}_{M,s} - G^0{}_{M,l} - R.T_{eu}.lnx}{(1-x)^2} \quad (11)$$

Where, $G^0_{M,s}$ and $G^0_{M,l}$ (J/mol) are the standard Gibbs energies of solid higher melting point metal and liquid higher melting point metal respectively, T_{eu} (K), is the eutectic temperature of the alloy, R (J/mol K) is the universal gas constant, x is the mole fraction of the higher melting point component in the eutectic composition. The data required was taken from [1, 137, 143]. Table 5.2-2. provides the calculated values of respective interfacial energy values.

Table 5.2-2. Interfacial energy values for Fe/Cu system calculated from Eq-s. (8-11)

σ_{sv}	2.1 ± 0.1 J/m^2
σ_{lv}	1.38 ± 0.06 J/m^2
σ_{sl}	0.64 ± 0.01 J/m^2
Cos θ	1.06 ± 0.12
θ	10 ± 10 degrees
W_a	2.84 ± 0.17 J/m^2

$$Cos\theta = \frac{2.1 \pm 0.1 - 0.64 \pm 0.01}{1.38 \pm 0.06} = 1.06 \pm 0.12 \quad (12)$$

From Eq. (12), we see the cosine of contact angle θ ranges between 0.94 to 1.08 J/m^2. From here it follows that the value of θ should range between 0° - 20°. This possible theoretical range is in agreement with experimentally observed values, Table 5.2-1.

Once contact has been established between the solid/liquid phases, the adhesion energy comes into play which is essential in maintaining the bond between atoms of dissimilar composition in our case atoms of steel and copper. The adhesion energy expressed in terms of contact angle and surface tension Eq. (13), which also follows from Eq. (3).

$$\frac{W_a}{\sigma_{lv}} = 1 + Cos\theta \quad (13)$$

By substituting the values from Eq. (12) into Eq. (13), we get the adhesion energy value W_a as 2.84 ± 0.17 J/m^2. The difference between the adhesion energy and surface tension provides the necessary driving force for the spread of copper on surface of steels.

Instantaneous spreading and excellent wetting of all the steels by liquid copper was observed. The contact angles of liquid copper on five different steels were below 10°, showing excellent wetting behavior of copper on steel. Further, simple model for calculation for driving force of spreading of liquid copper on steels was shown and theoretical contact angle limits were identified.

5.3. Grain boundary wetting and penetration of steels by liquid metals

5.3.1. Grain boundary wetting and penetration of steels by liquid tin

Wetting may or may not be accompanied by grain boundary wetting and grain boundary penetration. As established in the literature, both GB wetting and GB penetration are non-desirable phenomena taking place as a part of wetting. As molten liquid wets and spreads on the surface of solid steels, at the applied temperature (heat) the dissolution of solid grains occur in the liquid metal, which is pretty much unavoidable. Grain boundary wetting can be observed by phenomenon of grain boundary groove formation [84, 93, 100]. The behavior of both liquid metals – molten tin and molten copper are significantly different.

Though the formation of intermetallic compounds and intermetallic layer was observed in steel/Sn systems, no grain boundary penetration by liquid tin was observed in Armco, C45, S103 and CK60 steels. This can be understood from the formation of continuous intermetallic layer that closes the steel grain boundary for liquid tin to access. Thus, the dihedral angle $\varphi > 0$ and hence no penetration is observed, (see Fig.5.3.1-1). However, GB penetration was observed by liquid tin into the EN1.4034 steel grain boundary and a dihedral angle $\varphi = 0°$, (see Fig.5.3.1- 2-3). The GB penetration up to depth of 25 ± 3 µm was observed measured using Imagej image analysis software, shown in (Fig.5.3.1-2) at 600 s holding time and temperature between 1150-1250 K. This different GB behavior observed in EN1.4034 steel is attributed to its higher Cr – composition and the liquid Sn embrittlement of high Cr steel GB [86-87]. The EN1.4034 steel due to its higher Cr-content is susceptible to attack by liquid tin under the experimental temperature leading to the cracking of the grain boundary at the steel/tin interface. Once the grain boundary interface is cracked, penetration of liquid tin occurs through these cracks ending in a dry grain boundary at a certain depth as observed. Later due to the dissolution and diffusion of iron taking place from steel, intermetallic layer consisting of intermetallic compounds can be observed.

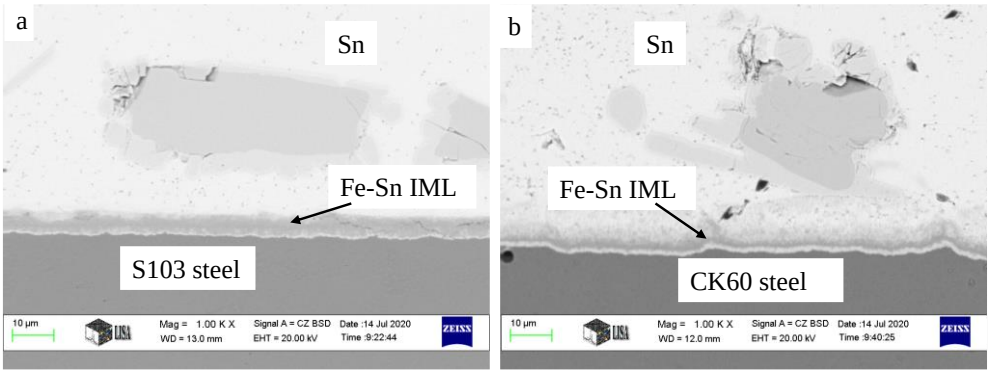

Fig.5.3.1-1. The Fe-Sn intermetallic layers formed in two different steels closing the grain boundary of the steels from liquid tin. Thus, no GB grooves or GB penetration is observed.

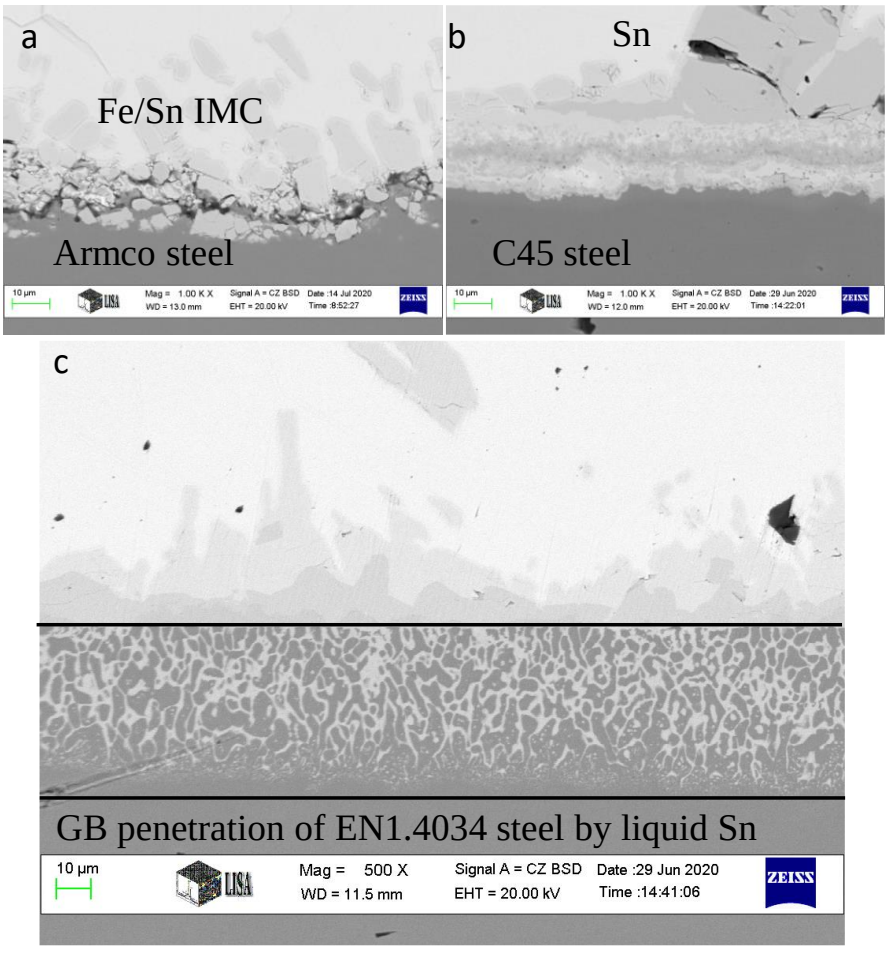

Fig.5.3.1-2. The tin penetration of steel grain boundary was only observed in EN1.4034 steel, Fig.5.3.1-2c. No grain boundary penetration by liquid tin was observed, Fig.5.3.1-2 a-b.

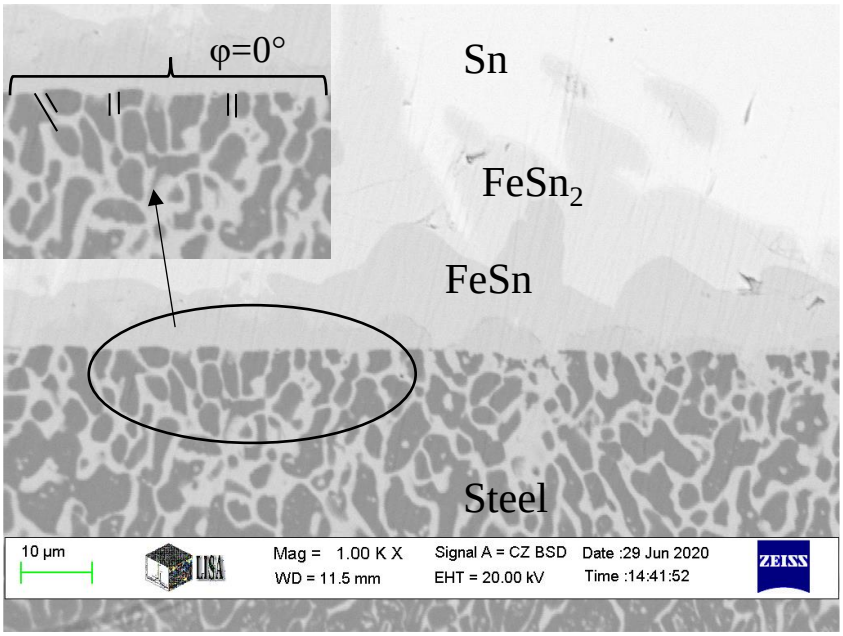

Fig.5.3.1-3. The dihedral angle ϕ = 0° and corresponding penetration of steel GB by liquid tin.

5.3.2. Grain boundary wetting and penetration of steels by liquid copper

For GB wetting and penetration study, in addition to C45, S103, CK60 and EN1.4034 steels, additionally 42CrMo4 steel was used. Chapter 5.2.2 showed perfect instantaneous wetting of steels by liquid copper. This perfect wetting by copper gives rise to GB wetting of steels by liquid copper.

Grain boundary groove formation is the first step during GB wetting. Grooves were observed at the interface of steel grain boundary with liquid copper in all the steel/Cu interactions, Fig.5.3.2-1 below.

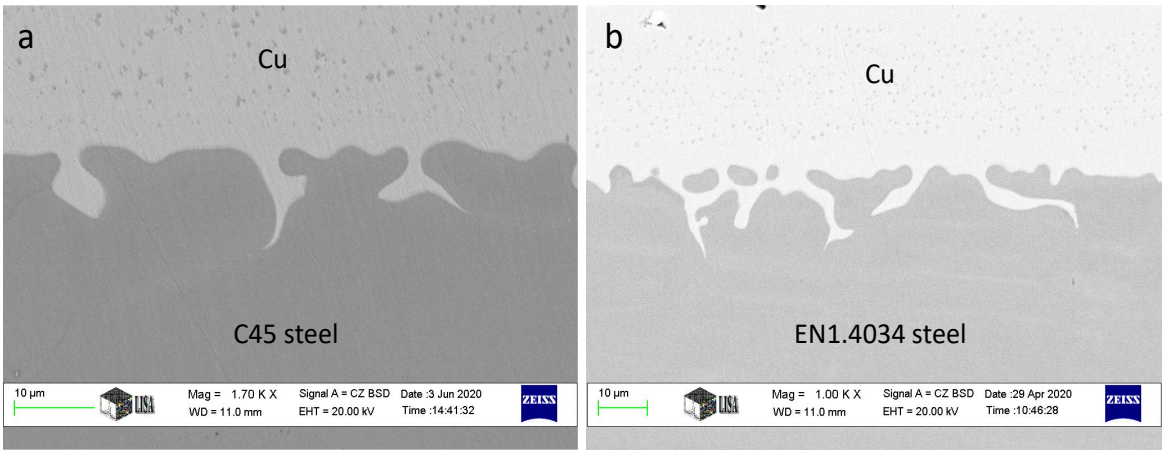

Fig.5.3.2-1. The grain boundary grooves formed at the steel/Cu interface indicating the GB wetting.

GB wetting between steel/Cu is accompanied by dissolution of Fe from the bulk steel in liquid copper during experiment. Fe grains from steel can be observed in the liquid copper solidified upon cooling. They are shown in Fig.5.3.2-2.

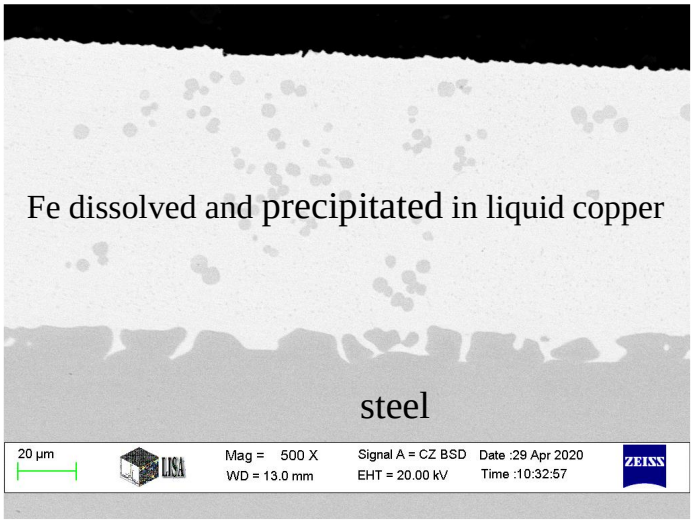

Fig.5.3.2-2. Dissolved Fe in the liquid copper solidified upon cooling. The dissolution takes place during the grain boundary wetting.

Besides good GB wetting, GB penetration was observed in all the steel/Cu systems. The GB groove formation and the subsequent penetration were observed, satisfying (Eq-s. 4-5). However, the depth of penetration varied depending on the alloying composition of the steel. The dihedral angle, $\phi = 0°$ was achieved in all the cases as can be seen in the Fig.5.3.2-3.

From Fig.5.3.2-3, we can observe the dihedral angle of 0° as already seen with the GB penetration by liquid Cu. Furthermore, the GB penetration can be seen in all the steels. The wetting experiment was conducted for 300 s and the following depth of penetration was measured post experiment. In Table 5.3.2-1, we observe an average depth of penetration between 10 – 20 µm is achieved by liquid copper in the five different steels under experimental conditions.

Table 5.3.2-1. Depth of penetration achieved by liquid Cu in five steels at 300s holding time

Steel	Depth of penetration (µm)
C45	15.3 ± 2
42CrMo4	19.1 ± 3
S103	11.1 ± 2
CK60	9.80 ± 1
EN1.4034	12.3 ± 2

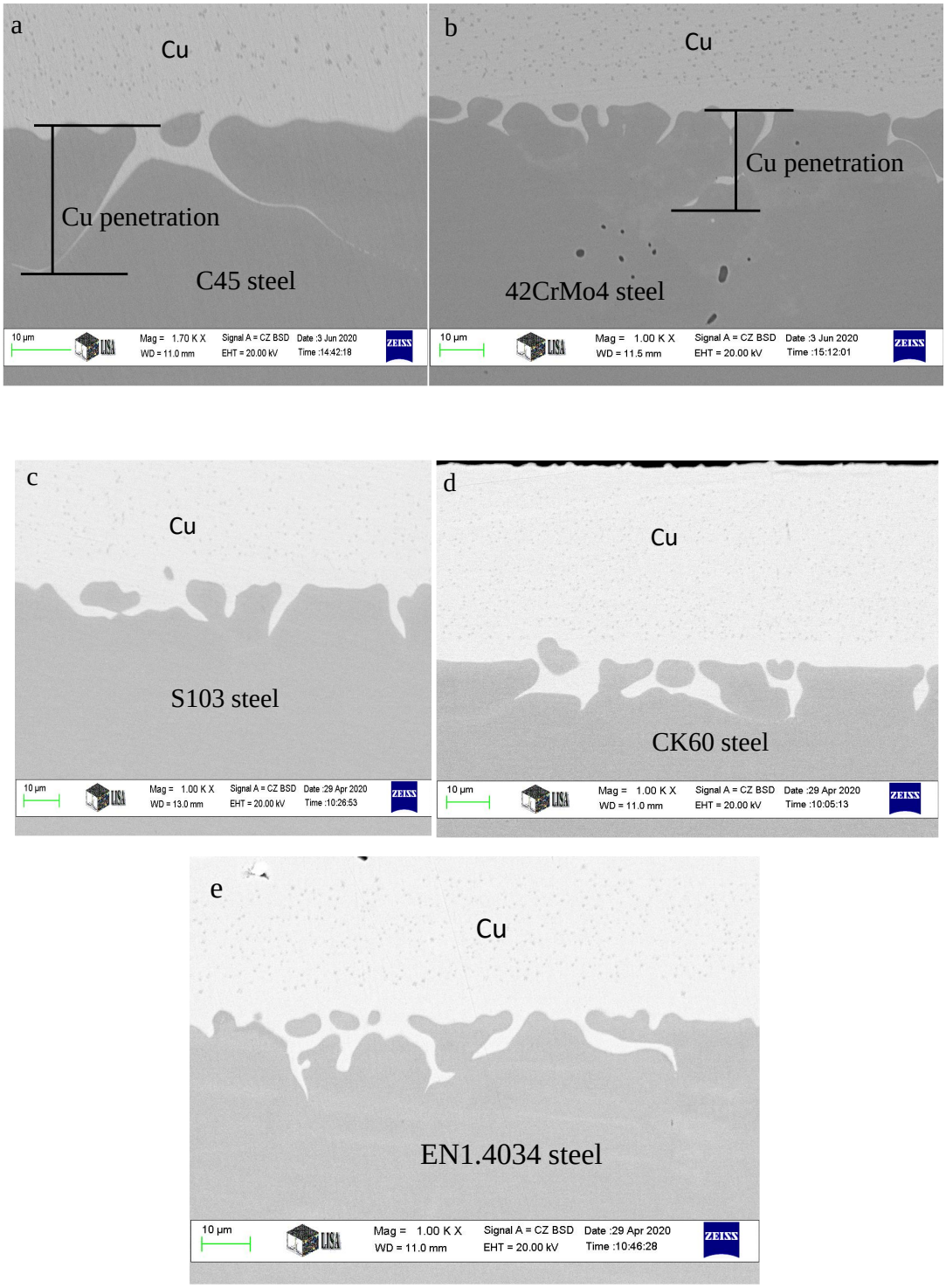

Fig.5.3.2-3. GB penetration of steels by liquid Cu. The dihedral angle, φ = 0° observed at the channels of Cu penetration.

Behavior of grain boundary wetting and penetration of the steels by both liquid tin and liquid copper were observed. Significant differences were observed between the two liquid metals interaction with steel GB. There is no formation of GB grooves at the steel interface by liquid tin nor the penetration of low alloyed steels. This is understood as consequence of formation of intermetallic layer of Fe-Sn at the liquid metal/solid steel interface which covers the grooves and creates a hindrance for the liquid tin to penetrate the steel GB. The formation of intermetallic layer and compounds are also the reason for a limiting contact angle of around 50° for steel/Sn wetting. GB penetration was observed only in high Cr steel with comparatively high Mn (EN1.4034 steel) due to liquid metal embrittlement of this particular steel by liquid tin. The observed penetration can be attributed to the composition of steel differing from other steels.

On contrary GB wetting and penetration was observed by liquid copper in all the steels. Grain boundary wetting was followed from groove formation at the steel GB, channel formation for copper to penetrate. The depth of penetration achieved by liquid copper in all steels was tabulated under similar experimental conditions.

5.4. Rapid thinning of the brazed joint

The phenomena discussed until now are the phenomena that usually takes place during the brazing process and are required for the formation of strong and reliable joints. The brazing process as explained in chapter 4 was carried out under vacuum at 10^{-8} bar residual pressure employing a sandwich structure, (see Fig.4.2-3). The experiment is carried out at 1373 K temperature (M.P. of Cu is 1356 K). The steels were ground and polished as explained. Before arranging the samples in a sandwich structure and placing in the furnace, the surface roughness of the samples was measured. The surface roughness of the steels is tabulated below, Table 5.4-1.

Table 5.4-1. Surface roughness of the steel samples post polishing

Steel	Surface roughness (R_a), µm
C45	0.020
S103	0.030
CK60	0.015
EN1.4034	0.020
42CrMo4	0.020
Armco	0.020

After experimentation, the samples were cooled down in the furnace using normal furnace cooling. No external cooling sources were used. The samples were taken out and first observation made is the reduction of thickness of Cu joint (d_j). In ideal case, the joint thickness should equal the thickness of the braze foil ~ 70µm. But, thickness of the joint between the two steel samples to be brazed was reduced significantly. The thickness of the joint has decreased rapidly with liquid time, (t_L, s). It is important at this point to define t_L, liquid time (s). The brazing experiments were conducted a fixed time – holding time, t_h, to generalize these results a new term called liquid time t_L was introduced. We call "liquid time" (t_L, s) the time duration for which the sample was in the interval of 1356 K … 1373 K. This equals the entire duration of the holding time at 1373 K + time interval during heating + the time interval of 1373 K …. 1364 K during cooling, Fig.5.4-1. Here T = 1364 K is obtained as average between holding temperature (1373 K) and melting point of pure Cu (1356 K). This is because during the holding time liquid Cu becomes saturated by Fe and the Fe—Cu system is peritectic, so the liquid alloy solidifies in the T-range of 1373 … 1356 K.

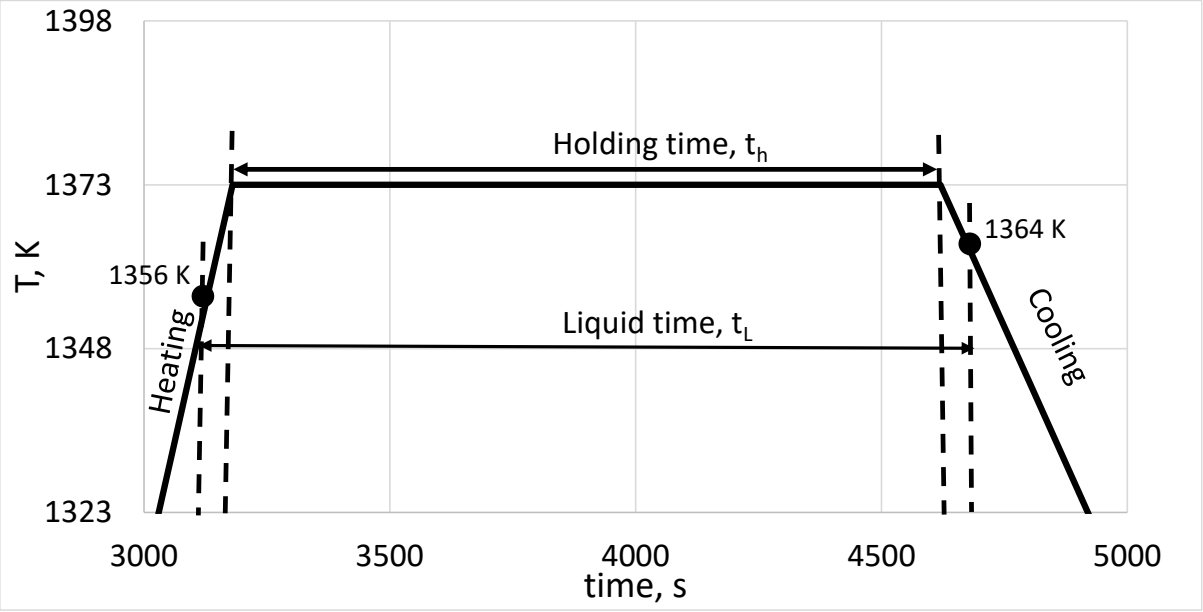

Fig.5.4-1. Schematic showing the relationship between holding time t_h and liquid time t_L

In our furnace, the measured liquid time was found to depend linearly on measured holding time (see Fig.5.4-2), and can be approximately written as:

$$t_L \cong t_h + 68 \qquad \text{(in seconds)} \qquad (14)$$

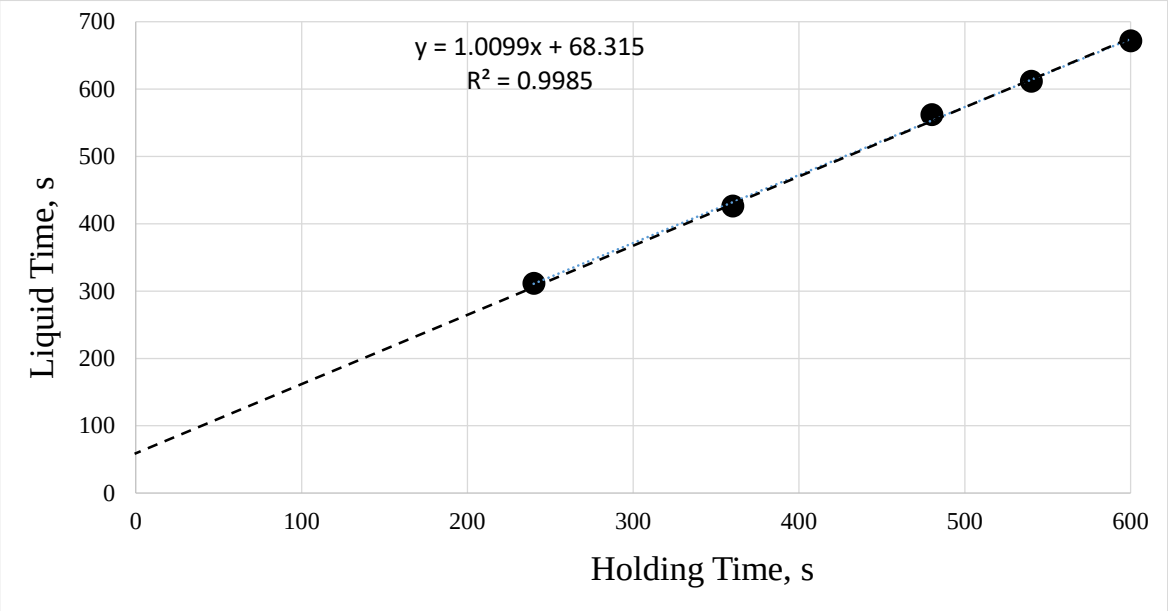

Fig.5.4-2. Dependence of liquid time defined above versus holding time in our furnace as follows from Fig.5.4-1.

Although overall reduction in thickness of the joint was observed as function of time, there was a difference in the rate of reduction of the thickness depending on the steel type. Correspondingly, I formulated and established three equations to describe the thinning of the joint as function of liquid time t_L.

The approximated general equation for the thickness of the joint and liquid time was given in Eq. (15).

$$d_j \cong \frac{70}{1+ z \cdot t_L} \tag{15}$$

where t_L is liquid time (s), d_j is thickness of joint (microns), z (1/s) is the semi-empirical coefficient. The boundary conditions for the equations are: at t_L = 0: d_j = 70 microns and at $t_L \to \infty$: $d_j \to 0$. This is shown below Fig.5.4-2.

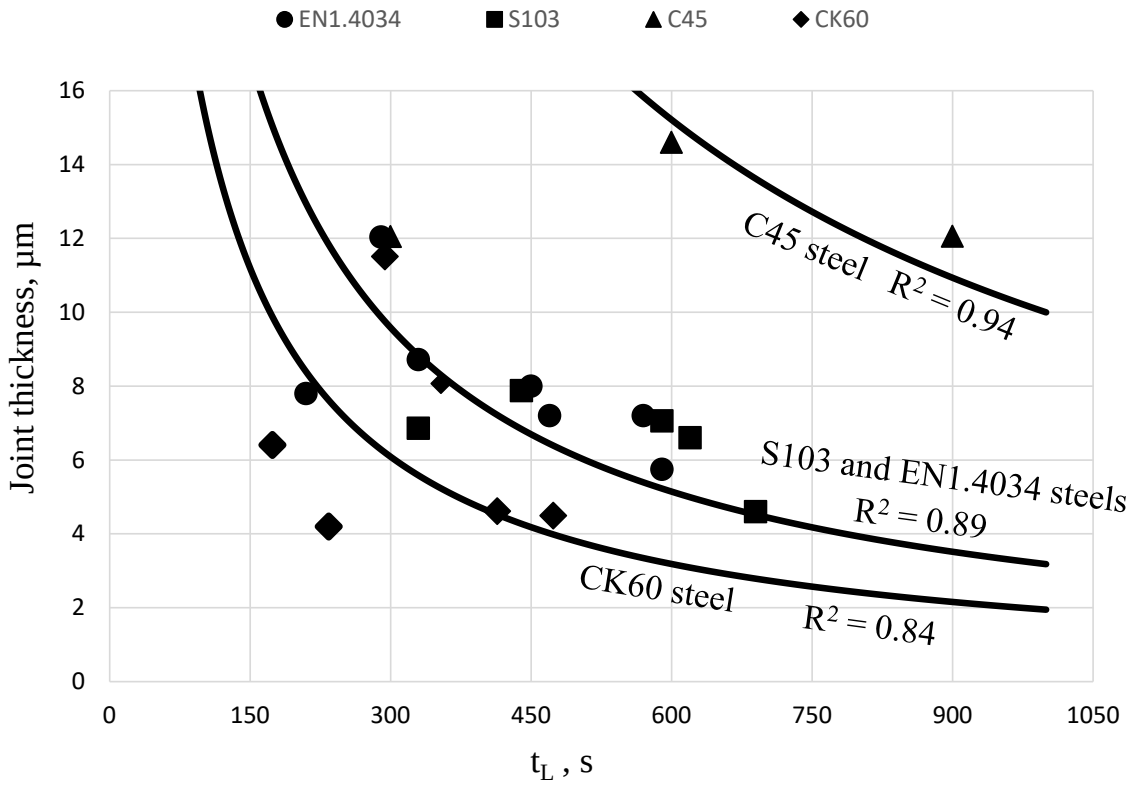

Fig.5.4-2. The measured joint thickness between the steel samples as function of the liquid time for various steel types. The three average lines obtained for steel types as indicated in figure by substituting z values from Table 5.4-2. in Eq. (15).

In Fig.5.4-2, we observe different thinning behaviors for different steels. They are devised from the same general equation Eq. (15) by changing the semi-empirical coefficient z (1/s). The value of z for different steel systems is tabulated in Table 5.4-2.

Table 5.4-2. Semi-empirical reduction coefficient for different steel grades to be used in Eq. (15)

Steel grade	Semi-empirical coefficient, z (1/s)
C45	0.0054 ± 0.001
EN1.4034 and S103	0.017 ± 0.003
CK60	0.045 ± 0.03

As soon as the copper foil melts, the thinning of the liquid layer occurs under the experimentation. This is accompanied by decreasing viscosity of molten copper promoting the wetting of steel. There is also an added effect of liquid coper being pushed out from between the steel samples by the force of bound wire around the sandwich and gravitational force acting on the sandwich. The out-pushed copper evaporates as the equilibrium vacuum

pressure of Cu is 7.94E-7 bar, higher than the residual pressure of vacuum used in the furnace 9E-8 bar.

Thus, the reduction in the thickness of the joint was observed across all the experiments as described above. The final thickness of the brazed joints is hence determined by the combination of the above phenomena – surface roughness (Table 5.4-1) determining the dissolution of Fe in liquid copper and the evaporation of the out-pushed Cu in the furnace besides the adhesive forces and gravity.

5.5. Cracking of the braze joint upon cooling

5.5.1. Observation of cracking in the brazed joints

The previous chapter 5.4 dealt with the reduction of the thickness of the joint as function of time carried out during the brazing experiments. Now, we deal with the spontaneous cracking of the copper brazed steel joints upon cooling

The study on the brazing is focused on the spontaneous cracking of the copper brazed steel joints upon cooling under no external loading conditions. The first two steels in the study, C45steel and Armco steel. C45 has only S (0.03 wt%) and Armco has very low concentrations of both S and Mn (0.0064 wt% S and 0.111 wt% Mn). The experiments were conducted at 30 min (1868 s) liquid time (minimum) and no cracking or any non-metallic precipitates were found in the brazed joint. The joints were clean, near perfect wetting and only metallic precipitates were found. These can be seen below, Fig-s.(5.5.1- 1-2).

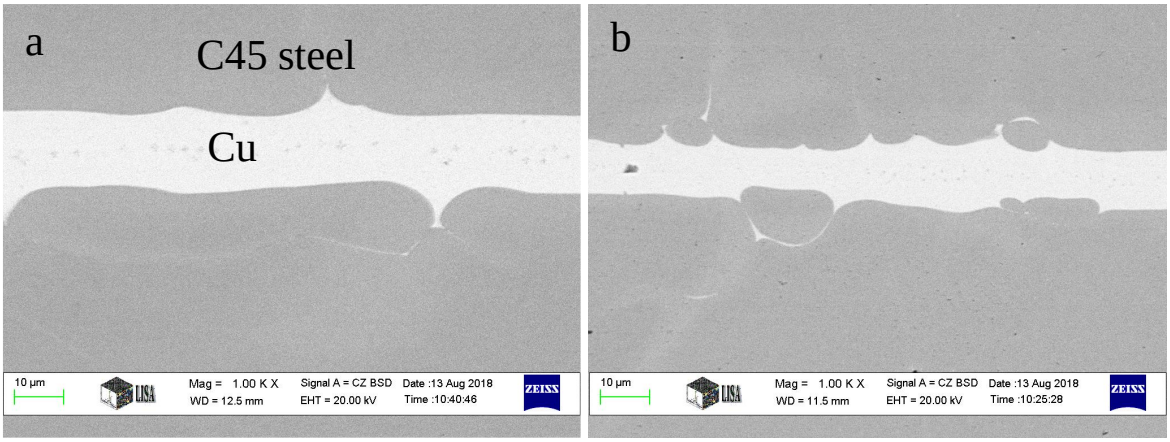

Fig.5.5.1-1 a-b. Brazed joint of C45steel/Cu/C45steel with no cracks and near perfect joint after at least 1868 s holding time.

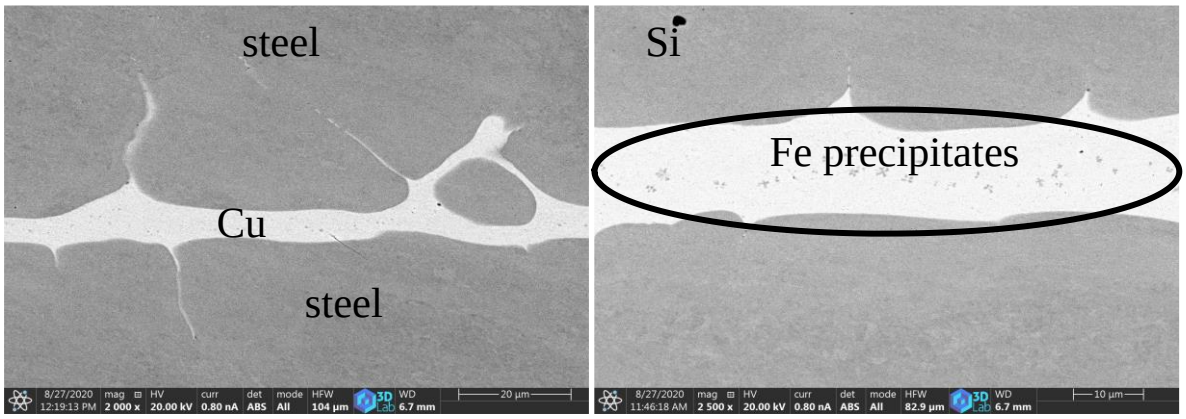

Fig.5.5.1-2 a-b. Brazed joint of Armco steel/Cu/Armco steel with no cracks and near perfect joint after at least 1868 s holding time.

The next study is conducted with S103 steel with increasing concentration of Mn and S. The experiments were conducted between 158 s and 668 s liquid time and the cracking in the joint was not found in the samples between 158 s and 548 s but was found in samples at 608 s and is shown below, Fig.5.5.1-3.

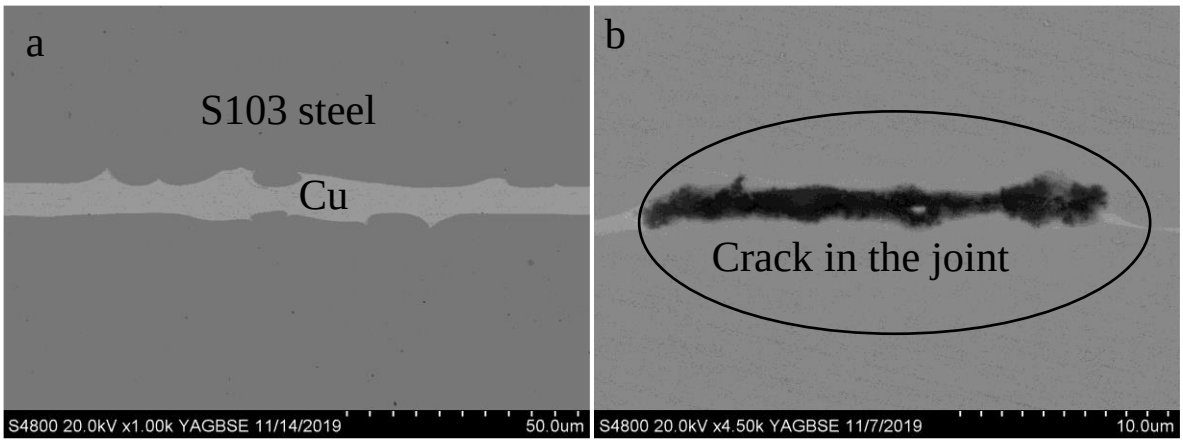

Fig.5.5.1-3. Brazed joint of S103steel/Cu/S103steel at 548 s (a) and 608 s (b)

The next steel in the series is CK60 with increasing Mn and S composition. As the Mn and S composition in the steel increased, the time required for cracking in the joint decreased. Similar relation of uncracked and cracked joints was observed with time. The cracking was observed in the joints after 338 s liquid time. Similar experiments and observations were conducted with EN1.4034 steel. The cracking of the brazed joint was observed after 368 s, Fig.5.5.1-5. The minimum liquid time required for cracking vs Mn and S concentration in the steel is tabulated below for the steels studied, Table 5.5.1-1.

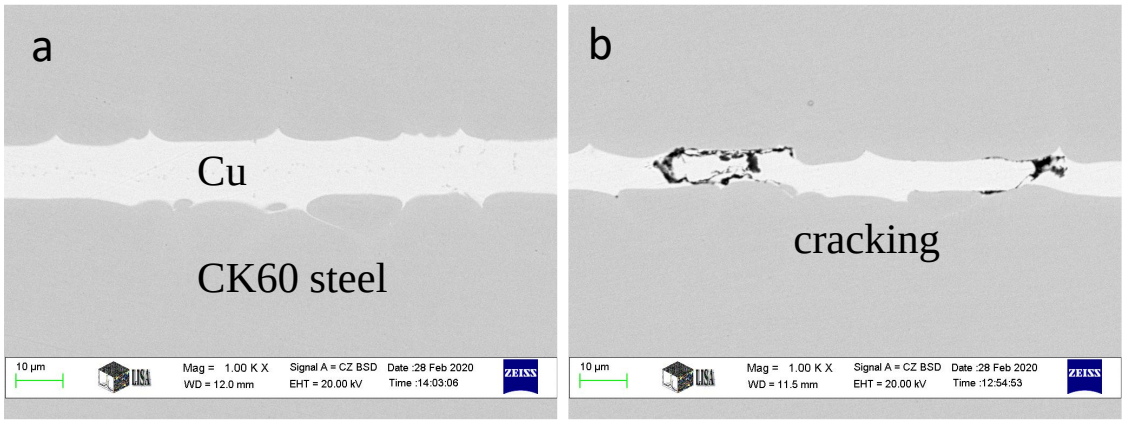

Fig.5.5.1-4. Brazed joint of CK60steel/Cu/CK60steel at 278 s (a) and 338 s (b)

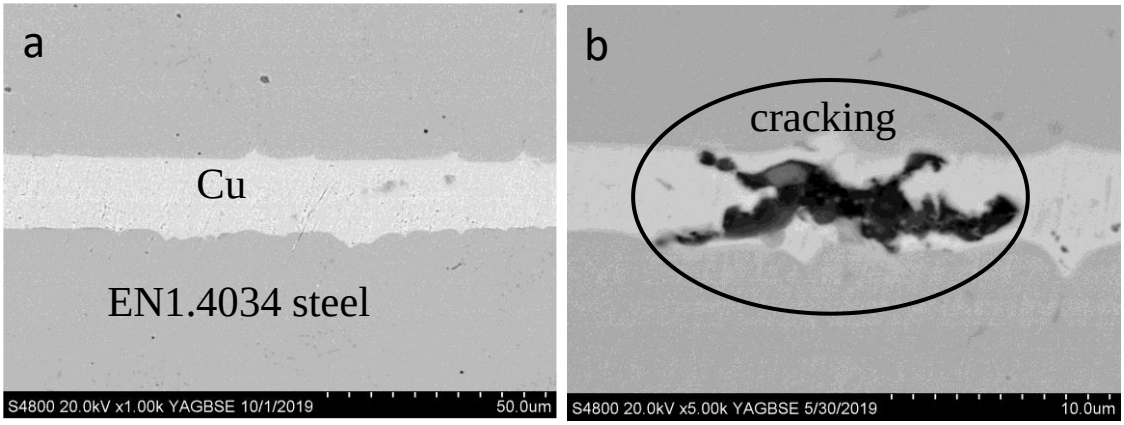

Fig.5.5.1-5. Brazed joint of EN1.4034steel/Cu/EN1.4034steel at 308 s (a) and 368 s (b)

Table 5.5.1-1. Mn and S concentration in the steel and minimum liquid time of cracking of the brazed joints

Steel	Mn wt%	S wt%	Liquid time required for cracking of the joint (s)
C45	-	0.03	no cracking up to 1868 s at least
Armco	0.11	0.0064	no cracking up to 1868 s at least
S103	0.25	0.02	578 ± 30
CK60	0.75	0.07	308 ± 30
EN1.4034	1	0.035	338 ± 30

5.5.2. Discussion on the reason for the observed cracking

From Table 5.5.1-1. we can see that higher the concentration of Mn and S in the steel, lower the time required for cracks to appear in the joint. Hence, the cracks in the joint was connected to Mn and S content in the steel. It was previously shown in the chapter 2.5, how MnS was linked to cracking in brazed joint [122]. It was also shown how MnS is formed in steels specially at GB during cooling [You2017, 123-125].

The copper joint is free of inclusions of any kind at the beginning of experiment. However, under the experimental conditions of time-Temperature, dissolution of Fe from bulk steel into liquid copper takes place. Dissolution of alloying elements like Cr, Mn, S from steel into the liquid copper also happens at the same time. Once dissolved, these components diffuse from steel/Cu interface into the liquid copper under experimental temperature and liquid time. The diffusion is known to be a time-Temperature dependent process. These diffused elements start to precipitate in the joint during the cooling down phase of the experiment. The non-metallic inclusion of MnS forms during precipitation as it is the most probable sulfide forming compound according to standard Gibbs energies of formation, tabulated Table 5.5.2-1.

Table 5.5.2-1. Standard melting points and standard formation Gibbs energies of some sulfides [137]

Sulfide	Melting point, K	$\Delta_f G^o$, kJ/mol 298 K	$\Delta_f G^o$, kJ/mol 1373 K
CuS	780*	-53.5	---
Cu_2S	1,400	-86.5	-86.2
FeS	1,463	-102.0	-75.6
CrS	1,840	-158.1	-127.6
MnS	1,803	-218.4	-187.5

*decomposition temperature into Cu_2S and S

Thus, MnS formation is very much probable at least from standard formation energies under the experimental conditions and subsequent cooling. From literature it is very much clear that formation temperature of MnS is around 1223 K to 1273 K [123]. Thus, it stands to hypothesize that the cracking in the joint is due to the formation of non-metallic MnS in the joint and they act as probable sites for crack initiation.

This hypothesis can be confirmed by the SEM micrographs obtained from the cracked joints of steels. In Fig.5.5.2-1, the cracking of the joint in S103 steel can be seen and MnS precipitates surrounding the joint can be noted from EDS spectra. In Fig-s (5.5.2- 2-3), similar observations can be made for EN1.4034 steel.

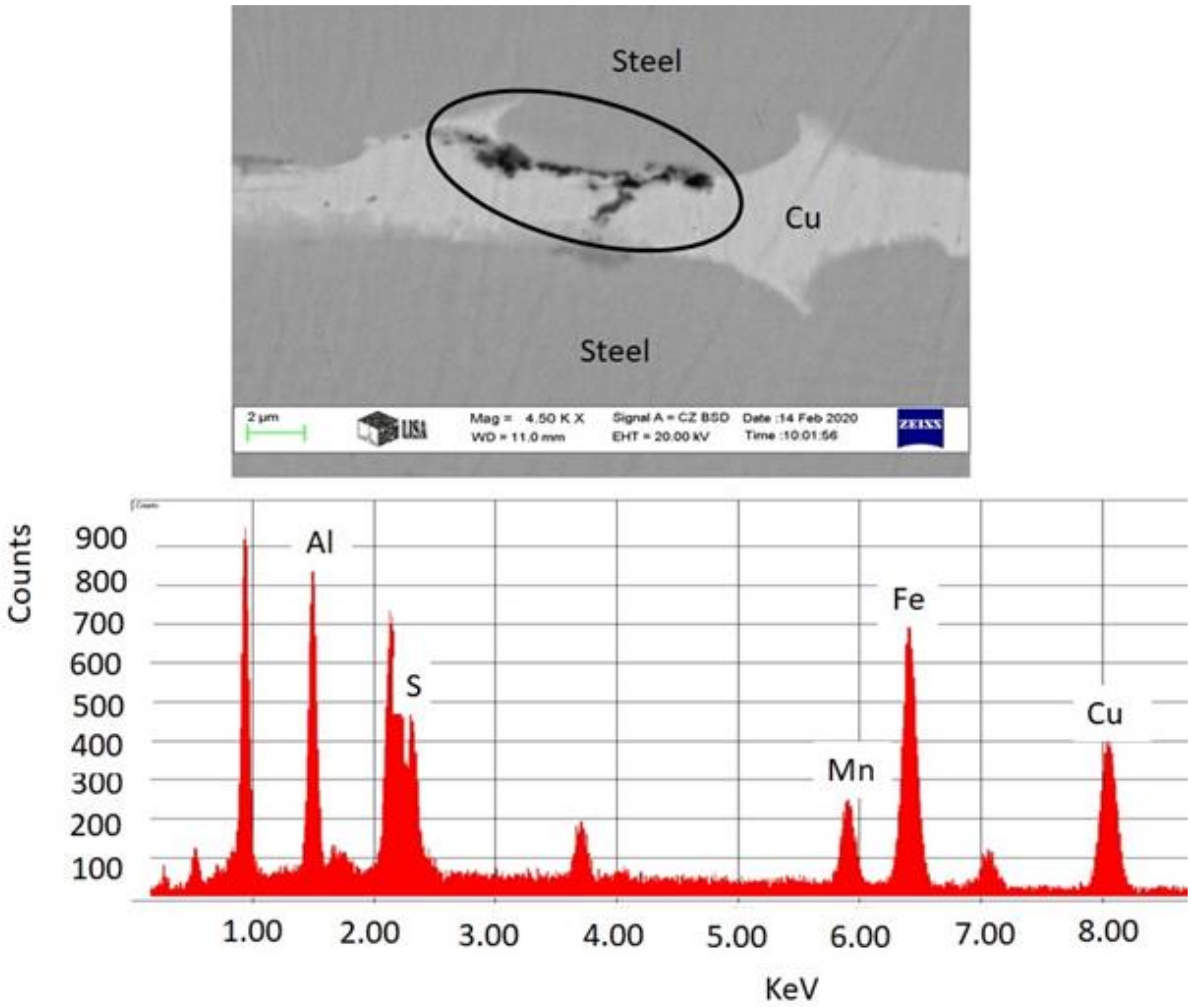

Fig.5.5.2-1. The SEM micrograph and EDS spectra of the encircled region showing the precipitates of MnS around the crack periphery. Besides MnS, polishing material (Al) was also detected.

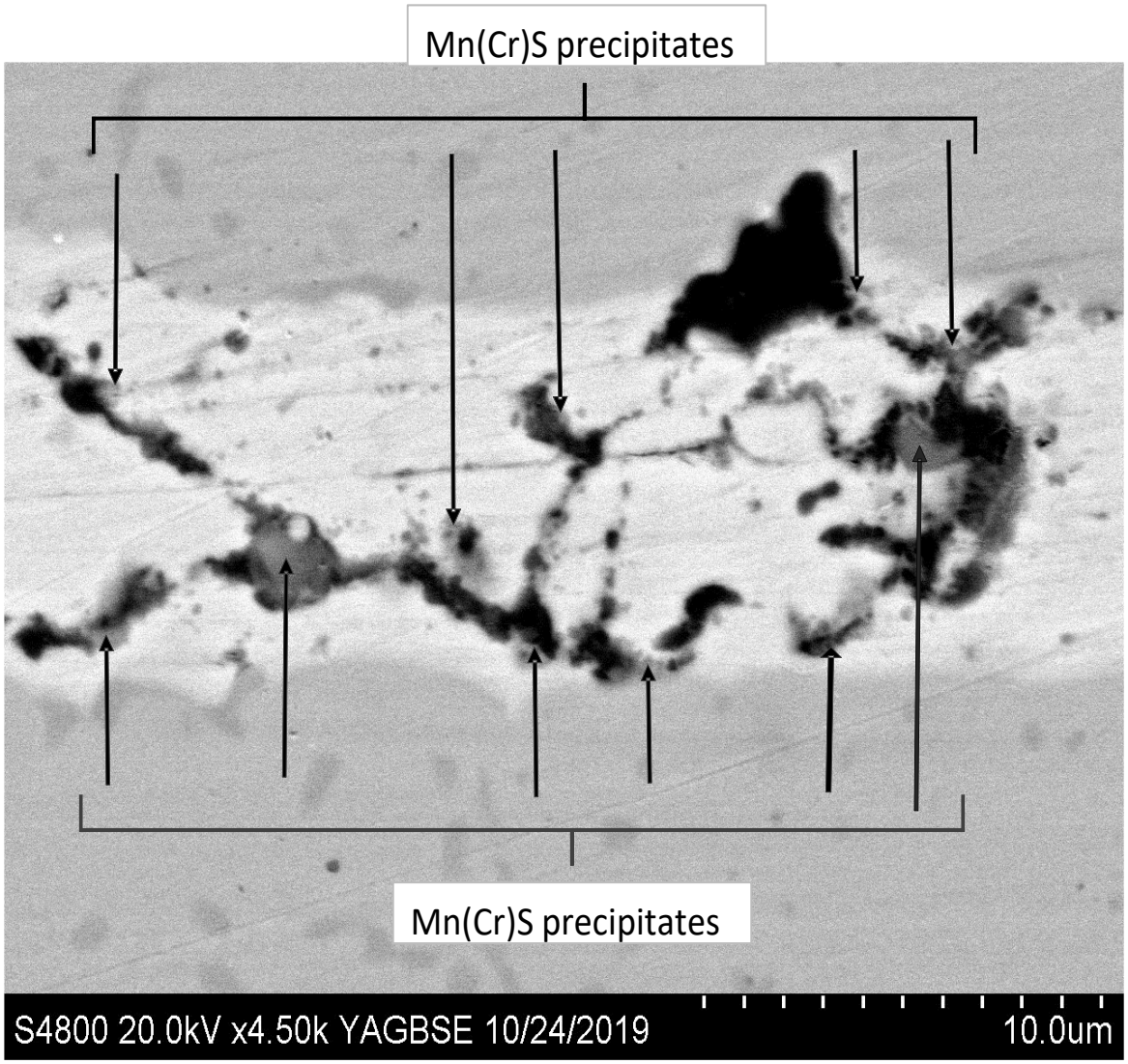

Fig.5.5.2-2. An enlarged SEM image of the EN 1.4034 joint showing how the cracks (dark areas) are interconnected with Mn(Cr)S precipitates (grey areas indicated by the arrows) within the Cu-rich matrix (light areas) of the joint.

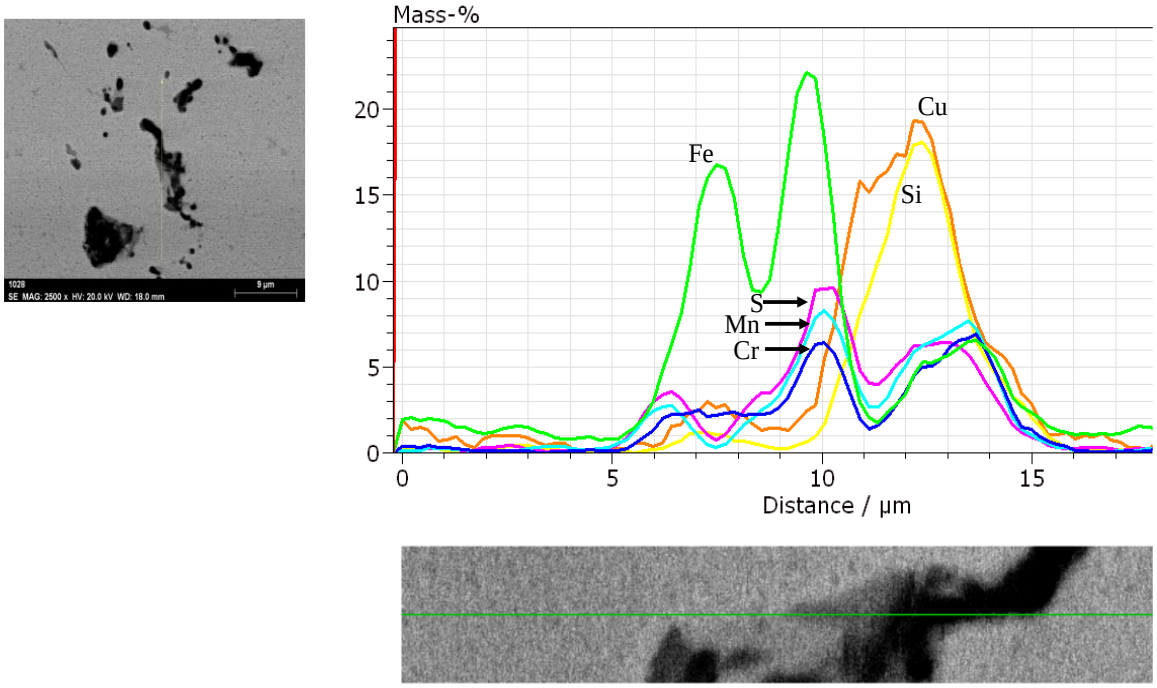

Fig.5.5.2-3. Line scan performed on the SEM micrograph and the EDS spectra of the cracked brazed joint.

The above figures Fig-s.(5.5.2- 1-3) evidently connect the manganese sulfide precipitates with cracking of the brazed joint.

The cracking of the brazed joints can be linked to sulfide precipitates by the following reasons. Firstly, from literature, we know the formation temperatures of MnS is between 1173-1273 K. By the time the temperature is down to 1273 K from 1373 K (experimental temperature), the joint is in the solid phase. The ionic MnS forms from the dissolved Mn and S atoms and precipitates in the solidified copper joint. The molar volume of ionic compound MnS is lower compared to the sum of partial molar volumes of Mn and S in copper. The volume loss at the MnS/Cu interface in the joint would act as crack initiator upon further cooling.

Second, the mismatch between the volume expansion coefficients of metals and non-metallic compounds like MnS. We observe the difference in the volume expansion values from Table 5.5.2-2, [144-145]. The metals involved here, Fe, Cr and Mn have similar expansion coefficients while the MnS phase has a volume coefficient which is 3 times lower. Hence, MnS when precipitates and solidifies within the joint (Cu-Fe-Cr-Mn-S rich), the mismatch in the expansion coefficients will lead to stress locally at the precipitate sites in the joint and leads to crack initiation.

Table 5.5.2-2. Volume expansion coefficients of elements/phases involved in the study at room temperature and at 1373 K

Phase	Volume expansion coefficient, 1/K	
	At 300 K	At 1373 K
Fe	$0.7 \cdot 10^{-4}$	$1.3 \cdot 10^{-4}$
Cu	$0.5 \cdot 10^{-4}$	$1.0 \cdot 10^{-4}$
Cr	$0.6 \cdot 10^{-4}$	$1.1 \cdot 10^{-4}$
Mn	$0.65 \cdot 10^{-4}$	$1.6 \cdot 10^{-4}$
MnS	$0.39 \cdot 10^{-4}$	$0.52 \cdot 10^{-4}$

The plausible third reason is the low adhesion energies between various precipitates forming within the copper joint. We know that the copper joint becomes saturated with metallic precipitates (such as Fe, Cr etc) from diffusion and dissolution of the respective elements under the experimental time and temperature. Besides metallic precipitates, non-metallic precipitates like MnS would be formed during the cooling down period of the experiment. The adhesion energy mismatch between the metallic copper and ionic MnS phase formed within the joint act as crack initiating zone. While a strong adhesion bond forms between the metals (Cu/Fe in our case), only a weak van-der-Waals bonds form between Cu (which is nonreactive) and ionic precipitate like MnS, both of which are known in literature [21, 46, 146-147].

Owing to the above reasons, one can conclude the localized stress developed at the MnS/Cu interface due to mismatch in volume expansion, partial volume and the weak adhesion between the MnS/Cu interface, the probability of crack formation is the highest at this interface. This crack initiation at the MnS/Cu interface was already seen from SEM micrographs

(Fig-s.5.5.2- 1-3).

Based on the above results, we construct a “braze integrity diagram” between two important parameters of engineering – i) solubility product of MnS – product of concentrations of MnS in the respective steels, $C_{Mn(Fe)}$ (wt%) and $C_{S(Fe)}$ (wt%). ii) Another parameter is the liquid time for the joint (t_L, s). Liquid time is taken here as a parameter because the dissolution and diffusion of elements (Fe, Mn and S) occur during this time. The braze integrity diagram provides two technologically different regions: i) the “stable, crack-free joints” region and ii). the “unstable cracked joints” region.

Since, the brazing temperature was fixed at 1373 K, temperature is considered as a constant parameter. Composition of Cu foil was also not an influential parameter as the Cu used was

pure and devoid of any contamination prior to experiment. This plot is shown below, Fig.5.5.2-4. Uncracked joints are shown in circles whereas cracked joints are shown in triangles. The demarcation line between the two was given by the semi-empirical equation, Eq. (16), between crack-free joint and cracked joint.

$$t_{L,cr} \cong \frac{151}{\sqrt[4]{c_{Mn(steel)} \cdot c_{S(steel)}}} \quad (16)$$

with 151 ($s/\sqrt{w\%}$) and power of 4 (dimensionless) as semi-empirical parameters.

Eq. (16) reasonably satisfies the boundary conditions:

i) at $c_{Mn(steel)}$ = 0 or at $c_{S(steel)}$ = 0 the critical liquid time tends to infinity, i.e. no cracking at least due to MnS precipitation.

ii). The higher is the value of the product $c_{Mn(steel)} \cdot c_{S(steel)}$, the shorter will be the liquid time leading to cracking of the joint.

The validity of Eq. (16) can be seen when the brazing experiments are conducted under the similar experimental parameters and materials as mentioned in the current thesis.

In principle the Eq. (16) can also be accommodated for Cr-content of the steel. However, the points with Cr-content in the steels also follow the same trend (Fig.5.5.2-4). Hence, we claim although there is Cr build up into MnS in these high Cr-steels, Cr has no significant effect on the observed cracking of the joint.

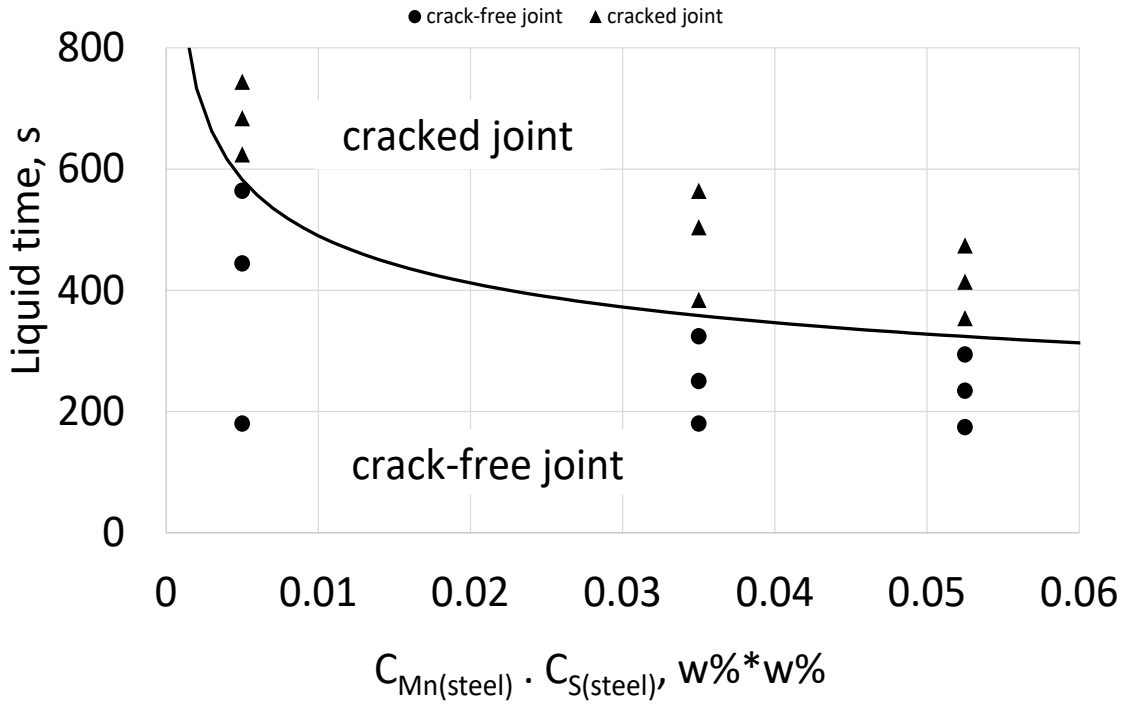

Fig.5.5.2-4. The *braze integrity diagram* for Cu braze used for different steels with different Mn- and S-contents as function of liquid time. The demarcation line between the two regions is given by Eq. (16).

In conclusion, spontaneous cracking of the unloaded copper brazed steel joints was observed when the microstructure was examined via SEM. The observed cracks were connected with the formation of manganese sulfide precipitates which form in the copper joint during cooling down phase of the experiment. The SEM-EDS (Fig-s.5.5.2- 1-3) results show the connection between the MnS precipitates in the joint and the observed cracks. The reason for cracking of the joint can be understood as a combination of following factors:

- Thermal expansion mismatch between the metallic Cu/ionic MnS both of which expand differently under same temperature leading to thermal stresses at the joint/precipitate interface.
- MnS precipitates in the copper joint forming from the dissolved Mn and S atoms. However, molar volume of MnS is lower than the sum of partial molar volumes of Mn and S in the copper joint. This leads to a localized crack initiation at the MnS/Cu interface in the joint upon further cooling.
- Further, the adhesion energy between an ionic precipitate MnS and metallic copper is much lower than the adhesion energy between metallic Fe and metallic copper. Only van-der-Waals forces exist between ionic/metallic systems. These in combination with the above two reasons would eventually lead to cracking in the joint at the site of MnS precipitate as shown.
- A braze integrity diagram was constructed between solubility product of MnS and liquid time showing the technological windows of cracked and uncracked joints.

Claims

All claims are based on the series of experiments conducted with a 70-micron thick pure copper foil placed in between two identical steel plates, Table C1, dimensions 10mm x 7mm x 4mm to form a sandwich structure as shown in Fig.C1. The sandwich is wound tightly by a high temperature wire to keep them in place during the experiments. The sandwich then is placed inside a resistance heating vacuum furnace. The experiments are conducted at a temperature of 1373 K at a residual pressure of around 10^{-8} bar (or in some cases at around 10^{-5} bar). The heating rate of the furnace is around 293 K/min and the temperature inside the furnace is measured by a Pt-Pt-Rh thermocouple. After given holding time at 1373 K the furnace is cooled down spontaneously overnight (keeping the vacuum) and the sample is removed the next morning.

Table C1. The composition of the various steels used in this study

Steel standard		Cr wt%	Mn wt%	S wt%	C wt%	Others (Si, P, Mo etc) wt%	Fe wt%
European	AISI						
Armco	-	0.016	0.11	0.0064	0.0010	< 0.050	Rest
C45	1045	-	-	0.030	0.45-0.50	~ 0.60	Rest
S103	-	-	0.20-0.25	0.010-0.020	0.60-1.00	~ 0.70	Rest
CK60	1060	0.15-0.20	0.75-0.80	0.070-0.075	0.25-0.60	~ 0.70	Rest
EN 1.4034	420	11-12	0.90-1.0	0.035	0.15-0.20	~ 0.50	Rest

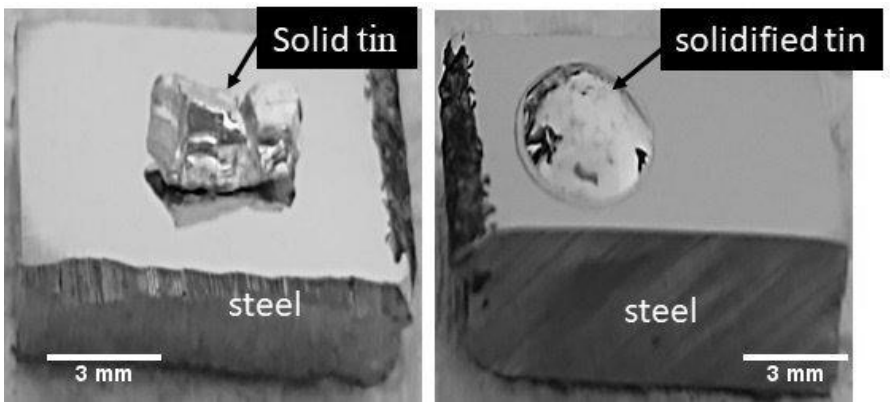

Fig.C1. The contact heating sessile drop technique used for wetting studies in thesis (left: before the experiment, right: after the experiment).

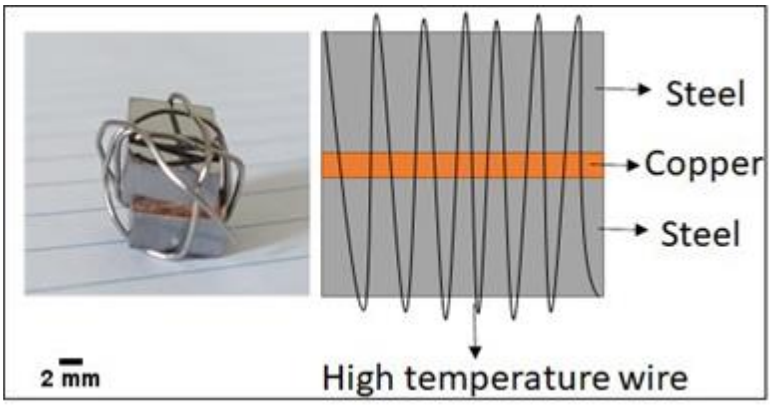

Fig.C2. The sandwich arrangement of the copper foil and steel plates used throughout the study

Though the experiments were conducted during given "holding time" at 1373 K, for consistency and generalization "liquid time" was used in the claims. Liquid time here is defined as time of the braze under liquid state (time maintained above the melting point of the braze) during the given experiment. It includes the entire duration of holding time of the experiment plus part of the heating time and part of the cooling time. The empirical relationship between the liquid time and holding time in our furnace was found as:

$$t_L = t_h + 68 \quad \text{(C1)}$$

where t_L is liquid time (s), t_h is holding time (s). As each furnace is different, Eq. (C1) is different for each furnace. That is why the claims in this thesis are formulated as function of liquid time, so the claims have general validity for any furnace.

The claims below are formulated according to the sequence of different phenomena that take place during brazing process.

Claim 1. Spontaneous removal of the native oxide layer from the surface of steels and wetting of the steel surfaces by liquid tin

The removal of the native oxide layer from the surface of steels was observed experimentally measuring the change from the non-wetting to wetting states of liquid tin on the surface of steels. The critical temperature of oxide removal on different steels at two different residual pressures of vacuum was tabulated in Table C2. Successful brazing of different steel types at given vacuum levels are possible only above the transition temperatures given in Table C2.

Table C2. Wetting transition temperatures of liquid tin on various steels

Steel	Transition temperature (K) at 10^{-8} bar vacuum	Transition temperature (K) at 10^{-5} bar vacuum
Armco	773-793	773-793
C45	823-843	823-843
S103	913-933	963-983
CK60	923-943	973-993
EN1.4034	1133-1153	No transition below 1273 K

After the oxide layer was removed and wetting transition was observed, wetting of the steel surfaces by liquid tin follows, see Fig.C3 and Table C3. The relatively high contact angles shown in Table C3 as compared to liquid copper/steel system are due to the formation of not-fully metallic intermetallic compounds at the steel/Sn interface, (see Fig.C4).

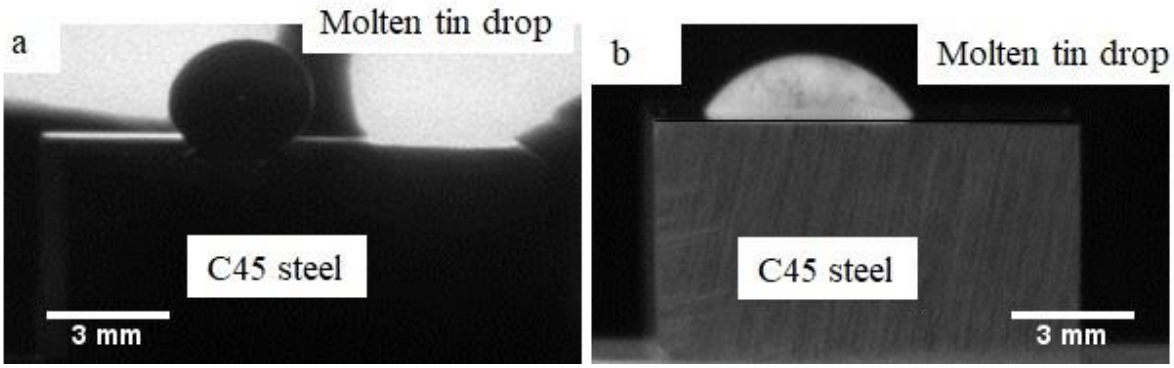

Fig.C3. Transition of liquid tin drop from non-wetting at 573 K (a) to wetting at 933 K (b) on the surface of C45 steel, at 10^{-8} bar residual pressure.

Table C3. final contact angles of liquid tin on the surface of steels at two different residual vacuum pressures

Steel	10^{-5} bar vacuum pressure		10^{-8} bar vacuum pressure	
	T, K	θ, (°)	T, K	θ, (°)
Armco steel	883	50 ± 10	923	50 ± 10
C45 steel	943	70 ± 10	933	45 ± 10
S103 steel	1033	75 ± 10	973	50 ± 10
CK60 steel	1073	70 ± 10	973	70 ± 10
EN1.4034 steel	1323	130 ± 10	1223	20 ± 10

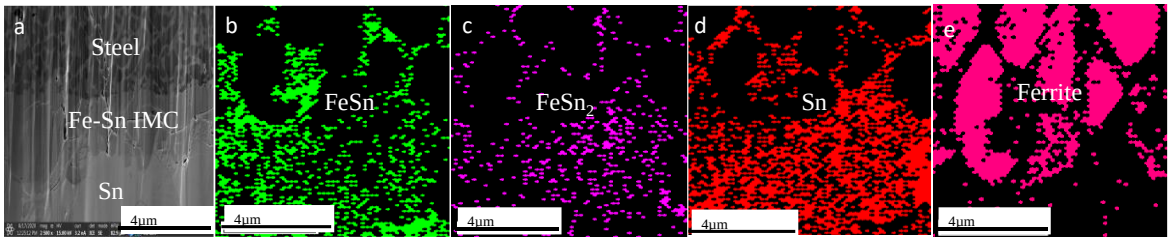

Fig.C4. Formation of Fe/Sn intermetallic compounds at the interface of steel and liquid tin limiting the spreading and wetting of steels by liquid tin.

Claim 2. Wetting of steel surfaces by liquid copper

Thanks to Claim 1, liquid copper was found spreading instantaneously (with near zero contact angle) along the surfaces of all steels at its melting (1083 ºC) point at 10^{-8} bar vacuum, which is the precondition to form strong joints, (see Fig.C5 and Table C4). The experimentally observed contact angle values were approximately confirmed by the theoretical calculations [13] providing the possible range of contact angles for the Fe/Cu systems between 0° and 20°.

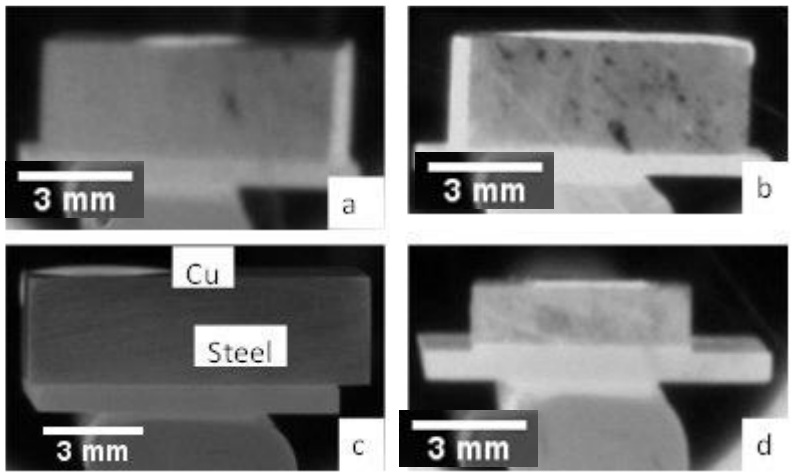

Fig.C5. Close-to-perfect wetting of the copper on various steels observed during the wetting experiments. a: C45 steel, b: S103 steel c: CK60 steel and d: EN1.4034 steel.

Table C4. Final contact angles of liquid Cu on the surface of various steels

Steel	contact angle of Cu on steel (°)
C45	2.7 ± 0.2
S103	1.3 ± 0.2
CK60	2.4 ± 0.3
EN1.4034	5.0 ± 0.5

Claim 3. Grain boundary penetration of liquid metals into GB-s of different steels

3a. GB penetration by liquid copper

Grain boundary penetration of steels by liquid copper was observed for all the steels studied here. However, the depth of penetration varied as function of composition of steels (see Fig.C6). Average depth of 10-20 μm was achieved by liquid Cu in steel GB's at 300 s holding time.

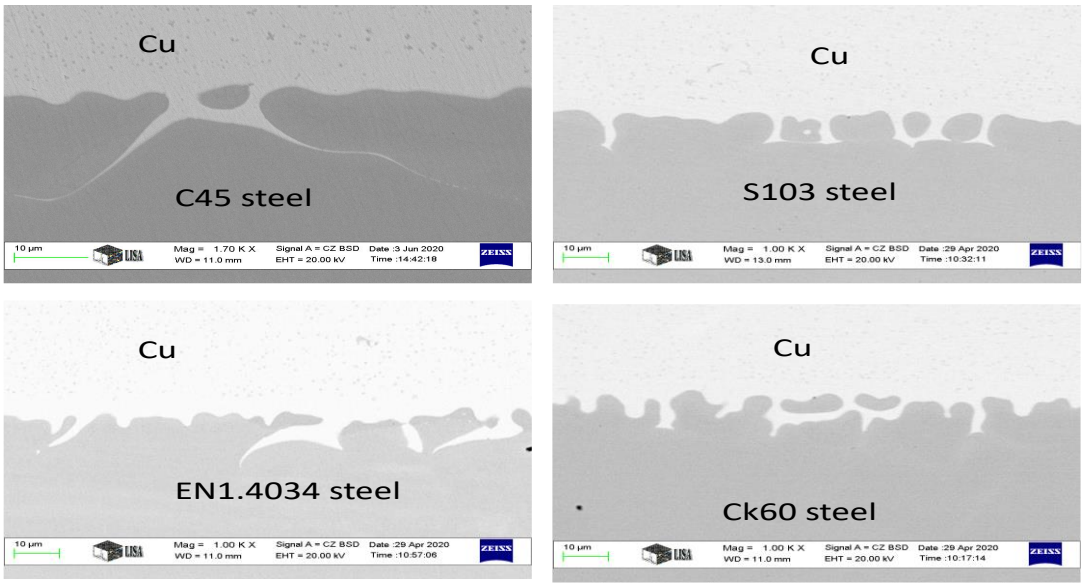

Fig.C6. Grain boundary penetration of steels by liquid copper at 300 s of holding time.

3b. GB penetration by liquid tin

GB penetration was not found by liquid tin in the following four steel types: Armco, C45, S103 and CK60. This can be explained by the formation of continuous FeSn and $FeSn_2$ intermetallic layer at the steel/tin interface, blocking the GB-s of steel, so liquid tin cannot penetrate into those GB-s (see Fig.C7). GB penetration was observed only in case of EN1.4034 steel due to its high Cr-content. This leads to liquid metal embrittlement of EN1.4034 steel by liquid tin. The average depth of penetration achieved by liquid tin in this steel was 25 ± 3 μm, at temperature between 1150-1250 K and 600 s holding time (Fig.C7e).

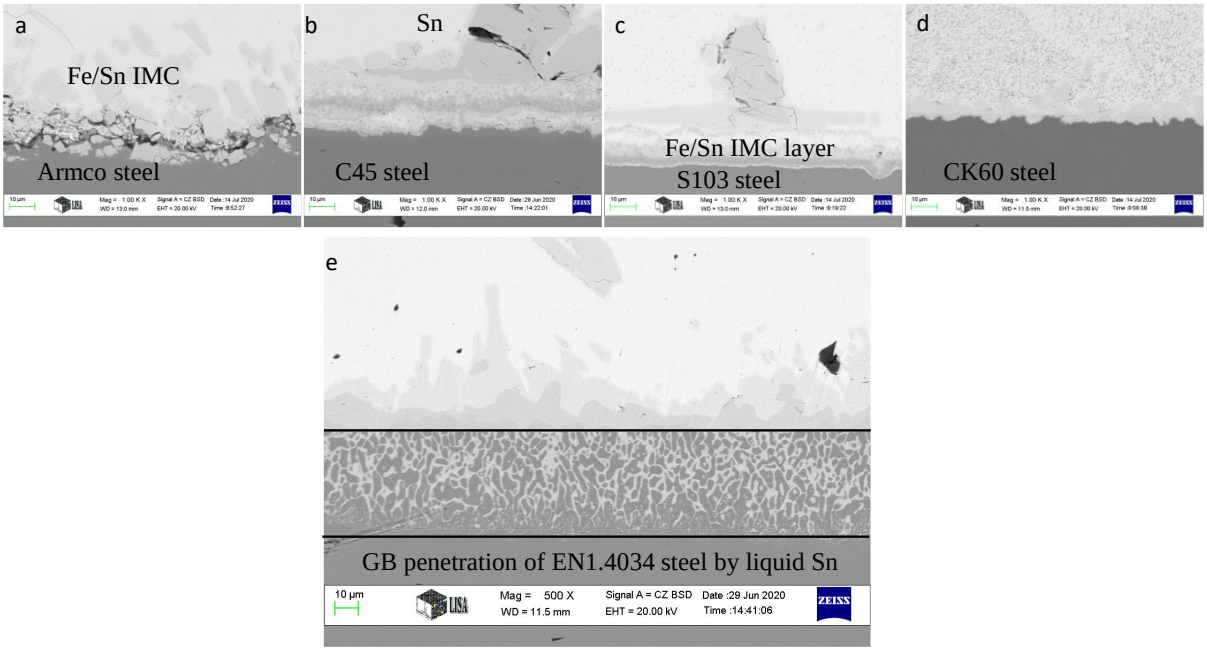

Fig.C7. No GB penetration of four steels by liquid tin seen in Fig-s. a-d. However, GB penetration of liquid tin in EN1.4034 steel (Fig.C7e) can be seen.

Claim 4. Rapid thinning of the joint after melting

After melting the copper foil, the joint thickness was found to decrease rapidly from its initial thickness of 70 µm as function of liquid time across all the experiments (see Fig.C8). The following general equation was found to describe the liquid time dependence of the thickness of the joint d_j, Eq. (C2):

$$d_j \cong \frac{70}{1+z \cdot t_L} \tag{C2}$$

where d_j (micron) is the thickness of the joint obtained post experimentation, t_L (s) is the liquid time for the experiment, 70 microns is the initial thickness of the Cu foil, while z (1/s) is the semi-empirical coefficient (see Table C5 for its values). As the copper melts, liquid copper is pushed out from between the steels due to the spring force from the wound wire and gravity force from the upper plate. This out pushed copper evaporates as the equilibrium vapor pressure of copper is 7.94 E-7 bar, being higher than 9 E-8 bar of residual pressure of vacuum inside the furnace.

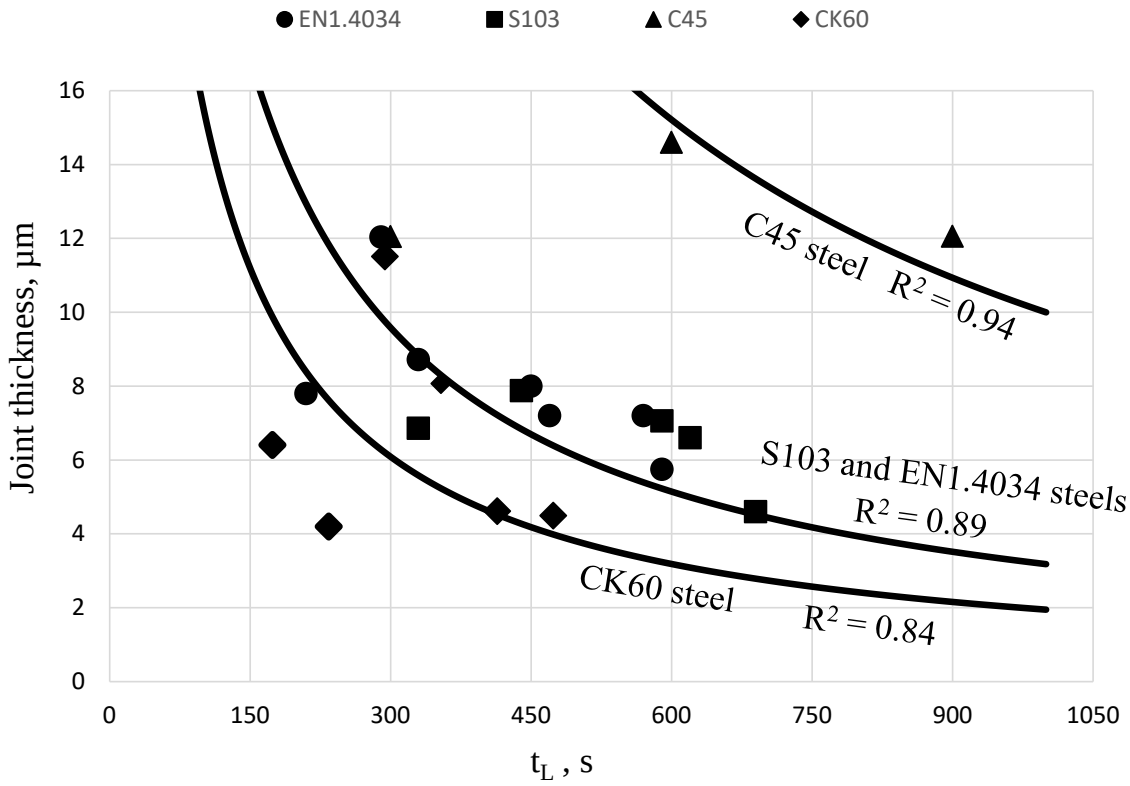

Fig.C8. Measured joint thickness between the steel samples as function of the liquid time for various steel types. The three average lines obtained for steel types as indicated in figure by substituting different z values from Table C5 into Eq. (C2).

Table C5. Semi-empirical coefficient for different steel grades to be used in Eq. (C2)

Steel grade	Semi-empirical coefficient, z (1/s)
C45	0.0054 ± 0.001
EN1.4034 and S103	0.017 ± 0.003
CK60	0.045 ± 0.03

Claim 5. Cracking in the unloaded brazed joint upon cooling

5a. Cracking observed

No cracking was observed in C45 and Armco steels with experiments after 1884 s liquid time, and the joints were free of any ionic precipitates. However, experiments with steels containing larger amounts of alloying elements (S103, CK60 and EN1.4034) show cracking after a certain liquid time (see Fig.C9). Table C6 shows the minimum liquid time t_L required for cracking the copper brazed joints as function of composition of steels.

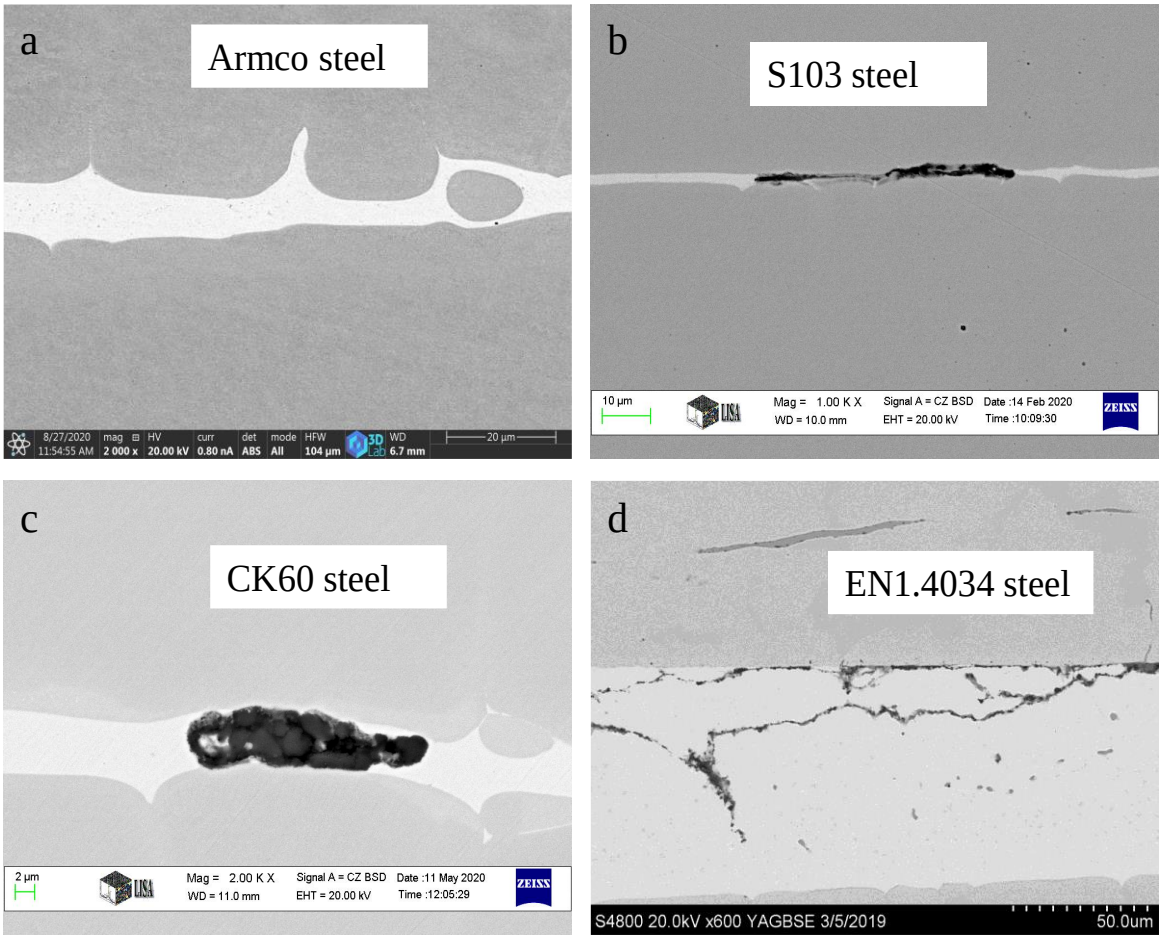

Fig.C9. SEM micrographs of the joints observed in unloaded brazed steel/Cu/steel joints. An uncracked joint is observed for Armco steel, while cracked joints were obtained for other three steels after certain critical liquid times: Armco steel after 1868 s (a), S103 steel after 578 s (b), CK60 steel after 308 s (c) EN1.4034 steel after 338 s (d).

Table C6. Mn-S composition in the steel and minimum liquid time needed for cracking the brazed joints

Steel	Mn wt%	S wt%	Liquid time required for cracking of the joint (s)
C45	-	0.03	no cracking up to 1868 s at least
Armco	0.11	0.0064	no cracking up to 1868 s at least
S103	0.25	0.02	578 ± 30
CK60	0.75	0.07	308 ± 30
EN1.4034	1	0.035	338 ± 30

5b. Reasons for cracking

Based on the experimental results, it was proven that the primary reason for the cracking is the formation of MnS / Mn(Cr)S sulfide phases, which form in the joint during cooling,

(see Fig.C10). The MnS / Mn(Cr)S phases are not present in the joint prior to the experiment. Instead, they form in the copper joint as a result of dissolution and diffusion of Mn, Cr and S elements from the bulk of steel into the liquid copper at the experimental temperature.

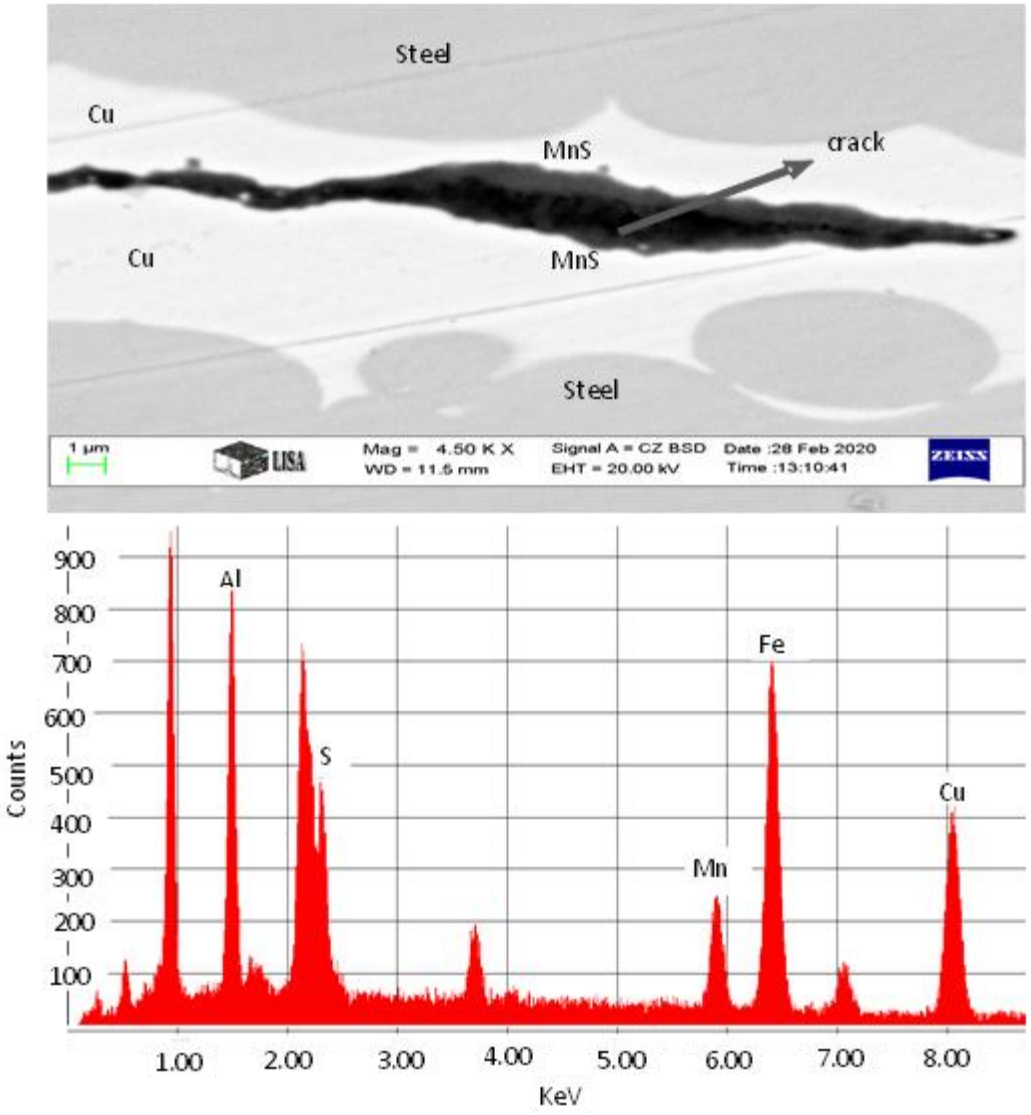

Fig.C10. The SEM image of the cross section of CK60 steel after 338 s liquid time of brazing experiment and the corresponding EDS spectra of the spot in the middle of the joint. We see Fe, Mn and S coming from steel while Cu being the joint. Additionally, we also observe Al which comes from polishing.

The reasons of cracking the joint at the MnS/Cu interface are the following:

i) The molar volume of ionic MnS precipitating in the solid copper joint is lower than the sum of partial molar volumes of Mn and S dissolved in copper joint. This local volume

decrease accompanying MnS precipitation acts as a crack initiator at the MnS/Cu interface in the joint.

ii) The MnS precipitate is ionic and it precipitates in metallic copper joint. During cooling, the ionic MnS precipitate and metallic Cu matrix contract differently owing to their significantly different thermal expansion coefficients leading to additional stress at the MnS/Cu interface.

iii) There is a weak adhesion energy at the interface of ionic MnS and metallic Cu due to van-der-Waals forces, only. Thus MnS/Cu interface is the most probable place to form a crack compared to other interfaces, which are all metal/metal interfaces, such as the Cu/steel interface.

5c. Braze-integrity diagram

The results obtained above were summarized in the "braze-integrity" diagram. The graph shows the relation between liquid time and solubility product of MnS in the steel. The graph is divided into two technological regions separated by a demarcation line between cracked and crack-free joints (see Fig.C11). The demarcation line is given by Eq. (C3):

$$t_{L,cr} \cong \frac{151}{\sqrt[4]{c_{Mn(steel)} \cdot c_{S(steel)}}} \qquad \text{(C3)}$$

with 151 ($s/\sqrt{w\%}$) and power of 4 (dimensionless) being semi-empirical parameters, valid for all steel types studied in this work.

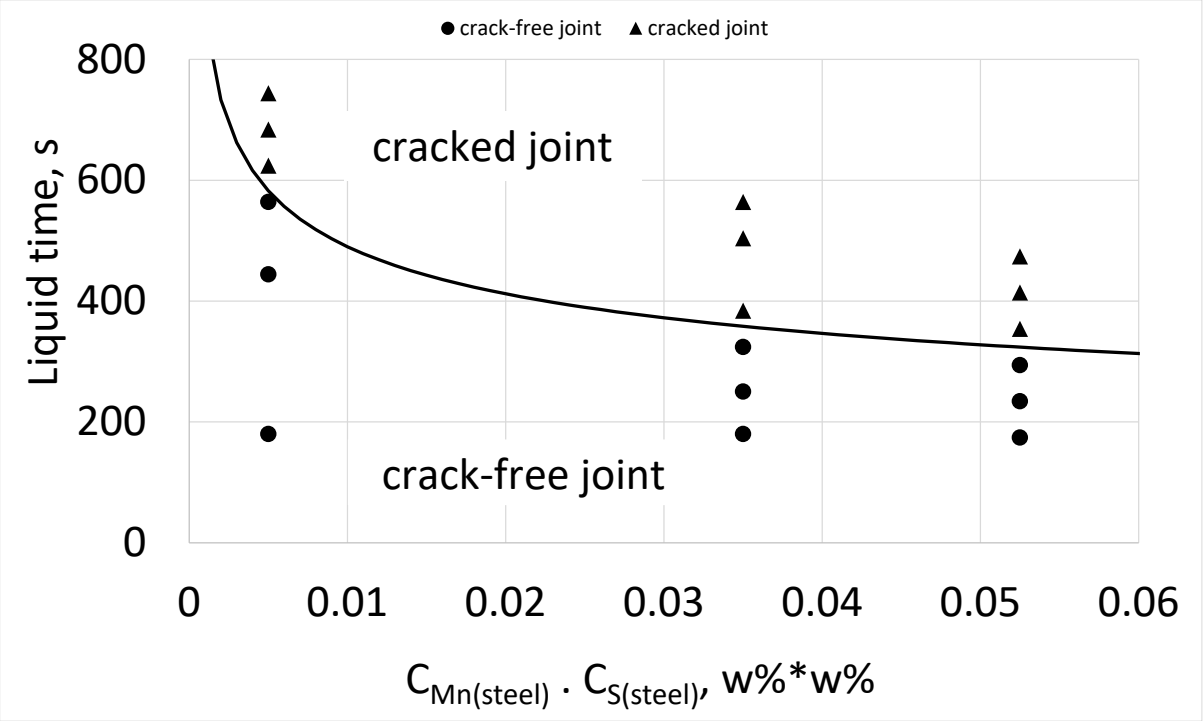

Fig.C11. The braze integrity diagram for Cu braze used for different steels with different Mn- and S-contents as function of liquid time.

Future possibilities

- The databank on the dependence of wetting transition of various metallic liquids (specially the braze alloys) on the surface of various steel types as function of temperature and pressure is missing.
- Further experiments are needed on better understanding the pressure dependence on the non-wetting to wetting transition of the said metallic liquids. This would help in better control of pressure and temperature parameters during the joining applications like brazing in the industries.
- It would also be interesting from science point of view to observe experimentally the conditions under which the joint thinning effect (reported throughout my study) occurs in a brazed joint. For example, change in brazing atmosphere may reduce/increase the joint thinning effect. Also, to observe if the composition of steels has any effect on the reduction of the joint thickness and extend the study to various steel grades.
- Grain boundary penetration of steel observed in my study with two different liquid metals (Cu, Sn) differ mainly as function of composition of steels and liquid Cu/Sn. There is a need for databank showing the alloying elements which enhances the GB penetration of steels by liquid metals and the elements which would reduce the GB penetration effect. Also, to formulate the time dependence of penetration depth achieved by liquids in steel GB's.
- The brazing experiments focusing on the quantitative analysis using mechanical testing is also a possible future research direction.

Acknowledgements

The success of my PhD dissertation is a combined effort of people and organizations alike. I am sincerely grateful to my supervisor Dr. Peter Baumli, who was more than just a supervisor in my journey. His continuous guidance has laid the foundation for my research direction and every day experimentation. My sincere and heartful gratitude to my co-supervisor Prof. George Kaptay whose eminent research profile and visionary guidance made my study more structured and refined. Their warmth and affectionate conversations made me feel right at home in a place away from home.

I would like to thank “Antal Kerpely Doctoral School of Material Science and Technology” and Prof. Zoltan Gacsi for accepting me as a PhD student and providing me an opportunity to conduct research at university of Miskolc. My gratitude extends to the Institute of Physical Metallurgy, Metal Forming and Nanotechnology and Prof. Valeria Mertinger for providing me with all the necessary equipment and an ambient work environment for carrying out my research.

I would like to thank Dr. Kovacs Arpad, Dr. Daniel Koncz-Horvath and Dr. Greta Gergely for extending their kind cooperation and scheduling of the SEM microstructural examination. I would also take the opportunity to show my gratitude to Dr. Anna Sycheva and Innovacios Laboratories for providing with SEM investigation of the samples. I would like to acknowledge the contributions of Bay-Zoltan non-profit kft and Mr. Jozsef T. Szabo for providing me with the experimental equipment in the initial phase of my PhD. A special thanks to Mrs. Aniko Markus and Mrs. Napsugar Bodnar for helping with both pre- and post-experimental sample preparation throughout the duration of my PhD. I show my appreciation to Adam Vegh and Korozs Jozsef for their invaluable support in the Calphad simulations. I would like to sincerely thank Mrs. Judit Szabo, Mrs. Agnes Solczi, Dr. Sveda Maria, Dr. Katalin Voith, Mrs, Nora Orosz-Forizs and Mrs. Stumpf Eva for their continued and valuable support in the administrative work at the university. Finally, I would like to thank my fellow colleagues both Hungarian and International for helping, interacting and supporting in realization of this thesis work.

I would like to show my appreciation for Tempus Public Foundation and Stipendium Hungaricum scholarship program for selecting and providing financial assistance for my wonderful journey in Hungary and Europe. This work was financed by GINOP2.3.2-15-2016-0027 “Sustainable operation of the workshop of excellence for the research and development of crystalline and amorphous nanostructured materials” project implemented in the framework of Szechenyi2020 program.

Finally, I am grateful for my family who were a constant support system in my life. I appreciate my friends Manoj Kumar Pal, Narender Saini, Ankit Santhoshi who were a part of my journey here in Hungary and Europe. A special mention to Pooja Kalpura Jagadeesh, who continuously cheered, supported and motivated me through out the PhD studies.

References

1. Kaptay, G. (2008). A unified model for the cohesive enthalpy, critical temperature, surface tension and volume thermal expansion coefficient of liquid metals of bcc, fcc and hcp crystals. *Materials Science and Engineering: A*, *495*(1-2), 19-26.
2. Kaptay, G. (2020). A coherent set of model equations for various surface and interface energies in systems with liquid and solid metals and alloys. *Advances in Colloid and Interface Science*, 102212.
3. Roberts, P. (2013). *Industrial brazing practice*, Crc.
4. Jacobson, D. M., & Humpston, G. (2005). *Principles of brazing*, ASM International.
5. Humpston, G., & Jacobson, D. M. (2004). *Principles of soldering*. ASM International.
6. Lang, J., & Hughes, M. J. (1991). Joining techniques. *Aspects of Early Metallurgy*, 169-177.
7. Pliny (the Elder.), & Rackham, H. (1952). *Pliny*. Harvard University Press
8. Sutton, M. A., Wolters, W. J., Peters, W. H., Ranson, W. F., & McNeill, S. R. (1983). Determination of displacements using an improved digital correlation method. *Image and vision computing*, *1*(3), 133-139.
9. Bradbury, F. (1912). A history of old Sheffield plate.
10. https://en.wikipedia.org/wiki/Sheffield_plate
11. Bauer, C. L., & Lessmann, G. G. (1976). Metal-joining methods. *Annual Review of Materials Science*, *6*(1), 361-387.
12. John, V. B. (1983). Metal-joining Processes. In *Introduction to Engineering Materials* (pp. 321-341). Palgrave Macmillan.
13. Kaptay, G. (2005). Modelling interfacial energies in metallic systems. *Materials Science Forum*, (473), 1-10.
14. Cadden, C. H. (2006). Encyclopedia of materials: science and technology.
15. Hans, W. (1929). *U.S. Patent No. 1,722,025*. Washington, DC: U.S. Patent and Trademark Office.
16. Alexander, H. W. (1952). *U.S. Patent No. 2,591,994*. Washington, DC: U.S. Patent and Trademark Office.
17. Chartet, A. (1973). *U.S. Patent No. 3,769,675*. Washington, DC: U.S. Patent and Trademark Office.

18. Chartet, A. (1973). *U.S. Patent No. 3,728,783*. Washington, DC: U.S. Patent and Trademark Office.
19. Schwartz, M. M. (2003). *Brazing*. ASM international.
20. Weis, S., Fedorov, V., Elssner, M., Uhlig, T., Hausner, S., Wagner, G., & Wielage, B. (2017). Research trends in brazing and soldering. *Welding Technology Review*, *89*(7).
21. Eustathopoulos, N., Nicholas, M. G., & Drevet, B. (Eds.). (1999). *Wettability at high temperatures*. Elsevier.
22. Kohl, W. H. (1967). Handbook of materials and techniques for vacuum devices.
23. Yearian, H. J., Derbyshire, W. D., & Radavich, J. F. (1957). The formation of oxide films on chromium and 18 Cr-8 Ni steels. *Corrosion*, *13*(9), 65-75.
24. Gesmundo, F., De Asmundis, C., Battilana, G., & Ruedl, E. (1987). High temperature oxidation of a commercial Cr-Mn austenitic steel in air. *Materials and Corrosion*, *38*(7), 368-375.
25. Song, S. H., & Xiao, P. (2003). An impedance spectroscopy study of oxide films formed during high temperature oxidation of an austenitic stainless steel. *Journal of materials science*, *38*(3), 499-506.
26. Chang, Y. N., & Wei, F. I. (1989). High temperature oxidation of low alloy steels. *Journal of materials science*, *24*(1), 14-22.
27. Chen, R. Y., & Yeun, W. Y. D. (2003). Review of the high-temperature oxidation of iron and carbon steels in air or oxygen. *Oxidation of metals*, *59*(5-6), 433-468.
28. Young, D. J. (2008). *High temperature oxidation and corrosion of metals* (Vol. 1), Elsevier.
29. Huntz, A. M., Reckmann, A., Haut, C., Sévérac, C., Herbst, M., Resende, F. C. T., & Sabioni, A. C. S. (2007). Oxidation of AISI 304 and AISI 439 stainless steels. *Materials Science and Engineering: A*, *447*(1-2), 266-276.
30. Vesel, A., Mozetic, M., Drenik, A., Hauptman, N., & Balat-Pichelin, M. (2008). High temperature oxidation of stainless steel AISI316L in air plasma. *Applied Surface Science*, *255*(5), 1759-1765.
31. Doyle, C. S., Seal, C. K., & James, B. J. (2011). Evolution of steel surface composition with heating in vacuum and in air. *Applied surface science*, *257*(23), 10005-10017.
32. Pour-Ali, S., Weiser, M., Nguyen, N. T., Kiani-Rashid, A. R., Babakhani, A., & Virtanen, S. (2020). High temperature oxidation behaviour of AISI 321 stainless

steel with an ultrafine-grained surface at 800° C in Ar–20 vol.% O2. *Corrosion Science*, *163*, 108282.

33. Silva, R., Vacchi, G. S., Santos, I. G. R., de Sousa Malafaia, A. M., Kugelmeier, C. L., Mendes Filho, A. A., & Rovere, C. A. D. (2020). Insights into high-temperature oxidation of Fe-Mn-Si-Cr-Ni shape memory stainless steels and its relationship to alloy chemical composition. *Corrosion Science*, *163*, 108269.
34. Ishigami, I., Tsunasawa, E., & Yamanaka, K. (1981). Effects of vacuum heating conditions on the surface brightness of various stainless steels. *Transactions of the Japan Institute of Metals*, *22*(5), 337-346.
35. Arata, Y., Ohmori, A., & Cai, H. F. (1983). Studies on vacuum brazing (report II). *Transactions of IWR112*, *1*, 27-34
36. Kozlova, O., Voytovych, R., Devismes, M. F., & Eustathopoulos, N. (2008). Wetting and brazing of stainless steels by copper–silver eutectic. *Materials Science and Engineering: A*, *495*(1-2), 96-101.
37. Kozlova, O. V., Rodin, A. O., & Eustathopoulos, N. (2008). Wetting and soldering of austenitic chromonickel steel by eutectic melts based on Cu-Ag. *Steel in Translation*, *38*(3), 195-200.
38. Rousseau, A. F., Partridge, J. G., Gözükara, Y. M., Gulizia, S., & McCulloch, D. G. (2016). Carbon evolution during vacuum heat treatment of High-Speed Steel. *Vacuum*, *124*, 85-88.
39. Young, T. (1805). III. An essay on the cohesion of fluids. *Philosophical transactions of the royal society of London*, (95), 65-87.
40. Adamson, A. W., & Gast, A. P. (1967). *Physical chemistry of surfaces* (Vol. 150, p. 180). New York: Interscience publishers.
41. Bico, J., Tordeux, C., & Quéré, D. (2001). Rough wetting. *EPL (Europhysics Letters)*, *55*(2), 214.
42. Seveno, D., Blake, T. D., & De Coninck, J. (2013). Young's equation at the nanoscale. *Physical review letters*, *111*(9), 096101.
43. Naidich, Y. V., Perevertailo, V. M., & Obushchak, L. P. (1975). Contact properties of the phases participating in the crystallization of gold-silicon and gold-germanium melts. *Soviet Powder Metallurgy and Metal Ceramics*, *14*(7), 567-571.
44. Wenzl, H., Fattah, A., & Uelhoff, W. (1976). Measurements of the contact angle between melt and crystal during Czochralski growth of copper. *Journal of Crystal Growth*, *36*(2), 319-322.

45. Surekh, T. (1976). Theory of shape stability in crystal growth from the melt. *Journal of Applied Physics*, *47*(10), 4384-4393
46. Naidich, J. V. (1981). The wettability of solids by liquid metals. In *Progress in surface and membrane science*, Vol. 14, 353-484, Academic Press, New York.
47. Ishida, T. (1988). Spreading kinetics of liquid metals on mild steel. *Materials science and technology*, *4*(9), 830-835.
48. Sun, Q., Jin, P., Liu, Y., Li, J., Wang, J., Ma, T., & Feng, J. (2019). Wetting of liquid copper on TC4 titanium alloy and 304 stainless steel at 1273–1433 K. *Materials & Design*, *169*, 107667.
49. Bernardo, E., de Oro, R., Campos, M., & Torralba, J. (2015). New findings on the wettability and spreading of copper on iron-base substrates. *International Journal of Powder Metallurgy*, *51*(4), 29-36.
50. Protsenko, P., Terlain, A., Traskine, V., & Eustathopoulos, N. (2001). The role of intermetallics in wetting in metallic systems. *Scripta Materialia*, *45*(12), 1439-1445.
51. Yin, L., Meschter, S. J., & Singler, T. J. (2004). Wetting in the Au–Sn system. *Acta Materialia*, *52*(10), 2873-2888.
52. Yin, L., Murray, B. T., & Singler, T. J. (2006). Dissolutive wetting in the Bi–Sn system. *Acta materialia*, *54*(13), 3561-3574.
53. Amore, S., Ricci, E., Borzone, G., & Novakovic, R. (2008). Wetting behavior of lead-free Sn-based alloys on Cu and Ni substrates. *Materials Science and Engineering: A*, *495*(1-2), 108-112.
54. Pstruś, J., Fima, P., & Gancarz, T. (2012). Wetting of Cu and Al by Sn-Zn and Zn-Al Eutectic Alloys. *Journal of Materials Engineering and Performance*, *21*(5), 606-613.
55. Rissanen, P. T. (1995). *U.S. Patent No. 5,378,294*. Washington, DC: U.S. Patent and Trademark Office.
56. Rassoul, E. S. M. (1997). Effect of carbon on the diffusion of copper in different carbon-steels. *Journal of materials science*, *32*(24), 6471-6474.
57. Májlinger, K., & Szabó, P. J. (2012). Intercrystalline cracking of austenitic stainless steels during brazing. In *Proceedings of the Eighth International Conference on Mechanical Engineering. Budapest: Budapest University of Technology and Economics Faculty of Mechanical Engineering*, 309-315.
58. Májlinger, K., & Szabó, P. J. (2013). Intercrystalline cracking of austenitic steel during brazing. In *Materials Science Forum*, 729, 442-447

59. He, Z., & Ding, L. (1997). Investigation on Ag-Cu-Sn brazing filler metals. *Materials chemistry and physics*, *49*(1), 1-6.
60. Song, R., Schroth, J. G., Speer, J. G., & Matlock, D. K. (2009). Copper brazing response of some advanced high strength steel grades. *journal of materials processing technology*, *209*(1), 70-76.
61. Hanson, W. B., Ironside, K. I., & Fernie, J. A. (2000). Active metal brazing of zirconia. *Acta materialia*, *48*(18-19), 4673-4676.
62. Abed, A., Jalham, I. S., & Hendry, A. (2001). Wetting and reaction between β′-sialon, stainless steel and Cu–Ag brazing alloys containing Ti. *Journal of the European Ceramic Society*, *21*(3), 283-290.
63. Kozlova, O., Voytovych, R., Protsenko, P., & Eustathopoulos, N. (2010). Non-reactive versus dissolutive wetting of Ag–Cu alloys on Cu substrates. *Journal of materials science*, *45*(8), 2099-2105.
64. Roy, R. K., Panda, A. K., Das, S. K., & Mitra, A. (2009). Development of a copper-based filler alloy for brazing stainless steels. *Materials Science and Engineering: A*, *523*(1-2), 312-315.
65. Roy, R. K., Singh, S., Gunjan, M. K., Panda, A. K., & Mitra, A. (2011). Joining of 304SS and pure copper by rapidly solidified Cu-based braze alloy. *Fusion engineering and design*, *86*(4-5), 452-455.
66. Tashi, R. S., Mousavi, S. A., & Atabaki, M. M. (2013). Diffusion Brazing of Ti-6Al-4V and Stainless Steel 316L Using AgCuZn Filler Metal. *Metallurgical and Materials Engineering*, *19*(3), 189-202.
67. Criss, E. M., & Meyers, M. A. (2015). Braze welding of cobalt with a silver–copper filler. *Journal of Materials Research and Technology*, *4*(1), 44-59.
68. Venkateswaran, T., Xavier, V., Sivakumar, D., Pant, B., & GD, J. R. (2017). Brazing of stainless steels using Cu-Ag-Mn-Zn braze filler: Studies on wettability, mechanical properties, and microstructural aspects. *Materials & Design*, *121*, 213-228.
69. McLean, D. Grain boundaries in metals. (1957), *London, Oxford University Press.*
70. H. Gleiter, B. Chalmers, High-Angle Grain Boundaries, Progress in Materials Science, vol. 16, 1–272. 1972, Oxford, U.K.
71. V. Randle, The Measurement of Grain Boundary Geometry, 1993, Institute of Physics Publications, Bristol, U.K.

72. Lejček, P., Hofmann, S., & Paidar, V. (2003). Solute segregation and classification of [100] tilt grain boundaries in α-iron: consequences for grain boundary engineering. *Acta Materialia*, *51*(13), 3951-3963.
73. Lejcek, P., *Grain boundary segregation in metals*, Vol. 136, (2010), Springer.
74. Rosenhain, W., & Ewen, D. (1913). The Intercrystalline Cohesion of Metals (Second Paper). *Journal of the Institute of Metals*, *10*, 119.
75. Read, W. T., & Shockley, W. (1950). Dislocation models of crystal grain boundaries. *Physical review*, *78*(3), 275.
76. Janczak-Rusch, J., Kaptay, G., & Jeurgens, L. P. H. (2014). Interfacial design for joining technologies: an historical perspective. *Journal of materials engineering and performance*, *23*(5), 1608-1613.
77. Kaptay, G. (2016). Modelling equilibrium grain boundary segregation, grain boundary energy and grain boundary segregation transition by the extended Butler equation. *Journal of materials science*, *51*(4), 1738- 1755.
78. Sutton, A. P. (1995). Interfaces in crystalline materials. *Monographs on the Physics and Chemistry of Materials*, 414-423.
79. Dragoo, A. L. (2000). The US Department of Energy's program on the fundamental material science of internal interfaces. *Acta materialia*, *48*(18-19), 4629-4633.
80. Pereiro-Lopez, E., Ludwig, W., Bellet, D., & Baruchel, J. (2003). Grain boundary liquid metal wetting: A synchrotron micro-radiographic investigation. *Nuclear Instruments and Methods in Physics Research Section B: Beam Interactions with Materials and Atoms*, *200*, 333-338.
81. Chatain, D., Rabkin, E., Derenne, J., & Bernardini, J. (2001). Role of the solid/liquid interface faceting in rapid penetration of a liquid phase along grain boundaries. *Acta materialia*, *49*(7), 1123-1128.
82. Savage, W. F., Nippes, E. F., & Stanton, R. P. (1978). Intergranular attack of steel by molten copper. *Welding Research Supplement*, *57*, 9-16.
83. Schmatz, D. J. (1983). Grain boundary penetration during brazing of aluminum. *Welding Journal*, *62*(10), 267-271.
84. Straumal, B. B., Gust, W., & Molodov, D. A. (1995). Wetting transition on grain boundaries in Al contacting with a Sn-rich melt. *Interface Science*, *3*(2), 127-132.
85. Straumal BB, Kogtenkova O, Zięba P. 2008. Wetting transition of grain-boundary triple junctions. Acta Mater 56(5): 925-933

86. Briant, C. L., & Banerji, S. K. (1978). Intergranular failure in steel: the role of grain-boundary composition. *International metals reviews*, *23*(1), 164-199.
87. Kameda, J., McMahon, C.J. The effects of Sb, Sn, and P on the strength of grain boundaries in a Ni-Cr Steel. *Metall Mater Trans A* 12, 31–37 (1981).
88. Evans, E. B., Thompson, I., & Erb, U. (1987). Grain-boundary wetting in Zn-Sn alloys as a function of tin concentration. *Journal of materials science letters*, *6*(7), 806-808.
89. Dolgopolov, N. A., Petelin, A. L., Rakov, S. V., & Simanov, A. V. (2007). Penetration of liquid tin along grain boundaries and triple grain-boundary junctions of aluminum. *Russian Journal of Non-Ferrous Metals*, *48*(2), 126-130.
90. Yin, L., Murray, B. T., Su, S., Sun, Y., Efraim, Y., Taitelbaum, H., & Singler, T. J. (2009). Reactive wetting in metal–metal systems. *Journal of Physics: Condensed Matter*, *21*(46), 464130.
91. Fisher, J. C. (1951). Calculation of diffusion penetration curves for surface and grain boundary diffusion. *Journal of Applied Physics*, *22*(1), 74-77.
92. Whipple, R. T. P. (1954). CXXXVIII. Concentration contours in grain boundary diffusion. The London, Edinburgh, and Dublin Philosophical Magazine and Journal of Science, 45(371), 1225-1236.
93. W. W. Mullins, "Theory of Thermal Grooving", *Journal of Applied Physics, 28(3)*, pp. 334-339, 1957.
94. Young, G., & Funderlic, R. E. (1973). On the grain boundary diffusion theory of Fisher and Whipple. Journal of Applied Physics, 44(11), 5151-5154.
95. Yoshida, T., & Ohmura, H. (1980). Dissolution and deposit of base metal in dissimilar carbon steel brazing. Welding journal, 59(10), 278
96. Ishida, T. (1986). The interaction of molten copper with solid iron. Journal of materials science, 21(4), 1171-1179.
97. Stoloff, N. S., & Davies, R. G. (1968). The mechanical properties of ordered alloys. *Progress in Materials Science*, *13*, 1-84.
98. Kelley, M. J., & Stoloff, N. S. (1975). Analysis of liquid metal embrittlement from a bond energy viewpoint. *Metallurgical Transactions A*, *6*(1), 159-166.

99. Steward, R. V., Grossbeck, M. L., Chin, B. A., Aglan, H. A., & Gan, Y. (2000). Furnace brazing type 304 stainless steel to vanadium alloy (V–5Cr–5Ti). *Journal of Nuclear Materials*, *283*, 1224-1228.

100. Fredriksson, H., Hansson, K., & Olsson, A. (2001). On the mechanism of liquid copper penetration into iron grain boundaries. Scandinavian journal of metallurgy, 30(1), 41-50.

101. López, G. A., Mittemeijer, E. J., & Straumal, B. B. (2004). Grain boundary wetting by a solid phase; microstructural development in a Zn–5 wt% Al alloy. *Acta materialia*, *52*(15), 4537-4545.

102. Garza, L. G., & Van Tyne, C. J. (2005). Surface hot-shortness of 1045 forging steel with residual copper. *Journal of Materials Processing Technology*, *159*(2), 169-180.

103. Ludwig, W., Pereiro-López, E., & Bellet, D. (2005). In situ investigation of liquid Ga penetration in Al bicrystal grain boundaries: grain boundary wetting or liquid metal embrittlement? *Acta Materialia*, *53*(1), 151-162.

104. Protasova, S. G., Kogtenkova, O. A., Straumal, B. B., Zięba, P., & Baretzky,B. (2011). Inversed solid-phase grain boundary wetting in the Al–Zn system. *Journal of materials science*, *46*(12), 4349-4353.

105. Zhevnenko, S. N., Vaganov, D. V., & Gershman, E. I. (2011). Rapid penetration of bismuth from solid Bi 2 Te 3 along grain boundaries in Cu and Cu-based alloys. *Journal of materials science*, *46*(12), 4248-4253.

106. Silze, F., Wiehl, G., Kaban, I., Wendrock, H., Gemming, T., Kühn, U., & Pauly, S. (2016). Wetting behavior of Cu–Ga alloys on 304L steel. *Materials & Design*, *91*, 11-18.

107. Straumal, B. B., Kogtenkova, O. A., Murashkin, M. Y., Bulatov, M. F., Czeppe, T., & Zięba, P. (2017). Grain boundary wetting transition in Al–Mg alloys. *Materials Letters*, *186*, 82-85.

108. Zimprich, P., Betzwar-Kotas, A., Khatibi, G., Weiss, B., & Ipser, H. (2008). Size effects in small scaled lead-free solder joints. *Journal of Materials Science: Materials in Electronics*, *19*(4), 383-388.

109. Nayeb-Hashemi, H., & Lockwood, M. (2002). The effect of processing variables on the microstructures and properties of aluminum brazed joints. *Journal of materials science*, *37*(17), 3705-3713.

110. Li, H., Sun, D., Gu, X., Dong, P., & Lv, Z. (2013). Effects of the thickness of Cu filler metal on the microstructure and properties of laser-welded TiNi alloy and stainless steel joint. *Materials & Design*, *50*, 342-350.

111. Zoeram, A. S., Rahmani, A., & Mousavi, S. A. (2017). Microstructure and properties analysis of laser-welded Ni–Ti and 316l sheets using copper interlayer. *Journal of Manufacturing Processes*, *26*, 355-363.

112. Wang, M., Chen, Y., Li, X., Hua, P., Gao, L., Zhou, W., & Wu, Y. (2019). Effect of Cu Interlayer on the Microstructure and Strength for Brazing of Tungsten/316L Steel. *Journal of Materials Engineering and Performance*, *28*(3), 1745-1752.

113. Han, K., Wang, T., Tang, Q., Zhang, B., & Feng, J. (2019). Effect of Cu66V34 filler thickness on the microstructure and properties of titanium/copper joint by electron beam welding. *Journal of Materials Processing Technology*, *267*, 103-113.

114. de Prado, J., Sánchez, M., Ruiz, A., & Ureña, A. (2020). Effect of brazing temperature, filler thickness and post brazing heat treatment on the microstructure and mechanical properties of W-Eurofer joints brazed with Cu interlayers. *Journal of Nuclear Materials*, 152117.

115. Stoloff, N. S. (1968). Liquid metal embrittlement. In *Surfaces and Interfaces II* (pp. 157-182). Springer, Boston, MA.

116. Nicholas, M. G., & Old, C. F. (1979). Liquid metal embrittlement. *Journal of Materials Science*, *14*(1), 1-18.

117. Heiple, C., Bennett, W., & Rising, T. (1982). Embrittlement of several stainless steels by liquid copper and liquid braze alloys. *Materials Science and Engineering*, *52*(3), 277-289.

118. Nippes, E. F., & Ball, D. J. (1982). Copper-Contamination Cracking: Cracking Mechanism and Crack Inhibitors. *WELDING J.*, *61*(3), 75.

119. Mukhopadhyay, N. K., Chowdhury, S. G., Das, G., Chattoraj, I., Das, S. K., & Bhattacharya, D. K. (1998). An investigation of the failure of low-pressure steam turbine blades. *Engineering failure analysis*, *5*(3), 181-193.

120. Maciejewski, J. (2005). Liquid metal induced embrittlement in fuel line braze joints. *Journal of Failure Analysis and Prevention*, *5*(2), 55-60.

121. Yue, X., He, P., Feng, J. C., Zhang, J. H., & Zhu, F. Q. (2008). Microstructure and interfacial reactions of vacuum brazing titanium alloy to stainless steel using an AgCuTi filler metal. *Materials characterization*, *59*(12), 1721-1727.

122. Ghovanlou, M. K., Jahed, H., & Khajepour, A. (2011). Mechanical reliability characterization of low carbon steel brazed joints with copper filler metal. *Materials Science and Engineering: A*, *528*(19-20), 6146-6156.

123. You, D., Michelic, S. K., Wieser, G., & Bernhard, C. (2017). Modeling of manganese sulfide formation during the solidification of steel. *Journal of materials science*, *52*(3), 1797-1812.

124. Temmel, C., Karlsson, B., & Ingesten, N. G. (2008). Fatigue crack initiation in hardened medium carbon steel due to manganese sulphide inclusion clusters. *Fatigue & Fracture of Engineering Materials & Structures*, *31*(6), 466-477.

125. Tanaka, Y., Pahlevani, F., Moon, S. C., Dippenaar, R., & Sahajwalla, V. (2019). In situ characterisation of MnS precipitation in high carbon steel. *Scientific reports*, *9*(1), 1-12.

126. Schmuki, P., Hildebrand, H., Friedrich, A., & Virtanen, S. (2005). The composition of the boundary region of MnS inclusions in stainless steel and its relevance in triggering pitting corrosion. *Corrosion Science*, *47*(5), 1239-1250.

127. Chiu, K. Y., Cheng, F. T., & Man, H. C. (2006). Corrosion behavior of AISI 316L stainless steel surface-modified with NiTi. *Surface and Coatings Technology*, *200*(20-21), 6054-6061.

128. Nathan, S. R., Balasubramanian, V., Malarvizhi, S., & Rao, A. G. (2015). Effect of welding processes on mechanical and microstructural characteristics of high strength low alloy naval grade steel joints. *Defence Technology*, *11*(3), 308-317.

129. Shi, W., Yang, S., Dong, A., & Li, J. (2018). Understanding the Corrosion Mechanism of Spring Steel Induced by MnS Inclusions with Different Sizes. *JOM*, *70*(11), 2513-2522.

130. Pantazopoulos, G., Sampani, A., & Tsagaridis, E. (2007). Torsional failure of a knuckle joint of a universal steel coupling system during operation–A case study. *Engineering Failure Analysis*, *14*(1), 73-84.

131. Sojka, J., Jérôme, M., Sozańska, M., Váňová, P., Rytířová, L., & Jonšta, P. (2008). Role of microstructure and testing conditions in sulphide stress cracking of X52 and X60 API steels. *Materials Science and Engineering: A*, *480*(1-2), 237-243.

132. Iida, T., Kita, Y., Okano, H., Katayama, I., & Tanaka, T. (1992). An equation for the vapor pressure of liquid metals and calculation of their enthalpies of evaporation. *High Temperature Materials and Processes*, *10*(4), 199-207.
133. Boinovich, L. B., Emelyanenko, K. A., Domantovsky, A. G., & Emelyanenko, A. M. (2018). Laser tailoring the surface chemistry and morphology for wear, scale and corrosion resistant superhydrophobic coatings. *Langmuir*, *34*(24), 7059-7066.
134. Mortensen, A., Drevet, B., & Eustathopoulos, N. (1997). Kinetics of diffusion-limited spreading of sessile drops in reactive wetting. *Scripta Materialia*, *36*(ARTICLE), 645.
135. Goldstein, J. I., Newbury, D. E., Michael, J. R., Ritchie, N. W., Scott, J. H. J., & Joy, D. C. (2017). *Scanning electron microscopy and X-ray microanalysis*. Springer.
136. Flegler, S. L., & Flegler, S. L. (1997). *Scanning & Transmission Electron Microscopy*. Oxford University Press.
137. Barin, I. (1989). Thermochemical data of pure substances. *VCH*.
138. Kaptay, G., & Báder, E. (2001). Ion-dipole adhesion energy model for wettability of oxide ceramics by non-reacive liquid metals. *Transactions-jwri*, *30*(SPI), 55-60.
139. Nesper, R. (1991). Bonding patterns in intermetallic compounds. *Angewandte Chemie International Edition in English*, *30*(7), 789-817.
140. Stenström, B. (1972). The Electrical Resistivity of FeSn Single Crystals. *Physica Scripta*, *6*(4), 214.
141. Armbrüster, M., Schnelle, W., Cardoso-Gil, R., & Grin, Y. (2010). Chemical bonding in compounds of the CuAl2 family: MnSn2, FeSn2 and CoSn2. *Chemistry–A European Journal*, *16*(34), 10357-10365.
142. Kasap, S. (2006). *Springer handbook of electronic and photonic materials*. Springer Science & Business Media.
143. Dinsdale, A. (1989). *SGTE data for pure elements*, Teddington, United Kingdom: National Physical Laboratory.
144. Iida, T., & Guthrie, R. I., (2015) The Thermophysical Properties of Metallic Liquids: Predictive Models (2). Oxford University Press.
145. Furuseth, S. & Kjekshus, A., (1965) On the properties of a-MnS and MnS2, *Acta Chem.* Scand, 19(6), pp 1405-1410.

146. Baumli, P., Sytchev, J., & Kaptay, G. (2010). Perfect wettability of carbon by liquid aluminum achieved by a multifunctional flux. *Journal of materials science*, *45*(19), 5177-5190.
147. Weltsch, Z., Lovas, A., Takács, J., Cziráki, Á., Toth, A., & Kaptay, G. (2013). Measurement and modelling of the wettability of graphite by a silver–tin (Ag–Sn) liquid alloy. *Applied surface science*, *268*, 52-60.

Author publications in the subject of the thesis

Journal papers

- J1: Varanasi, D., & Baumli, P.: Grain boundary behavior of copper with C45 medium carbon steel. *Resolution and Discovery*, *3*(2) (2018), 24-28.
- J2: Varanasi, D., Szabo, J. T., & Baumli, P.: Investigation of the Copper Penetration and Joint Microstructure Observed in Low Alloyed Steels. *NanoWorld J*, *5*(3) (2019), 36-40.
- J3: D.Varanasi, D.Koncz-Horvath, A.Sycheva, P.Baumli, G.Kaptay. Cracking of copper brazed steel joints due to precipitation of MnS upon cooling. J Mater Eng Perform (2020) doi:10.1007/s11665-020-05293-9. (2019-IF = 1.652, Q2 in 2019 in "Mater Sci (misc)").
- J4: Dheeraj Varanasi, Khaldun E. Aldawoudi, Daniel Koncz-Horvath, Peter Baumli and George Kaptay, "Non-wetting / wetting transition of liquid tin on solid steels indicating the oxidation state of steel surfaces and its role in joining technologies", submitted to AMM (Q3), Under review.

Conference presentations

- Con1: Dheeraj Varanasi, "Comparison of penetration of copper into C45 and CrMo4 steel", conference for PhD students, oral presentation, Miskolc, Hungary – 24/04/2018.
- Con2: Dheeraj Varanasi, "Grain boundary penetration of low alloyed steels by copper", Tavaszi-Szel conference, oral presentation, Gyor, Hungary – 05/05/2018.
- Con3: Dheeraj Varanasi, "Grain boundary penetration of steels by Nickel", Tavaszi – Szel conference, oral presentation, Gyor, Hungary – 05/05/2018.
- Con4: Dheeraj Varanasi, Peter Baumli and George Kaptay, "Effect of chromium content of steel on grain boundary penetration of liquid copper", FEMS Junior Euromat 2018, oral presentation, Budapest, Hungary – 09/07/2018.
- Con5: D. Varanasi, J. T. Szabo, P. Baumli and G. Kaptay, "Influence of Cr-content on the joining & GB penetration of steels by copper", FM&NT 2018, poster presentation, Riga, Latvia – 03/10/2018.
- Con6: D. Varanasi, J. T. Szabo, P. Baumli and G. Kaptay, "Effect of alloying elements on steel-Cu joint microstructure at smaller holding times", Nano Boston conference, Poster presentation, Boston, USA – 23/04/2019.

- Con7: Dheeraj Varanasi, Jozsef T. Szabo, Peter Baumli and George Kaptay, “On the joint microstructure and grain boundary penetration by copper in low alloyed steels”, 1st Science Unlimited conference – EOTVOS symposium, oral presentation, Miskolc, Hungary – 24/05/2019.
- Con8: Dheeraj Varanasi, Jozsef T. Szabo, Peter Baumli and George Kaptay, “Effect of holding time on the microstructure evolution of steel/Cu/steel joints”, FEMS Euromat 2019, oral presentations, Stockholm, Sweden – 02/09/2019
- Con9: D. Varanasi, J. T. Szabo, P. Baumli and G. Kaptay, “Modelling the diffusion of alloying elements from bulk steel into molten copper during brazing”, 18th Austrian Chemistry Days, poster presentation, Linz, Austria – 25/09/2019.
- Con10: D. Varanasi, P. Baumli and G. Kaptay, “Wetting & grain boundary wetting of steels by copper”, e-HTC 2020, poster presentation, Visegrad, Hungary – 24/06/2020.